# INFORMATION TO USERS

This manuscript has been reproduced from the microfilm master. UMI films the text directly from the original or copy submitted. Thus, some thesis and dissertation copies are in typewriter face, while others may be from any type of computer printer.

**The quality of this reproduction is dependent upon the quality of the copy submitted.** Broken or indistinct print, colored or poor quality illustrations and photographs, print bleedthrough, substandard margins, and improper alignment can adversely affect reproduction.

In the unlikely event that the author did not send UMI a complete manuscript and there are missing pages, these will be noted. Also, if unauthorized copyright material had to be removed, a note will indicate the deletion.

Oversize materials (e.g., maps, drawings, charts) are reproduced by sectioning the original, beginning at the upper left-hand corner and continuing from left to right in equal sections with small overlaps.

Photographs included in the original manuscript have been reproduced xerographically in this copy. Higher quality 6" x 9" black and white photographic prints are available for any photographs or illustrations appearing in this copy for an additional charge. Contact UMI directly to order.

ProQuest Information and Learning
300 North Zeeb Road, Ann Arbor, MI 48106-1346 USA
800-521-0600

UMI®

# SINGLE BUBBLE VELOCITY PROFILE: EXPERIMENTS AND NUMERICAL SIMULATION

**Yongqin Zhang**

Department of Mining and Metallurgical Engineering
McGill University
Montreal, Canada
January, 2000

A thesis submitted to the faculty of Graduate Studies and Research in partial fulfillment of the requirements for the degree of Doctor of Philosophy

National Library
of Canada

Acquisitions and
Bibliographic Services

395 Wellington Street
Ottawa ON K1A 0N4
Canada

Bibliothèque nationale
du Canada

Acquisitions et
services bibliographiques

395, rue Wellington
Ottawa ON K1A 0N4
Canada

Your file Votre référence

Our file Notre référence

0-612-64706-4

Canada

*To my parents, my husband and my son*

# ABSTRACT

A new technique to study the dynamic adsorption of a surfactant on a rising bubble is established, which combines the single bubble velocity profile and numerical solution of the governing equations. Through investigation of the single bubble velocity profiles in water and surfactant solutions, a physical model describing the surface retardation of the bubble and surfactant mass transfer is proposed. A pseudo-steady state approach is employed to solve the mass transfer and fluid flow interactively. Various models are tested against the velocity profile of a 0.8 mm bubble in Triton X-100 solutions as a function of concentration and temperature. The combination of stagnant cap model and boundary layer mass transfer gave good agreement with experiment at 6 °C and 25 °C. Failure of the model to converge at 45 °C is discussed. Terminal velocity in water and surfactant solutions was defined from the profiles and tested against the available models. A new empirical correlation is proposed to estimate terminal velocity in pure water. Surfactant concentration on the bubble surface was estimated from the numerical solution and showed a bubble size and temperature dependence. The application of single bubble velocity profiles to systems of practical interest is considered.

# RESUMÉ

La nouvelle téchnique pour étudier la dynamique d'adsorption des agents de surface sur une bulle qui se lève est établi. Cette technique combine le profil de la vélocité de la bulle simple et la solution numérique des équations qui les gouvernent. Pendant la recherche des profiles de la vélocité de la bulle simple dans l'eau et la solution surfactant un modèle physique que décrit le ralentissement de la bulle et le transfer de la masse des agents de surface est proposé. Un méthode d'état pseudo-soutenu est employé pour résoudre l'interaction du transfer de la masse et l'écoulement du fluide. Beaucoup des modèles ont été utilisés contre les profiles de la vélocité d'une bulle de 0.8 mm à solution de Triton X-100 comme une fonction de la concentration et la température. La combination du modèle "stagnant cap" est tranferée de la masse à la couche frontière a donnée une bonne conductance de l'expérimentation entre 6° et 25°C. L'échec du modèle à 45°C est discuté. La vélocité finale dans l'eau et solution des agents de surface a été defini du profile et contrôlé contre les modèles disponibles. Une corrélation empirique est proposé pour estimer la vélocité finale dans l'eau pure. La concentration des agents de surface sur la surface de la bulle a été estimé de la solution numérique et montré comme a taille de la bulle et de la température. L'application des profiles de la vélocité de la bulle simple à systèmes d'intérêts pratiques sont considerés.

# ACKNOWLEDGEMENTS

I wish to express my grateful thanks to:

Porf. J. A. Finch, my supervisor, for his guidance, enthusiasm, keen insight, and constant encouragement throughout this work.

Prof. J. McLaughlin, Chemical Eng. Clarkson University, for his generosity in supplying the original computation program and some fruitful discussions.

Dr. C. O. Gomez, for his help in the experimental work and useful discussions.

Dr. R. Rao, for his resourceful suggestions in flotation chemistry.

Dr. C. Sui, for her friendship and enthusiasm.

I want to thank Prof. M. Weber in Chemical Eng. McGill, Prof. M. Hasan, Prof. A. Laplante and all members of mineral processing group for the valuable discussions during the course of this project.

# TABLE OF CONTENTS

# NOMENCLATURE

| | |
|---|---|
| $a'$ | Constant in Frumkin's isotherm |
| $A$ | Solute |
| $A$ | Project area of the bubble, $m^2$ |
| $b$ | Characteristic intermolecular spacing |
| $c$ | Concentration of surfactant in solution, $mol/m^3$ |
| $c_s$ | Concentration of surfactant in solution at the bubble surface, $mol/m^3$ |
| $c_\infty$ | Concentration of surfactant in the bulk solution, $mol/m^3$ |
| $c_e$ | Concentration of surfactant in solution at the bubble surface in equilibrium with surfactant on the bubble surface, $mol/m^3$ |
| $\Delta c$ | Concentration difference of surfactant in solution, $mol/m^3$ |
| $C_D$ | Drag coefficient |
| $d$ | Diameter of rigid sphere, m |
| $d_e$ | Equivalent diameter of the bubble or fluid sphere, m |
| $D$ | Diffusion coefficient in water, $m^2/s$ |
| $D_0$ | Diffusion coefficient in water at absolute temperature zero, $m^2/s$ |
| $D_s$ | Diffusion coefficient on bubble surface, $m^2/s$ |
| $E_a$ | Activation energy of molecular diffusion, J/mol |
| $Eo$ | Eotvos number, $Eo = \frac{g\Delta\rho d_e^2}{\gamma}$ |
| $f$ | $h_\eta/h_\xi$ |
| $F$ | Force, N |
| $F_B$ | Buoyant force, N |
| $F_D$ | Drag force, N |
| $g$ | Acceleration constant, $m/s^2$ |
| $g$, $h$ | Functions in Sawi's correlation |
| $G(\chi)$, $H(\chi)$ | Functions in Moore's theory |

| | |
|---|---|
| $h_\xi$, $h_\eta$, $h_\phi$ | Metric functions |
| $J_{ad}$ | Adsorption flux to the interface, mol/(m$^2$·s) |
| $J_{des}$ | Desorption flux from the interface, mol/(m$^2$·s) |
| $J_z$ | Flux of surfactant in z direction, mol/(m$^2$·s) |
| k | Mass transfer coefficient, m/s. |
| $k_B$ | Boltzmann's constant |
| m | Mass of the bubble, kg |
| Ma | Marangoni number, $Ma = \frac{RT\Gamma_\infty}{\mu U}$ |
| $M_B$ | Molar weight of the solvent |
| Mo | Morton number, $Mo = \frac{g\Delta\rho\mu^4}{\rho^2\gamma^3}$ |
| $N_\eta$, $N_\xi$ | Grid numbers in $\eta$ and $\xi$ directions |
| p | Static pressure, N/m$^2$ |
| Pe | Peclet number, $Pe = \frac{d_e U}{D}$ |
| $r_0$ | Solute molecular radius |
| $r_c$ | Radium of the capillary, m |
| $r_e$ | Equivalent radium of the bubble, m |
| $r_m$ | Average surfactant transfer rate, mol/s |
| $r_{m\theta}$ | Local surfactant transfer flux, mol/(m$^2$·s) |
| R | Gas constant, 8.314 N·m/(mol·K) |
| Re | Reynolds number, $\mathrm{Re} = \frac{U\rho d_e}{\mu}$ |
| S | Area, m$^2$ |
| $S_b$ | Area of the bare surface, m$^2$ |
| Sc | Schmidt number, $Sc = \frac{\mu}{\rho D}$ |

| | |
|---|---|
| $S_{stc}$ | Area of the stagnant cap, $m^2$ |
| $t$ | Time, s |
| $\Delta t$ | Pseudo-time step in the numerical simulation |
| $T$ | Absolute temperature, K |
| $u_\eta$ | Dimentionless normal fluid velocity |
| $u_\xi$ | Dimentionless tangential fluid velocity |
| $U$ | Bubble velocity in vertical direction, m/s |
| $U_t$ | Bubble terminal velocity in vertical direction, m/s |
| $U_{max}$ | Bubble maximum velocity in vertical direction, m/s |
| $Us$ | Liquid velocity along the surface, m/s |
| $V_A^0$ | Molar volume of pure A at its normal boiling point ($cm^3$/mol) in Wilke-Chang equation |
| We | Weber number, $We = \frac{\rho d_e U^2}{\gamma}$ |
| $z$ | Mass flux direction |
| $x, \sigma, \phi$ | Cylindrical coordinates |
| $\alpha$ | Desorption rate constant, 1/s |
| $\beta$ | Adsorption rate constant, $m^3/(s \cdot mol)$ |
| $\beta_\eta$ | Relaxation parameter for the vorticity boundary condition |
| $\beta_\omega$ | Relaxation parameter of normal stress balance |
| $\gamma$ | Surface tension of surfactant solution, N/m |
| $\gamma_0$ | Surface tension of water, N/m |
| $\Gamma$ | Surfactant concentration on bubble surface, $mol/m^2$ |
| $\Gamma_e$ | Equilibrium surfactant concentration at air water interface, $mol/m^2$ |
| $\Gamma_\infty$ | Maximum surfactant concentration at air water interface, $mol/m^2$ |
| $\theta$ | Angular coordinate of the spherical coordinate, radian |
| $\theta$ | Contact angle between capillary and water, radian |
| $\kappa_\eta, \kappa_\phi$ | Normal curvatures of the interface in the $\eta$ and $\phi$ directions |

| | |
|---|---|
| $\mu$ | Viscosity of liquid, N·s/m$^2$ |
| $\mu_B$ | Viscosity of solvent in Wilke and Chang's equation, cp |
| $\nu$ | Kinetic viscosity, m$^2$/s |
| $\nu_0$ | Frequency of molecular vibration |
| $\xi$, $\eta$, $\phi$ | Boundary fitted orthogonal coordinates |
| $\rho$ | Liquid density, kg/m$^3$ |
| $\Delta\rho$ | Density difference between bubble and solution, kg/m$^3$ |
| $\tau_{\xi\eta}$ | Dimensionless tangential stress on the bubble |
| $\tau_{\xi\eta}$ | Dimensionless normal stress on the bubble |
| $\nabla_s$ | Vector operator along bubble surface |
| $\chi$ | Axis ratio of the bubble |
| $\psi$ | Dimentionless streamfunction of the flow around a bubble |
| $\omega$ | Dimentionless vorticity component in angular direction |
| $\phi$ | Association factor for the solvent in Wilke-Chang's equation. |

Superscripts

| | |
|---|---|
| ' | Dimensionless parameters |
| n | n th time-step |

# LIST OF FIGURES

# LIST OF TABLES

# CHAPTER 1

# INTRODUCTION

## 1.1 Adsorptive bubble separation

Processes in which gas bubbles rise through a liquid or slurry are common to several industries. The first large-scale use was in mineral flotation (Richards, 1909). Now, "adsorptive bubble" processes are found in extractive metallurgy, chemical engineering, agriculture, environmental engineering and biotechnology (Lemlich, 1972; Clarke and Wilson, 1983; Thind and Wallace, 1984; Tharapiwattananon et al., 1996). Adsorptive bubble separations are used to extract minerals, metal ions and complexes, proteins, surfactants and organics.

Adsorptive bubble separation is based on differences in hydrophobicity of the components in aqueous systems. Particles or molecules can be selectively adsorbed onto bubble surfaces and be removed from solution. The process using gas bubbles and small amounts of chemical reagents offers a variety of attractive aspects such as low energy requirements, high removal efficiency, reasonable capital and operating costs with comparatively low level of maintenance and operational requirements (Rubin, 1981; Clarke and Wilson, 1983).

With the expansion of applications has come the question of equipment (reactor) design and scale-up. Such investigations on one type of reactor, the bubble column, started in the early 1960's. In non-mineral applications experimental studies carried out to investigate the effects of column configuration on the separation efficiency extend from the work of Kown (1971) to Keyser et al. (1996). One common observation made was that an increase of column height to increase retention time of the bubble did not improve the separation after a certain value had been reached.

Some researchers also tried to develop design models based on theoretical analysis of the adsorption and mass transfer processes. Chen (1994) modelled surfactant removal in foam fractionation by analysing the velocity of bubbles and the mass transfer processes from the bulk to the surface. By approximation of the model for Stokes flow, he derived a simplified equation relating surfactant removal rate to the terminal velocity of the bubble and the diffusion coefficient of the surfactant in water. Smith et al. (1996) assumed that the convective mass transport was dominant and developed models for a solvent sublation column by using an axial dispersion model (ADM) with a series of well-mixed stages (CSTR). They found that for strongly surface active material the removal efficiency was independent of the diameter of the column, which means that back mixing does not affect the adsorption.

Common to the fundamental approaches is the significance of bubble rise velocity and the effect of surfactant on the bubble surface properties and mass transfer.

### 1.2 Single bubble velocity

There have been numerous studies on the motion of single bubbles. Clift et al. (1978) reviewed the research prior to 1978. The most recent experimental studies on bubble velocity include Zhou et al. (1992), Jordan et al. (1994) and Fdhila and Duineveld (1996). However, because of restrictions imposed by the experimental set-up and deficiencies in understanding the nature of bubble velocity especially in surfactant solutions, there are problems with the previous work. For example, most studies report the terminal velocity as an average velocity of a bubble over a given distance, e.g., the height of a column of liquid. Others use the velocity at a fixed distance above the point of bubble release. Both measures overlook a possible time-dependence of the velocity which has led, for instance, to confusion over interpreting the role of surfactant concentration. It is important to clarify what velocity is being determined experimentally. Sam (1995) was the first to us an adjustable speed moving video camera system to measure the velocity of a rising bubble as a function of time or height and defined this as the "velocity profile". It was recognized recently by Dewsbury et al. (1999) that the movable video camera unit is "the most effective method" for the study of "drag coefficient, trajectory of rise and terminal velocity as a function of the shape and the volume of gas bubbles and solid particles and the rheological properties of the non-Newtonian (pseudoplastic) liquid". Using the movable video camera system and the velocity profile has opened a new approach in the fundamental study of the surfactant adsorptive process.

Adsorbed surfactants retard the motion of a mobile surface (gas bubble or liquid droplet) resulting in increased drag (Frumkin and Levich, 1947). Two principal models have been used to explain surface retardation, uniform retardation and stagnant cap models, depending on the relative rate of bulk diffusion and surface convection to the kinetics of adsorption and desorption. In both models, the velocity of a free rising single bubble in a surfactant solution is directly determined by the accumulation of surfactant molecules on the bubble surface.

Theoretically, the velocity of a single bubble rising in surfactant solution can be solved by a combination of the Navier-Stokes equation, the mass transfer equation and the Marangoni effect. These govern the fluid flow around the bubble, the amount of surfactant on the bubble, and the extent of surface retardation and distribution of surfactant on the surface, respectively.

The simultaneous solution of these equations at high Reynolds number is difficult and an analytical solution is not possible. Ryskin and Leal (1983, 1984a, 1984b) developed a finite-difference technique for simulating axisymmetric bubble motion and used it to compute the flow around bubbles for a large range of Reynolds numbers and Weber numbers. McLaughlin (1996) further refined the method to include the effect of a surfactant cap, which makes the modeling of single bubble motion in surfactant solution tractable.

### 1.3 The single bubble velocity profile

Sam et al. (1996) characterised the single bubble velocity profile by three stages (Fig. 1.1): first, a rapid increase to a maximum value; second, a decrease; and third, a constant velocity stage.

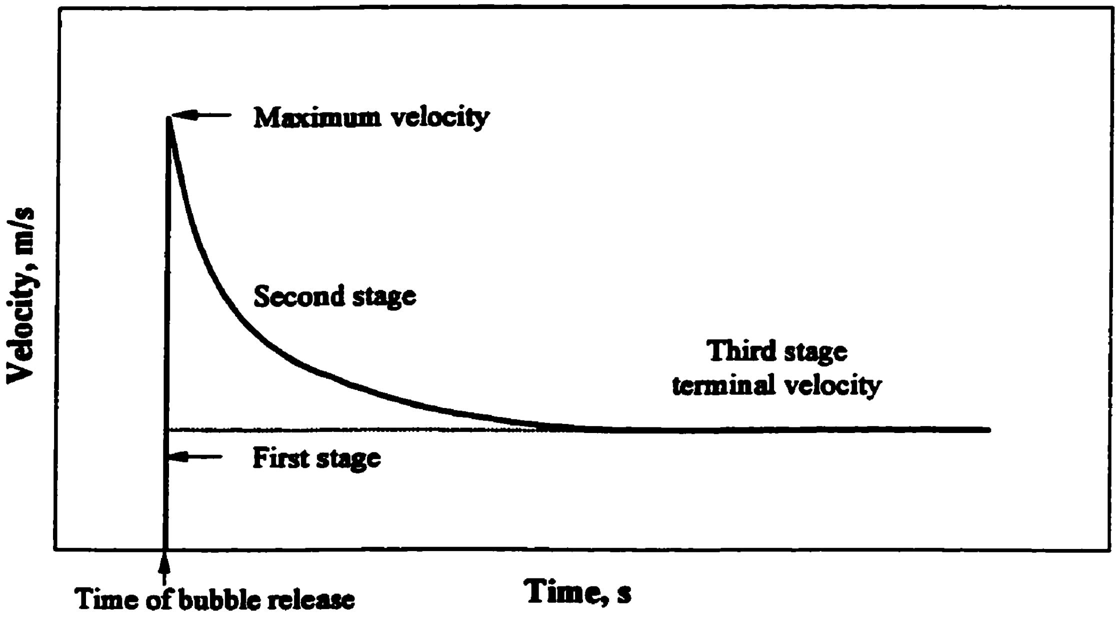

Fig. 1.1 Single bubble velocity profile (after Sam, 1995)

Different stages in the profile correspond to a different amount of adsorbed surfactant. Initially the bubble surface is free of surfactant and the bubble tries to reach the maximum possible velocity (equivalent to the terminal velocity in a completely surfactant-free system). As surfactant molecules accumulate, the bubble will gradually decelerate. When adsorption reaches equilibrium, the velocity of the bubble will become constant. The latter is a measure of the terminal velocity in a surfactant solution.

From an understanding of the mechanism of bubble motion, the following should be possible from analysis of the velocity profile:

- Estimation of the flow pattern around the bubble;

- Discrimination among different retardation models from the shape of the profile and the value of terminal velocity;
- Determination of adsorption kinetic parameters;
- Determination of mass transfer coefficient of a surfactant.

## 1.4 Objectives of the study

Knowledge of the fundamentals, including the velocity of free rising single bubbles in liquid media, is of great importance to understanding the characteristics of adsorptive bubble separation processes and in the design of reactors. With reactor design as the long term objective, the objectives of this thesis are:

- Measure velocity profile and establish reproducibility;
- Model the profile;
- Discriminate among models of terminal velocity;
- Establish mass transfer control vs. adsorption kinetics control;
- Investigate temperature effect on velocity profile;
- Explore the use of single bubble velocity in estimating surfactant mass transfer coefficients.

## 1.5 Structure of the thesis

The background and literature review of single bubble motion, mass transfer from bulk solution to bubble, the Marangoni effect and the role of surfactants on the velocity of bubbles, and computational methods for fluid dynamics are covered in chapter 2.

Chapter 3 establishes the physical and mathematical models related to the modeling of velocity profiles. The selection of suitable chemicals and the experimental procedure to study the dynamic adsorption of surfactant are established in chapter 4.

Chapter 5 discusses the terminal velocity of bubbles in water and surfactant solutions. Models to predict terminal velocity are discriminated. In chapter 6 the numerical simulation is validated using the maximum and terminal velocities in the profile. The effect of surfactant type and the simulated surface coverage are discussed. Chapter 7 investigates the mass transfer mechanism of Triton X-100 from bulk solution to a bubble surface by simulating the experimental single bubble velocity. The mass transfer models and terminal velocity are further investigated as a function of temperature in chapter 8.

Chapter 9 contains final conclusions, the claims to original research and suggestions for further research.

# CHAPTER 2

# BACKGROUND AND LITERATURE REVIEW

### 2.1 Single bubble motion

The rise of gas bubbles has been the subject of casual observation for centuries and the subject of systematic study since about 1900.

Bubble motion is governed by the laws of conservation of mass, momentum and energy. In an isothermal system, the conservation of energy equation can be ignored and the combination of mass and momentum conservation is the Navier-Stokes equation. For incompressible pure liquids the Navier-Stokes equation is expressed as:

$$\rho \frac{DU}{Dt} = -\nabla p + \mu \nabla^2 U + \rho g \qquad (2\text{-}1)$$

If only linear momentum conservation is considered, the forces acting on a bubble are the buoyant force and the drag force parallel to and opposing the direction of motion. According to Newton's second law:

$$\Sigma F = F_B - F_D = m \frac{dU}{dt} \qquad (2\text{-}2)$$

The drag force ($F_D$) is often conveniently represented with a suitable frontal or projected area of bubble, A:

$$F_D = C_D \times \frac{\rho U^2}{2} \times A \qquad (2\text{-}3)$$

where $\rho$ is the liquid density; $C_D$ is the proportional factor defined as the drag coefficient.

Experiments on rising bubbles and developments of models to predict the rise velocity have been reported widely in the literature. A classic collection of the works on bubble rise velocity is by Clift et al. (1978).

Many equations to predict the rise velocity have been proposed (Hadamard, 1911; Rybczynsky, 1911; Moore, 1959; Levich, 1962; Mehdelson, 1967, Clift et al., 1978; Karamanev, 1994). Very small bubbles behave as solid spheres and the velocity is given by Stokes' law (eq. 2-4) derived for solid sphere at small Reynolds number (Re<<1).

$$F_D = 3\pi\mu dU \tag{2-4}$$

The terminal velocity for a falling sphere would be:

$$U_t = \frac{gd^2\Delta\rho}{18\mu} \tag{2-5}$$

Levich (1962), using boundary layer theory, developed an equation for terminal velocity of spherical bubbles with a mobile surface in the range of 1<Re<1500, expressed as:

$$U_t = \frac{gd_e^2\Delta\rho}{36\mu} \tag{2-6}$$

Moore (1959) considered bubble deformation and derived an equation to estimate bubble velocity based on Levich's theory and extended the upper limit on Re. For spherical bubbles the terminal velocity in pure water was obtained as:

$$U_t = \frac{g d_e^2 \Delta\rho}{24\mu} \tag{2-7}$$

The terminal velocity for a deformed bubble is a function of the ratio of the bubble major and minor axes, $\chi$, which is correlated with the Weber number (We) for $\chi$ <2:

$$\chi = 1 + \frac{9}{64} We + O(We^2) \tag{2-8}$$

If We is small, the shape is known and then the terminal velocity of the bubble is given by:

$$U_t = \frac{g d_e^2 \Delta\rho}{36\mu G(\chi)\left(1 + \frac{H(\chi)}{\mathrm{Re}^{1/2}}\right)} \tag{2-9}$$

where G($\chi$) and H($\chi$) are the functions listed in Table 2.1 (Harper, 1972). In general, Moore's theory is valid for any Re>>1.

Sawi (1974) studied the steady rise of a bubble in an inviscid incompressible liquid and developed an expression relating We and the axis ratio $\chi$.

$$We = \frac{2(h\chi^2 - g)^2[g\chi(3\chi^2 - g^2) - (3\chi^2 + g^2)\tanh^{-1}(g/\chi)]}{g^4(3h\chi^2 - 2hg^2 3g)\chi^{\frac{7}{3}}} \tag{2-10}$$

where

$$\begin{aligned} g &= (\chi^2 - 1)^{\frac{1}{2}} \\ h &= \sec^{-1} \chi \end{aligned} \tag{2-11}$$

The relationship agrees with Moore's result up to $\chi$ = 2.

Table 2.1 G(χ) and H(χ) functions in Moore's theory

| χ | G(χ) | H(χ) | χ | G(χ) | H(χ) |
|---|---|---|---|---|---|
| 1.0 | 1.000 | -2.211 | 2.6 | 4.278 | 1.499 |
| 1.1 | 1.137 | -2.129 | 2.7 | 4.565 | 1.884 |
| 1.2 | 1.283 | -2.025 | 2.8 | 4.862 | 2.286 |
| 1.3 | 1.437 | -1.899 | 2.9 | 5.169 | 2.684 |
| 1.4 | 1.600 | -1.751 | 3.0 | 5.487 | 3.112 |
| 1.5 | 1.772 | -1.583 | 3.1 | 5.816 | 3.555 |
| 1.6 | 1.952 | -1.394 | 3.2 | 6.155 | 4.013 |
| 1.7 | 2.142 | -1.186 | 3.3 | 6.505 | 4.484 |
| 1.8 | 2.341 | -0.959 | 3.4 | 6.866 | 4.971 |
| 1.9 | 2.549 | -0.714 | 3.5 | 7.237 | 5.472 |
| 2.0 | 2.767 | -0.450 | 3.6 | 7.620 | 5.987 |
| 2.1 | 2.994 | -0.168 | 3.7 | 8.013 | 6.517 |
| 2.2 | 3.231 | 0.131 | 3.8 | 8.418 | 7.061 |
| 2.3 | 3.478 | 0.448 | 3.9 | 8.834 | 7.618 |
| 2.4 | 3.735 | 0.781 | 4.0 | 9.261 | 8.189 |
| 2.5 | 4.001 | 1.131 | | | |

Mendelson (1967) drew an analogy between wave and bubble motion based on the available experimental data. The terminal velocity was predicted from:

$$U_t = \sqrt{\frac{2\gamma}{d_e \rho} + \frac{g d_e}{2}} \tag{2-12}$$

This theory was defined for bubbles with an equivalent diameter $d_e \geq 1.4$mm or Re>450. Clift et al. (1978) empirically modified Mendelson's model (eq. 2-12) and predicted the terminal velocity to be:

$$U_t = \sqrt{\frac{2.14\gamma}{d_e\rho} + 0.505gd_e} \qquad (2\text{-}13)$$

For a bubble rising in contaminated water Karamanev and Nikolov (1992) found the drag coefficient of free rising particles is different from that of free falling particles for Re>130 and density of particle less than 300 kg/m$^3$. In this range the drag coefficient is constant, ca. 0.95, which is larger than the drag coefficient of a free falling sphere. Only when Re<130 and the density of the particle is larger than 300 kg/m$^3$, can the free rising particle be described by the laws of free settling. Later Karamanev (1994) collected the available experimental data on bubble rise velocity. He recalculated the drag coefficient by taking account of non-sphericity. The results showed the drag coefficient of free rising bubble is in good agreement with the results for free rising solid sphere of density <300 kg/ m$^3$, which confirmed the assumption that there is no internal recirculation in a bubble rising in a contaminated aqueous solution.

There are various empirical correlations of the drag coefficient for a falling sphere which can be substituted into the general equation for terminal velocity. A common one is that due to Schiller and Naumann (1933), for example as employed by Finch and Dobby (1990).

More recently, Duineveld (1995) measured the velocity of rising bubbles over the range of (equivalent) radius 0.33-1.00 mm in "hyper clean" water at a distance of 10 to 12 cm from the point of bubble generation. He concluded that for small bubbles (radius < 0.6 mm) there is good agreement with Moore's theory. For larger bubbles (radius > 0.6 mm) the theory underestimated the rise velocity. He attributed the difference to the overestimation of bubble deformation in the theory.

Most of the studies mentioned above apart from Duineveld report an average velocity of the bubble over a given distance, e.g., the height of a column of liquid. Some authors have reported a difference in bubble velocity in columns of different height.

Aybers and Tapuccu (1969) measured average rise velocities as a function of the distance travelled. Their results showed a maximum velocity after which a decrease as the distance travelled increased. This decrease was relatively large for small bubbles and small for large bubbles, and suggested an effect due to the presence of surface-active impurities. Wesselingh (1987) concluded in his theoretical work that the velocity of a bubble in surfactant solution is a function of surfactant saturation on the surface. Jordan et al. (1994) found that the addition of surfactant caused a concentration-dependent and height-dependent decrease in bubble velocity. The explanation offered was that bubbles became covered with surfactant as they rose until saturation was reached. With Serum and Pluronic 68 surfactants they found that the progressive covering of the bubble surface was proportional to the height the bubble had risen. The distance to reach saturation reasonably decreased with increased concentration of surfactant. Fdhila and Duineveld (1996) observed that the rise velocity in surfactant solutions at 3.5 cm from the generation point decreased with increasing concentration until a minimum velocity was reached. A further increase in concentration did not affect this velocity.

Sam et al. (1996) studied single bubble velocity in frother[1] solutions at 30 °C. They found the velocity had three stages. The velocity first increased to a maximum, then decreased until a constant or terminal velocity was reached. The time over which this occurred depended on frother type and concentration. They termed this a "velocity profile" (an example was given in Fig 1.1). In water, the maximum velocity on the profile was close to the predicted terminal velocity in pure water. In surfactant solutions the final, constant velocity (i.e., stage 3) was largely independent of surfactant type and concentration.

From the above several points relevant to the present study emerge. It is clear that the behaviour of free rising bubbles is different from that of free falling particles. The velocity of a bubble rising in an aqueous liquid depends on the nature of the bubble surface. The bubble surface states are different in pure water and surfactant containing water. If the bubble surface is clean, the surface moves with the fluid outside. This results in an increased rise velocity of the bubble, higher than that of a rigid sphere. In surfactant containing water, surfactant molecules adsorb on the bubble surface retarding surface

---

[1] Frother is the term used in mineral flotation to designate the reagent causing a froth to form.

motion and air circulation inside the bubble. As a consequence, drag increases. The maximum drag can be as large as that on a light rigid sphere.

## 2.2 Models of surfactant adsorption kinetics at air water interface

A surfactant (a contraction of surface active agent) is a compound that in very small quantities significantly changes a surface property but often no other property (e.g., viscosity and density in the case of a liquid). A surfactant, therefore, exhibits surface activity. Surface activity is most widely encountered in the lowering of surface tension of water (Tsujii, 1997). Surfactants are surface active because of the mixed hydrophilic/hydrophobic nature of their structure: a polar group with a long hydrocarbon chain. By residing at the interface with the polar part in the water and the hydrocarbon chain in air both the hydrophilic and hydrophobic properties are satisfied simultaneously. Hence surfactant accumulates at the interface. Dukhin et al. (1995) reviewed the developments in the theory, experiment methods, and applications of surfactant adsorption at a liquid interface. One of the models of surfactant distribution between interface and bulk solution is schematically shown in Fig. 2.1.

In this representation, the air water interface is divided into three regions: the interface, where the surfactant molecules accumulate; the sublayer, which is adjacent to the interface and in equilibrium with the interface at all times; and the bulk solution, which has a uniform concentration of surfactant. The transport of surfactant from bulk solution to the interface proceeds with two consecutive steps after the boundary layer is formed:

surfactant migrates from the bulk to the sublayer then adsorbs (and orientates) at the interface.

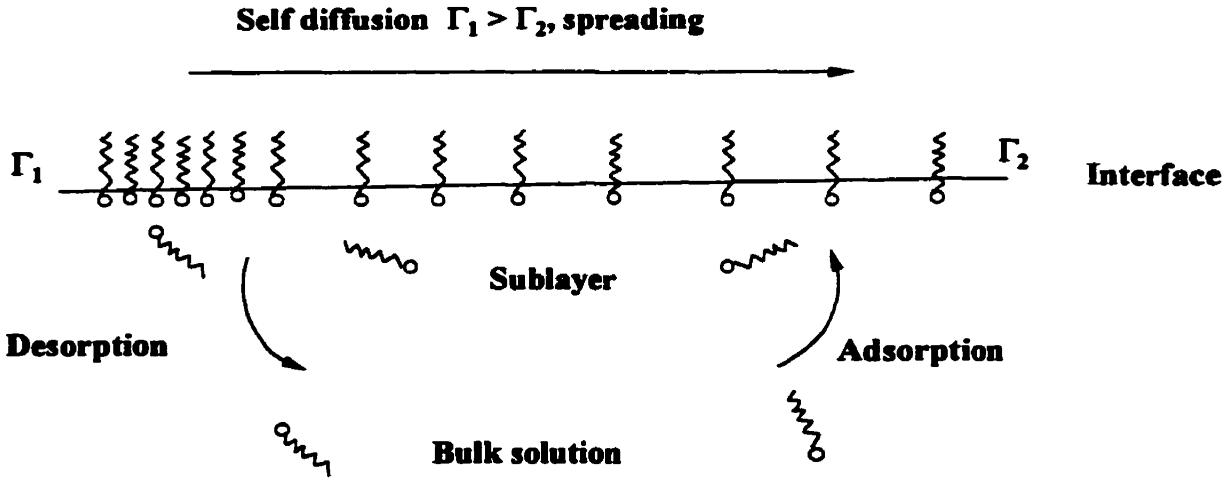

Fig. 2.1 Accumulation of surfactant at air water interface (after Dukhin et al., 1995)

The exchange rate of surfactant between the bulk solution and interface depends on the surfactant concentration and surface activity. For highly surface active (or "strong") surfactant at low concentration, diffusional transport is the exchange rate control process; for weak surfactants and solutions of comparatively high concentration, non-diffusional adsorption kinetics is observed (Bleys and Joos, 1985; Feinerman, 1985).

The foundation of surfactant adsorption kinetics is the Langmuir model. The adsorption rate for a kinetic controlled mechanism is given by the balance of surfactant adsorption and desorption fluxes to and from the interface:

$$\frac{d\Gamma}{dt} = J_{ad} - J_{des} \tag{2-14}$$

The Langmuir model is:

$$\frac{d\Gamma}{dt} = \beta c(0,t)(\Gamma_\infty - \Gamma) - \alpha\Gamma \tag{2-15}$$

Fainerman et al. (1998) suggested that for most surfactants non-diffusional adsorption kinetics can be expected if the ratio of desorption rate constant to adsorption rate constant ($a=\alpha/\beta$, called the Langmuir Von Szyskowski constant, which is a measure of surface activity) is larger than ca. 1 mol·m$^{-3}$.

When equilibrium is reached the Gibbs adsorption isotherm relates the surfactant concentration on the surface with the surface tension:

$$\Gamma = -\frac{1}{RT}\frac{d\gamma}{d\ln c} \tag{2-16}$$

Combining the Langmuir kinetic model with the Gibbs adsorption isotherm results in the Langmuir adsorption isotherm:

$$\gamma_0 - \gamma = -RT\Gamma_\infty \ln(1 - \frac{\Gamma}{\Gamma_\infty}) \qquad (2\text{-}17)$$

where $\gamma_0$ is the surface tension for water. If the surface concentration is very low, $\Gamma/\Gamma_\infty$ is close to zero and Langmuir's isotherm simplifies to:

$$\gamma_0 - \gamma = RT\Gamma \qquad (2\text{-}18)$$

that is, a linear dependence of surface tension on surface concentration. Frumkin (1925) introduced additional interaction forces between adsorbed molecules into the Langmuir adsorption isotherm.

$$\gamma = \gamma_0 + RT\Gamma_\infty \ln\left[\left(1 - \frac{\Gamma}{\Gamma_\infty}\right) + a'\left(\frac{\Gamma}{\Gamma_\infty}\right)^2\right] \qquad (2\text{-}19)$$

where a' represents this intermolecular force.

## 2.3 The Marangoni effect and the role of surfactant on the velocity of bubbles

Velocity changes during bubble rise in a surfactant solution are due to adsorption of surfactant at the air water interface. After a bubble is freshly created and during its motion, surfactant adsorbs at the surface. The motion of the bubble pushes the adsorbed surfactant molecules from the front of bubble to the rear, inducing a layer of non-uniformly distributed surfactant. There are two explanations for the reduction in the rise velocity associated with the presence of surfactant on the bubble surface. One is that when the surfactant molecules are transported to the rear of the bubble, the compacted surfactant layer becomes immobile and the associated no-slip boundary condition increases the drag coefficient. The second explanation arises from the fact that the concentration of surfactant at the rear is much larger than that at the front. This non-uniformity induces a surface tension gradient toward the front of the bubble which generates a tangential shear stress that retards the surface velocity and increases the drag coefficient. This phenomenon is called the Marangoni effect (Frumkin and Levich, 1947, Levich 1962). Experimentally, Warszynski et al. (1996) demonstrated a non-uniform distribution of surfactant over the surface which changed with the life of the bubble i.e., after rising different distances.

The distribution of surfactant over the bubble surface depends on the adsorption kinetics and transport properties of the surfactant. The nature of the adsorbed layer at the interface can be characterised by two extremes: soluble and non-soluble. If the surfactant flux from the bulk is extremely slow compared to surface convection, the adsorbed surfactant behaves as an insoluble monolayer. At this extreme the interface can be divided into two regions, the leading end, which is swept free of surfactant, and the trailing end, which is stagnated by a surfactant concentration gradient (Cuenot et al., 1997). The size of this stagnant region is specified by a cap angle measured from the trailing pole to the edge of the stagnated region. At the opposite extreme, when the surfactant flux from the bulk is only slightly less than the surface convective flux, a smoothly changing concentration gradient develops over the entire surface. The bubble surface can then be classified into four cases according to the surface velocity: the unretarded surface; the uniformly retarded surface; the partly stagnated surface (with a stagnant cap); and the completely stagnant interface. The distribution of surfactant and surface velocity on the bubble for the two extremes of the adsorption layer are illustrated in Fig. 2.2.

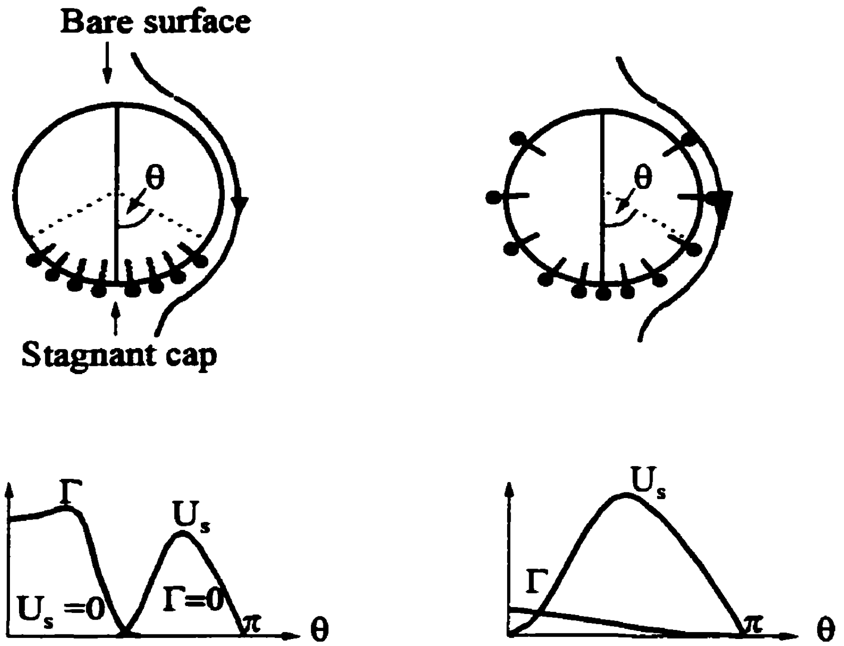

a) Stagnant cap model

b) Smoothly changing concentration gradient model

Fig. 2.2 Surfactant and velocity distribution on bubble surface for the two extremes

Andrews et al. (1988) proposed a two-phase adsorption isotherm model and divided the bubble into two regions, the surfactant desorption and surfactant adsorption regions. In the former the interface is saturated, $\Gamma = \Gamma_\infty$, and $d\Gamma/d\theta = 0$, and in the latter surfactant coverage is less than $\Gamma_\infty$.

The uniformly retarded surface model has been studied by many researchers (Levich, 1962; Schechter and Fairley, 1963; Newman, 1967; Harper, 1972; He et al., 1991a). However, from the analysis above and the experimental evidence (Savic, 1953; Garner and Skelland, 1955; Elzinga and Banchero, 1961; Griffith, 1962; Horton el al., 1965; Huang and Kintner, 1969; Beitel and Heidegger, 1971; Yamamoto and Ishii, 1987) it is concluded that the stagnant cap model is appropriate in most cases.

The majority of the theoretical treatments of the Marangoni effect have concentrated on small bubbles or drops considering a relatively small Reynolds number (often in Stokes regime, Re<1) and a relatively rigid shape (Frumkin and Levich, 1947; Levich 1962; Davis and Acrivos, 1966; Saville, 1973; Harper, 1973, 1983; Holbrook and Levan, 1983a, b; Sadhal and Johnson, 1983; Dukhin et al., 1987; He el al., 1991b; Dukhin et al., 1995). Analytical solutions have been obtained. However, at small and even intermediate Re (Re < O (10)) the bubble surface can initially behave as immobile and the formation of a stagnant cap is almost impossible (Dukhin et al., 1995).

For high Re, numerical methods were developed to solve the governing equations. Usually, the models were simplified by either ignoring the mass transfer from the bulk solution (Fdhila and Duineveld, 1996; McLaughlin, 1996) or fixing the fluid field (Cuenot et al., 1997; Takagi and Yamamoto, 1999). Andrews et al. (1988) used boundary layer theory to solve the fluid flow and mass transfer with the proposed two-phase adsorption isotherm model.

Usually, linear relations between the surface tension, the surface coverage and the bulk concentration were used (Levich, 1962; Schechter and Fairley 1963; Harper, 1974, 1988; He et al., 1991a, b). Recently, Chen and Stebe (1996) employed a non-linear adsorption model for monolayer saturation and non-ideal surfactant interactions to calculate the terminal velocity of a droplet settling through a surfactant solution. A numerical solution to the problem was obtained for a "very strong" Marangoni effect (i.e., a stagnant cap existed at the rear of the bubble).

Fdhila and Duineveld (1996) studied the effect of surfactant on the rise of a spherical bubble at high Reynolds number (from 50 to 200) and Peclet number. They assumed the no-slip condition held at the rear part of the bubble (i.e., stagnant cap model). A finite-difference numerical method was used to solve the full Navier-Stokes equations around the bubble. The concentration on the bubble surface is obtained for surfactants having a desorption rate much lower than the convective rate. In their model, the distribution of the tangential velocity, the vorticity, the pressure and the surfactant concentration on the bubble surface were all considered. They tested the model for bubble velocities obtained at 3.5 cm from the capillary as a function of bulk concentration of the surfactant. In their numerical solution, the deformation of the bubble was not considered. They related the cap angle with the surfactant concentration in bulk solution, although this clearly ignores the mass transfer process. The assumption of the cap angle and the concentration dependency of the bubble velocity is in contradiction to the observations of Sam et al., (1996) and Zhang and Finch (1996).

McLaughlin (1996) considered the deformation of the bubble. He modelled single bubble motion at different cap angles by solving the free boundary problem and stagnant cap model. The bubble Reynolds number ranged up to roughly 600. He assumed the bubble motion is still axisymmetric.

Cuenot et al. (1997) modelled the transient evolution of the flow around a spherical bubble (Re=100) in a weakly soluble surfactant solution. They assumed the velocity far from the bubble was constant while the transient process of surfactant adsorption occurs. The influence of surfactant characteristics was studied. They concluded that:

- The stagnant cap model is valid for weakly soluble surfactants;
- In steady state the local mass fluxes are non-zero;
- Adsorption is still present on the front part of the bubble while desorption affects most of the contaminated part;
- There is no simple relation between the cap angle and the bulk concentration because diffusion from the bulk plays a significant role.

As a criticism, the assumption of constant flow field outside the bubble is illogical. The flow field changes with time during the transient process.

Takagi and Yamamoto (1999) combined the approaches by McLaughlin (1996) and Cuenot et al. (1997) to investigate the motion of a contaminated bubble by allowing the bubble to deform in a system of boundary fitted coordinates. The adsorption of surfactant decreases the surface tension and causes the bubble to deform, thus increasing the drag. On the other hand, the increase in the drag reduces the deformation due to the flow field change. They concluded that the influence of bubble deformation and the Marangoni effect on drag are far stronger than the effect of increased drag on bubble deformation.

From the results of these recent studies a new approach to solve the bubble motion at high Re can be introduced. This includes the following considerations. First, the stagnant cap model is valid for bubbles in motion in most surfactant solutions. Second, the mass transfer of surfactant from bulk solution to bubble surface can not be ignored. And third, the transient evolution of the bubble velocity can be solved by a combination of mass transfer and momentum transfer. It should be added that the lack of experimental data is a handicap to the understanding of the physical model and the design of appropriate theoretical studies.

## 2.4 Mass transfer from bulk solution to a bubble

In a surfactant solution when the bubble is formed and released from the orifice, the surface is initially essentially free of surfactant. As the bubble rises transfer of surfactant molecules from the bulk solution to the bubble surface occurs. The Reynolds number of fluid flow outside the bubble is far greater than 1. According to Clift et al. (1978) the effect of viscosity can be taken into account in a thin layer adjacent to boundary in the flow. The thin layer is called the flow boundary layer. The concentration gradient of surfactant can also be regarded as restricted to a thin boundary layer. The mass transfer occurs in this concentration boundary layer.

In the concentration boundary layer two basic modes of mass transfer exist: molecular diffusion induced by the concentration gradient and advection induced by the bulk motion of fluid with different concentrations. The cumulative transport is termed convection.

Molecular diffusion can be defined as the transport of a particular species relative to an appropriate reference plane resulting from the random motion of molecules in a region of space in which a composition gradient exits (Rousseau, 1987). The molecular diffusivity (or diffusion coefficient) D is defined as the proportionality constant between the diffusive flux and the negative of the composition gradient (in z direction, dc/dz), which results from Fick's first law of diffusion:

$$J_z = -D\frac{dc}{dz} \tag{2-20}$$

The energy barrier to molecular diffusion is dependent on the mechanism of the diffusive process. The diffusivity in the condensed phase would be given by an expression of the form $v_0 b^2 \exp(-E_a/RT)$, where b is the characteristic intermolecular spacing, and $v_0$ is the frequency.

Diffusion coefficients in liquids are of the order of $10^{-9}$ m$^2$/s unless the solution is highly viscous or the solute has very high molecular weight (Rousseau, 1987). It is probably safe to say that most of the reported experimental diffusivities were computed based on Fick's second law (eq. 2-21) without consideration of whether or not the system was thermodynamically ideal:

$$\frac{\partial c}{\partial t} = D\frac{\partial^2 c}{\partial z^2} \qquad (2\text{-}21)$$

Hydrodynamic theories for prediction of liquid phase diffusion coefficients at infinite dilution are represented by the Stokes-Einstein equation (eq. 2-22) which views the diffusion process as the motion of a spherical solute molecule A through a continuum made up of solvent molecules B where the ratio of solute to solvent size exceeds five:

$$D = \frac{k_B T}{6\pi\mu r_0} \qquad (2\text{-}22)$$

where $k_B$ is Boltzmann's constant, and $r_0$ the solute radius.

Wilke and Chang (1955) correlated the experimental data available for estimating infinite dilution diffusion coefficients of different solutes in various solvents:

$$D = \frac{7.4 \times 10^{-12} (\phi M_B)^{1/2} T}{\mu_B \left(V_A^0\right)^{0.6}} \tag{2-23}$$

where $V_A^0$ is the molar volume of pure A at its normal boiling point (cm$^3$/mol); $M_B$ is the molar weight of the solvent; $\mu_B$ is the viscosity of solvent (cp); and $\phi$ is an association factor for the solvent.

In equation (2-23) the dependency of diffusion coefficient on temperature is represented by the temperature dependency of viscosity. The ratio D/T may be assumed constant over a modest temperature range. Over a wide temperature range or when viscosity data are unavailable, the diffusivity is conveniently correlated by an equation of the Arrhenius form:

$$D = D_0 \exp\left(\frac{-E_a}{RT}\right) \tag{2-24}$$

The activation energy $E_a$ for a diffusion process is typically a few kilocalories per mole.

The convective mass transfer flux from bulk solution to an interface (in z direction) is assumed to be proportional to the concentration difference, with the proportional factor k defined as the mass transfer coefficient:

$$J_z = k(c_\infty - c_s) \tag{2-25}$$

The diffusion coefficient and mass transfer coefficient are connected by mass transfer models.

Different physical models have been proposed for interfacial mass transfer. The simplest is the film theory. It assumes that a stagnant film exists near every interface. The concentration in the film changes with position linearly. This film, also called an "unstirred layer", is almost always hypothetical, for fluid motion commonly occurs right up to even a solid interface (Campbell and Hanratty, 1982). Nonetheless, such a film, suggested first by Nernst in1904, gives the simplest model of the interfacial region. Later models provided a better physical picture of mass transfer than the film theory. Higbie (1935) suggested a penetration model for diffusion into a falling film. It assumes the falling film is thick and, in the direction perpendicular to the fluid flow, diffusion is more important than advection, while in the direction parallel to the fluid flow, diffusion is less important than advection. Predictions of the penetration theory support the experimental observations. However, the physical model and assumptions are restrictive. Dankwerts (1951) proposed an alternative model, the surface-renewal theory. This theory divides the liquid into two regions: the "interfacial" and "bulk". Mass transfer in the interfacial region is described by the penetration theory. However, small volumes or elements of this interfacial region are constantly exchanging with elements of the bulk region.

Boundary layer theory offers a more complete description of mass transfer (Levich, 1962; Skelland, 1974; Schlichting, 1979). Boundary layer theory is based on parallels with earlier studies of fluid mechanics and heat transfer. The situation is shown in Fig. 2.3 for the case of a flat plate immersed in a smoothly flowing fluid. Boundary layer theory assumes that most of the velocity or concentration change occurs over a short distance from the plate. Usually the concentration boundary layer is much smaller than the flow boundary layer.

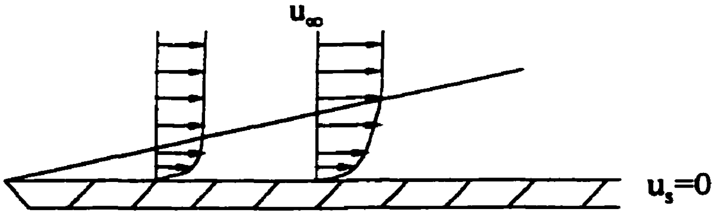

(a) Flow boundary layer

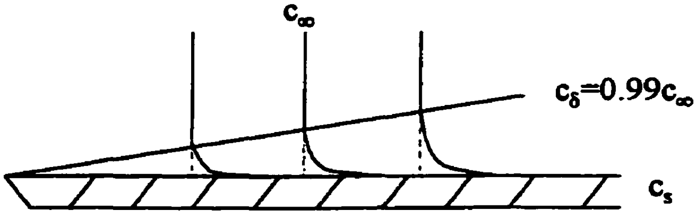

(b) Concentration boundary layer

Fig. 2.3 Boundary layer theory

The mass transfer from bulk solution to the bubble surface depends on bubble Reynolds number (Re) and the state of the bubble surface. Clift et al. (1978) reviewed the work on mass transfer for mobile bubbles and rigid spheres. At high Re, the thin concentration boundary layer approximation is valid and the mass transfer from bulk solution to a spherical surface for the case of fluid and rigid spheres has been solved numerically from boundary layer theory (LeClair and Hamielec, 1971; Oellrich et al., 1973). The mass transfer reaches a maximum at the front of a moving bubble and decreases along the bubble surface toward the rear. For a mobile bubble surface the average Sherwood number (Sh) for the boundary layer can be correlated by (Lochiel and Calderbank, 1964; Winnikow, 1967):

$$Sh = \frac{2}{\sqrt{\pi}}\left(1 - \frac{2.89}{\mathrm{Re}^{1/2}}\right)^{1/2} Pe^{1/2} \tag{2-26}$$

The result is within 7% of the numerical solution obtained by LeClair and Hamielec, and Oellrich et al.

For a rigid sphere freely rising in water with d>0.1 mm, the following correlation can be used (Calderbank and Lochiel, 1964).

$$k(Sc)^{2/3} = 0.45(\Delta\rho/\rho)^{0.3} g^{0.3} \nu^{0.4} d^{-0.1} \tag{2-27}$$

## 2.5. Computational method for fluid dynamics

Fluid flow and related phenomena can be described by partial differential (or integro-differential) equations (PDE), which can not be solved analytically except in special cases. To obtain an approximate solution numerically, a discretization method has to be used which approximates the differential equations by a system of algebraic equations. The resulting algebraic equations can then be solved on a computer. The approximations are applied to small domains in space and/or time so the numerical solution provides results at discrete locations in space and time. The accuracy of numerical solution is dependent on the quality of discretizations used. Discretization errors can be reduced by using more accurate interpolation or approximations or by applying the approximations to smaller regions although this usually increases the time and cost of obtaining the solution. Compromise is usually needed.

Compromises are also needed in solving the discretized equations. Direct solvers, which yield accurate solutions, are seldom used, because they are too costly. Iterative methods are more common but the errors due to stopping the iteration process too soon need to be taken into account.

Numerical solution of a fluid dynamics problem starts with the mathematical model obtained from the physical model. Conservation equations can be written in many forms; one has to choose the coordinate and basis vector systems. Depending on the target flow, Cartesian, cylindrical, spherical, curvilinear orthogonal or non-orthogonal coordinate systems, which may be fixed or moving, are selected. A suitable discretization method is chosen after the mathematical model is established.

The discrete locations at which the variables are to be calculated are defined by the numerical grid which is essentially a discrete representation of the geometric domain on which the problem is to be solved. It divides the solution domain into a finite number of subdomains.

After the numerical grid is selected, the approximation method in the discretization process has to be determined. In a finite difference method, approximations for the derivatives at the grid points have to be selected. In a finite volume method, one has to select the method of approximating surface and volume integrals. In a finite element method one has to choose the functions (elements) and weighting function.

Discretization yields a large system of non-linear algebraic equations. The method of solution depends on the problem. For unsteady flows, methods based on those used for initial value problems for ordinary differential equation (marching in time) are used. At each time step an elliptic problem has to be solved. Steady state flow problems are usually solved by pseudo-time marching or an equivalent iteration scheme. Since the equations are non-linear, an iteration scheme is used to solve them. These methods use successive linearization iteration techniques. The choice of solver depends on the grid type and the number of nodes involved in each algebraic equation. Finally, the criteria of convergence for the iterative method have to be set.

### Finite difference method

The finite difference (FD) method is the oldest method for numerical solution of PDE's, believed to have been introduced by Euler in the 18th century. It is also the easiest method to use for simple geometries.

The starting point is the conservation equation in differential form. The solution domain is covered by a grid. At each grid point, the differential equation is approximated by replacing the partial derivatives by approximations in terms of the nodal values of the functions. The result is one algebraic equation per grid node, in which the variable value at that and a certain number of neighbor nodes appear as unknowns.

In principle, the FD method can be applied to any grid type. However, in most applications, the grid lines serve as local coordinate lines.

Taylor series expansion or polynomial fitting is used to obtain approximations to the first and second derivatives of the variables with respect to the coordinates. When necessary, these methods are also used to obtain variable values at locations other than grid nodes (interpolation).

For simple geometries, the FD method is simple and effective. It is especially easy to obtain higher-order schemes on a regular grid; the disadvantage of FD methods is that conservation is not enforced unless special care is taken. Also, the restriction to simple geometries can be a significant disadvantage.

# CHAPTER 3

# THEORETICAL ANALYSIS

The velocity of a free rising bubble in a surfactant solution of an isothermal system is governed by the momentum balance, mass balance constraints and the Marangoni effect with the boundary conditions imposed by the dynamic adsorption layer model.

### 3.1 Bubble shape

The bubble shape changes in response to the fluid forces exerted on the bubble. If the surface tension force and viscous force exceed the dynamic inertia forces, the bubble will remain spherical. In contrast, if the inertia forces dominate, the bubble will deviate from spherical because of the asymmetrical nature of the inertia forces at the front and rear of the bubble. For small bubbles rising through a liquid with small Eotvos (Eo) and Re numbers, and a large Morton (Mo) number the shape can be regarded as spherical (Fig. 2.5, page 27 of Clift et al., 1978).

From the experimental data listed in Table 3.1, the shape of a 0.8 mm bubble (of interest here as shown later) at 6 and 25°C can be regarded as spherical but not at 45°C. Therefore, It is necessary to account for the shape change to solve for the bubble motion at this temperature. The boundary fitted curvilinear coordinate system was chosen for the task.

Table 3.1 Maximum Eo, Re and Mo for 0.8 mm bubble at different temperatures

| **Temperature, °C** | **Eo $\times 10^2$** | **Re** | **Mo $\times 10^{12}$** |
|---|---|---|---|
| 6 | 8.39 | 90.6 | 119 |
| 25 | 8.68 | 205 | 17.3 |
| 45 | 9.04 | 396 | 3.95 |

### 3.2 Boundary fitted coordinates

Ryskin and Leal (1983) proposed a technique of orthogonal mapping to construct boundary-fitted orthogonal curvilinear coordinate systems in two dimensions (2-D). Later, they (1984a, 1984b) used the technique and computed the fluid flow around a bubble for a large range of Reynolds number. McLaughlin (1996), incorporating the Marangoni effect, used the technique to solve bubble motion in surfactant solution.

The boundary-fitted orthogonal curvilinear coordinate is denoted as ($\xi$, $\eta$, $\phi$) where $\phi$ is the azimuthal angle measured about the axis of symmetry. The curvilinear coordinates can be connected with cylindrical coordinates ($\sigma$, $\phi$, x) through the Laplace equations:

$$\left.\begin{aligned}\frac{\partial}{\partial\xi}\left(f\frac{\partial x}{\partial\xi}\right)+\frac{\partial}{\partial\eta}\left(\frac{1}{f}\frac{\partial x}{\partial\eta}\right)=0\\ \frac{\partial}{\partial\xi}\left(f\frac{\partial\sigma}{\partial\xi}\right)+\frac{\partial}{\partial\eta}\left(\frac{1}{f}\frac{\partial\sigma}{\partial\eta}\right)=0\end{aligned}\right\} \tag{3-1}$$

where f is the distortion function which represents the ratio of scale factors $h_\eta/h_\xi$. The scale factors in the mapping are:

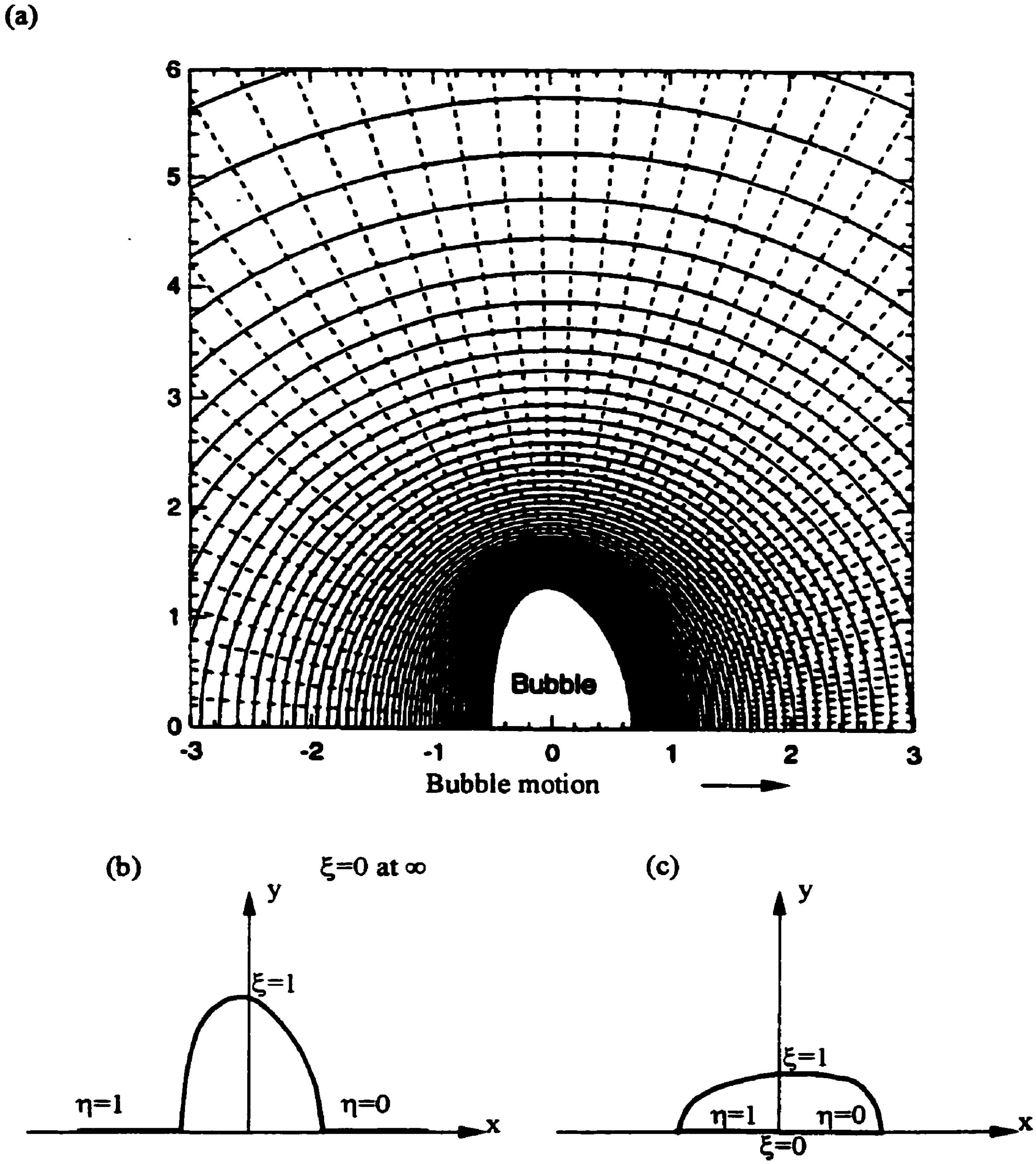

Fig. 3.1 Sketch of the coordinate system for the exterior of axisymmetric bubble: (a) the grid in Cartesian coordinate; (b) the boundary fitted orthogonal coordinate system; (c) the auxiliary mapping for the finite domain (after McLaughlin, 1996, and Ryskin and Leal, 1983).

$$\left.\begin{aligned} h_\xi &= \left\{\left(\frac{\partial x}{\partial \xi}\right)^2 + \left(\frac{\partial \sigma}{\partial \xi}\right)^2\right\}^{\frac{1}{2}} \\ h_\eta &= \left\{\left(\frac{\partial x}{\partial \eta}\right)^2 + \left(\frac{\partial \sigma}{\partial \eta}\right)^2\right\}^{\frac{1}{2}} \end{aligned}\right\} \qquad (3\text{-}2)$$

The infinite domain outside of the bubble in Fig. 3.1 (b) is then transformed into the finite domain inside the bubble (c) by conformal mapping. The solution domain becomes the unit square for any arbitrary fixed $\phi$:

$$0 \le \xi, \eta \le 1 \qquad (3\text{-}3)$$

### 3.3 Fluid Flow

Since bubbles in the size range of interest rise along rectilinear paths, the flow around a bubble may be assumed to be axisymmetric. This justifies the use of the streamfunction-vorticity formulation of the governing equations.

For axisymmetric flow the equation of motion and continuity can be conveniently expressed by vorticity transport and stream function equations:

$$\frac{\mathrm{Re}}{2}\left(\frac{\partial \omega}{\partial t}\right)_{\xi,\eta} + \frac{\mathrm{Re}}{2}\frac{1}{h_\eta h_\xi}\left(\frac{\partial \psi}{\partial \xi}\frac{\partial}{\partial \eta}\left(\frac{\omega}{\sigma}\right) - \frac{\partial \psi}{\partial \eta}\frac{\partial}{\partial \xi}\left(\frac{\omega}{\sigma}\right)\right) = L^2(\omega\sigma) \qquad (3\text{-}4)$$

and

$$L^2\psi + \omega = 0 \qquad (3\text{-}5)$$

where

$$L^2 = \frac{1}{h_\xi h_\eta}\left(\frac{\partial}{\partial \xi}\left(\frac{f}{\sigma}\frac{\partial}{\partial \xi}\right) - \frac{\partial}{\partial \eta}\left(\frac{1}{f\sigma}\frac{\partial}{\partial \eta}\right)\right) \tag{3-6}$$

The distortion function f for the rising bubble is chosen as:

$$f = \pi\xi(1 - \tfrac{1}{2}\cos\pi\eta) \tag{3-7}$$

In the case of bubble acceleration and deceleration, the vorticity transport equation should consider the vorticity change with time. However, if the time interval is very small the bubble can be considered to be at steady state. In this work the pseudo-steady state assumption is applied to simplify the mathematical models, save computing time and minimize the numerical experimental work for some of the relaxation parameters.

### 3.4 Mass transfer

Surfactant in solution will be transported from the bulk solution to the bubble surface sublayer then adsorbed onto the bubble surface. The fluid flow around the bubble will cause the surfactant to form a compact layer at the rear of the bubble (advection). The concentration difference along the bubble surface can also cause back diffusion. Therefore, surfactant transportation in a spherical coordinate system (r, θ, ϕ) can be expressed as:

$$\frac{\partial \Gamma}{\partial t} - \nabla_s(\Gamma u_\theta - D_s \nabla_s \Gamma) = r_{m,\theta} \tag{3-8}$$

The local mass transfer rate of surfactant from bulk solution to the bubble surface, $r_{m,\theta}$, is determined by the control step between surfactant boundary layer mass transfer from the bulk solution to the sublayer of the interface and the adsorption kinetics of the surfactant from the sublayer to the bubble surface. For the stagnant cap model to hold, it is supposed that the bulk diffusion is much slower than the desorption rate at the stagnant cap. Fitting to the experimental velocity profiles is used to discriminate among the mass transfer control steps.

To simplify the numerical solution and save computing time, it is practical to decouple the solution for the mass transfer from the fluid flow. When the bubble rises in a surfactant solution, the velocity is high (e.g., the velocity of 0.8 mm bubble is larger than 9 cm/s). Therefore, the adsorbed surfactant molecules are considered to be transported to the rear of the bubble instantaneously by advection while the surface diffusion flux can be ignored.

### 3.4.1 Boundary layer mass transfer control

Mass transfer from the bulk solution to the bubble surface at high Re and high Pe can be simplified using the boundary layer theory. The mass balance is solved by integrating eq. (3-8) over the bubble surface:

$$\int \frac{\partial \Gamma}{\partial t} - \int \nabla_s (\Gamma U_s - D_s \nabla_s \Gamma) = r_m \tag{3-9}$$

The integration of the item in the bracket over the whole surface is 0.

Supposing the average mass transfer coefficient is k, then the mass transfer rate integrated over the surface can be approximated in terms of Sh:

$$r_m = kS\Delta c \tag{3-10}$$

and:

$$k = \frac{ShD}{d_e} \tag{3-11}$$

The surfactant in the sublayer is always in equilibrium with the adsorbed surfactant on the bubble surface, i.e., $c_s$=$c_e$,

$$c_s = \frac{\alpha}{\beta}\frac{\Gamma}{\Gamma_\infty - \Gamma} \tag{3-12}$$

Therefore the concentration difference across the boundary layer is,

$$\Delta c = c_\infty - c_s \tag{3-13}$$

In this thin concentration boundary layer approximation, the concentration gradient normal to the bubble surface is much larger than that parallel to the surface. In dilute solution, the diffusion-induced advection can be ignored. Therefore the mass transfer is mainly by diffusion in the normal direction.

The mass transfer coefficient depends on the position in accordance to the bubble surface. Empirical correlations can be used to approximate the average mass transfer coefficient at both the mobile and the stagnant part of the surface. As discussed in chapter 2, for a mobile bubble surface the average Sh is correlated by eq. (2-26) (Lochiel and Calderbank, 1964; Winnikow, 1967). For a rigid sphere freely rising in water with d>0.1 mm, eq. (2-27) can be used (Calderbank and Lochiel, 1964).

Integration of the mass balance equation over the whole surface gives:

$$S_b k\Delta c|_{S_b} + S_{stc} k\Delta c|_{S_{stc}} = \frac{d(S_{stc}\Gamma)}{dt} \tag{3-14}$$

If the stagnant cap angle (θ) is known, the area of bare surface ($S_b$) and the stagnant cap ($S_{stc}$) can be calculated by:

$$S_b = 2\pi r_e^2(1+\cos\theta) \tag{3-15}$$

and

$$S_{stc} = 2\pi r_e^2(1-\cos\theta) \tag{3-16}$$

### 3.4.2 Adsorption kinetic control

If the boundary layer mass transfer of surfactant is sufficiently fast the concentration of surfactant in the sublayer would be the same as in the bulk, $c_s=c_\infty$. The mass transfer rate is then determined by the adsorption kinetics:

$$r_{m,\theta} = \beta c_\infty(\Gamma_\infty - \Gamma) - \alpha\Gamma \tag{3-17}$$

Integration of the above equation over the bubble surface gives:

$$r_m = \beta S_b c_\infty \Gamma_\infty + \beta S_{stc} c_\infty(\Gamma_\infty - \Gamma) - \alpha S_{stc}\Gamma \tag{3-18}$$

### 3.5 Boundary conditions

According to the stagnant cap model, the tangential stress at the clean surface is zero. The boundary condition at the clean surface ($\xi$=1) is therefore expressed as:

$$\omega - 2\kappa_\eta u_\eta = 0 \tag{3-19}$$

where $\kappa_\eta$ is the normal curvature of the interface in the $\eta$ direction.

Surfactant coverage at the bare surface is zero:

$$\Gamma = 0 \tag{3-20}$$

Normal velocity on the bubble surface is zero, therefore;

$$\psi = 0 \tag{3-21}$$

The $\tau_{\xi\xi}$ the total normal-stress due to the contributions of pressure and viscous forces can be calculated by the equation:

$$\tau_{\xi\xi} = -p - \frac{8}{\mathrm{Re}} \frac{1}{\sigma h_\eta} \frac{\partial}{\partial \eta}(\sigma u_\eta) \tag{3-22}$$

$\tau_{\xi\xi}$ balances the capillary force:

$$\tau_{\xi\xi} - \frac{4}{We}(\kappa_\eta + \kappa_\phi) = 0 \tag{3-23}$$

where $\kappa_\phi$ is the normal curvature of the interface in the $\phi$ direction

The normal curvatures of the interface in the $\eta$ and $\phi$ direction $\kappa_\eta$, $\kappa_\phi$ can be calculated by:

$$\kappa_\eta = \frac{1}{h_\eta{}^3}\left(\frac{\partial x}{\partial \eta}\frac{\partial^2 \sigma}{\partial \eta^2} - \frac{\partial^2 x}{\partial \eta^2}\frac{\partial \sigma}{\partial \eta}\right) \tag{3-24}$$

$$\kappa_{\phi} = -\frac{1}{\sigma h_{\eta}} \frac{\partial x}{\partial \eta} \tag{3-25}$$

The tangential shear stress balances the surface tension force at the stagnant cap,

$$\tau_{\xi\eta} = -\frac{\mathrm{Re}}{h_{\eta} We} \frac{\partial \gamma'}{\partial \eta} \tag{3-26}$$

where $\gamma'$ is the dimentionless surface tension, $\gamma'=\gamma/\gamma_0$.

The adsorbed surfactant layer is compressed to a compact layer by the shear stress. The equation of state, the Langmuir isotherm, is used to correlate the surface tension and concentration of adsorbed surfactant:

$$\gamma_0 - \gamma = -RT\Gamma_{\infty} \ln(1 - \frac{\Gamma}{\Gamma_{\infty}}) \tag{3-27}$$

The concentration in the sublayer at the stagnant cap is in equilibrium with the surface concentration at any time.

$$c_s = \frac{\alpha}{\beta} \left( \frac{\Gamma}{\Gamma_{\infty} - \Gamma} \right) \tag{3-28}$$

For a dilute solution, it is assumed that at the edge of the stagnant cap the surface tension equals the surface tension of water. In the case of full coverage, the surface tension at the top of the bubble equals the surface tension of water.

### 3.6 Solution algorithm

The fluid flow and the Marangoni effects are solved numerically in a boundary fitted coordinate system. At a fixed stagnant cap angle the covariant Laplace equations and the streamfunction-vorticity equations are solved with the constant step alternating directions implicit (ADI) method which is developed from that presented by McLaughlin (1996). In each time step the orthogonal coordinates (interface shape) are adjusted by considering the normal stress balance. The new scale factor for the next time step can be expressed in the explicit manner as:

$$h_\xi^{n+1} = h_\xi^n + \beta_h \Pi^n \tag{3-29}$$

where Π is the local excess of total normal stress over capillary forces:

$$\Pi \equiv \tau_{\xi\xi} - \frac{4}{We}(\kappa_\eta + \kappa_\phi) \tag{3-30}$$

The boundary vorticity value at the stagnant cap for the next time step is adjusted by considering the tangential stress excess:

$$\omega^{n+1} = \omega^n - \beta_\omega(\omega^n - 2\kappa_\eta u_\eta^n) \tag{3-31}$$

The cap angle step is chosen to be small, ≤ 1/60, and it was assumed the bubbles decelerate sufficiently slowly that the fluid flow between two consecutive cap angles remains in steady state (quasi-steady state condition). The time derivative term in the vorticity equation is negligible. Once the flow field was computed, the balance between the shear stress and the Marangoni force was used to compute the surface tension as a function of position on the surfactant cap and the Langmuir isotherm was then used to determine the surface concentration of surfactant.

The initial condition for a run was a clean bubble moving at the steady-state speed. This is a reasonable assumption for sufficiently small bulk concentrations of surfactant since the experiments indicate that the bubble attains a maximum velocity that is close to the steady-state velocity in pure water before beginning to slow down (Zhang and Finch, 1999). At each time step, a cap angle was selected and the Re and We of the flow around the bubble were computed by iteration. To begin the iterative process, the Re and We were chosen as the values from the previous time step. On each iteration, the program computed the drag coefficient for specified values of the Re and We. The drag coefficient was then used to compute new values of the bubble velocity, Re and We. This process was continued until Re converged.

The value of the relaxation parameters for the vorticity boundary condition ($\beta_\omega$ and $\beta_h$) was obtained by numerical experiments. The iteration number for the coordinates and vorticity solution is also selected by monitoring the convergence of the solution. The spatial grid generated by the program was orthogonal and non-uniform in both the angular and radial directions. Grid numbers in both directions depend on the bubble size considered.

Finally, the time needed to attain a cap angle must be computed. This is done by using mass transfer correlations discussed in the above section 3.4.1 with the computed flow field. Fig. 3.2 is a flow chart of the algorithm.

McLaughlin (1996) estimated the Re for each cap angle as the input to solve the hydrodynamic equations. The tangential stress balance was used to obtain the drag coefficient on the bubble and the total amount of surfactant adsorbed. The result was checked by monitoring Mo calculated by the following equations:

$$Mo = \frac{3}{4} C_D \frac{We^3}{\mathrm{Re}^4} \tag{3-32}$$

$$Mo = \frac{g\mu^4}{\rho\gamma^3} \tag{3-33}$$

If the calculated Mo from eq. (3-32) did not equal the value from eq. (3-33), a new estimation of Re was made to re-run the program. In their solution algorithm, the We is fixed. Therefore, the bubble size is a function of velocity.

The program used in this work is improved by adding the iteration loop for Re. By comparing the computed Re from the program with the input Re, a new Re input is chosen as the average of the two. And hence, a new We is obtained from the relationship with Re for a fixed bubble size. If the Re converges, the Mo automatically equals the physical value. Numerical experiments showed the program converges well at any initial value of Re. To fix the bubble size in the modeling is more physically meaningful than to fix We.

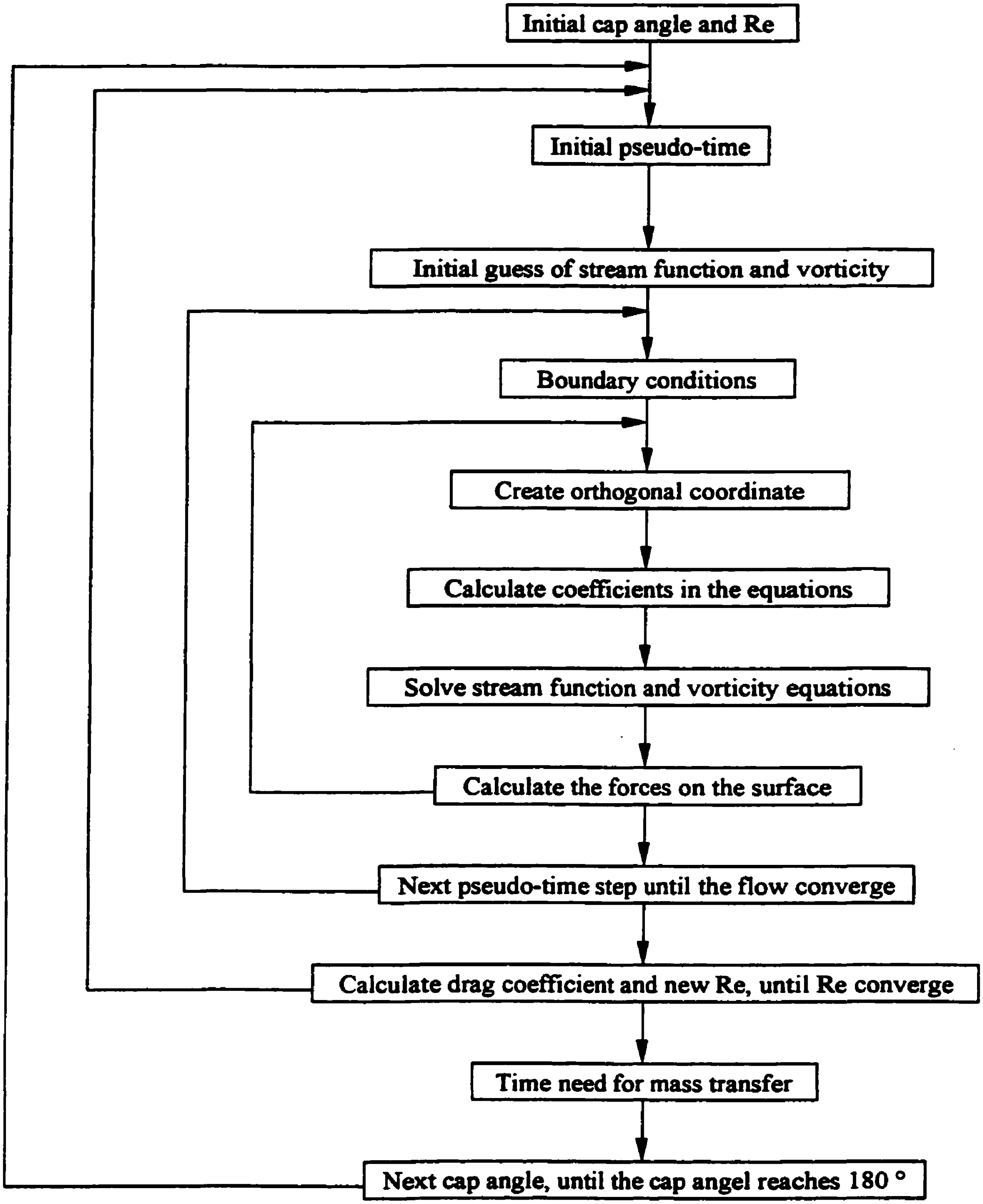

Fig. 3.2 The algorithm of the numerical solution

# CHAPTER 4

# EXPERIMENTAL PROCEDURE AND ESTABLISHMENT OF REPEATABILITY

*"The state of experiments in general seems to be underdeveloped as compared with the level of broad theoretical studies of dynamic adsorption layers on moving bubbles and drops. Most of all [is] the lack of systematic studies, which are obviously necessary for a further development of this area of physico-chemical hydrodynamics. This is clearly an important area for the optimisation of many technological processes. Only experiment can prove the existence of different states of a dynamic adsorption layer proposed by the theories. Two questions remain to be answered: 'does the motion of the bubble surface in absence of surfactants arise at small or intermediate Reynolds numbers' and 'is it possible to attain a low surfactant concentration at which its effect on the surface motion remains small?'"*

——Excerpt form "Dynamics of Adsorption at Liquid Interfaces" by Dukhin, S. S., Kretzschmar, G. and Miller, R. (1995), pp. 320-321.

*"Unfortunately, accurate experimental data with known surfactant concentrations do not appear to be available. Thus theories cannot be tested except by fitting the contaminant concentration to match the data. Moreover, the conditions which must be satisfied for the theories to hold are so stringent that theories are of little practical importance."*

——Excerpt form "Bubbles, Drops, and Particles " by Clift, R., Grace, J. R. and Weber, M. E. (1978), p. 135.

The lack of experimental study of dynamic adsorption of surfactant onto moving bubbles has hindered the development of the field of physico-chemical hydrodynamics. Adsorption on the bubble modifies the bubble surface, which is manifested in the mobility of the bubble surface and the drag opposing the bubble motion. The measure of single bubble velocity in water and surfactant solutions is a promising means to study the dynamic adsorption process.

## 4.1 Equipment

Comparison of the available methods to measure single bubble velocity revealed that the most suitable is to use photography because of its simplicity and relative accuracy (Sam, 1995). The photographic method combined with a moving camera setup to track the bubble is well suited for the measurement of bubble velocity as a function of position along a column.

The equipment used is sketched in Fig. 4.1. The column is 4 m high with a square cross section of $10\times10$ cm$^2$. Bubbles are produced by introducing air through a glass capillary with a known inner diameter. The column has a jacket for circulating water to control the temperature (6-50 °C). A fibreglass measuring tape is installed inside the column to determine the position of the bubble.

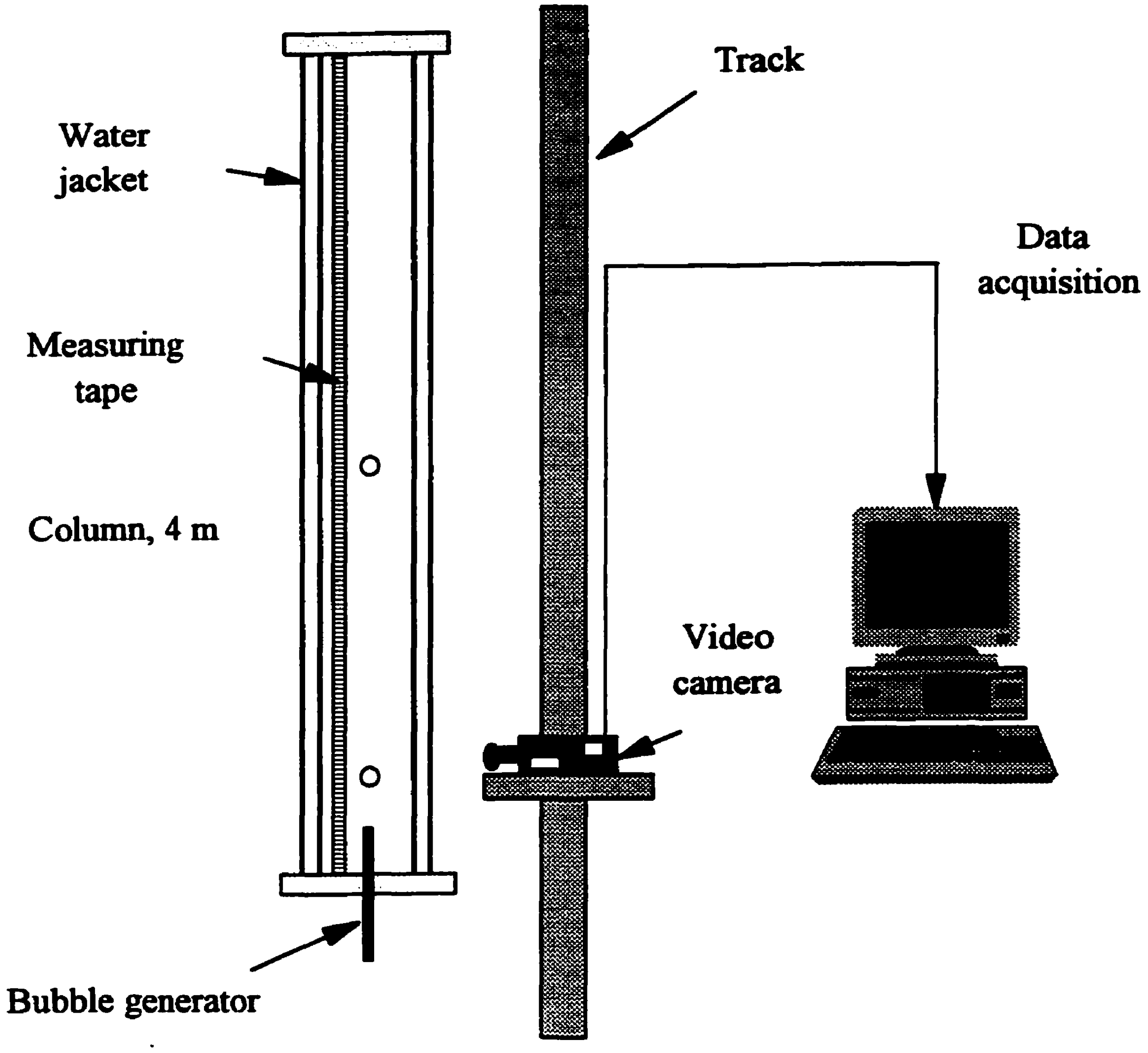

Fig. 4.1 Experimental set-up

The test solution was heated to the experimental temperature and aerated (to air-saturate the water) before being placed in the column. After filling the column, the temperature was maintained by circulating water in the jacket with a variance of temperature < ±0.25 °C along the column. The bubble frequency was adjusted to less than 80 per minute whereby bubbles do not interfere with each other (Sam, 1995). A high resolution CCD video camera recorder (Sony Hi8-V801) mounted on a track was used to record the bubble motion. The video camera recorded 30 frames per second. The movement of the camera was controlled by the operator at a speed between 0-50 cm/s to follow a rising bubble. The motion of the bubble recorded on a videotape was processed off-line.

## 4.2 Chemicals

Various surfactants were used for the experimental measurement of single bubble velocity. The surfactants can be classified into three categories: flotation frothers, such as Dowfroth 250 (DF 250, which is polypropylene glycol ether), Methyl Isobutyl Carbinol (MIBC) and Pine oil (largely terpineol); alcohols (ethanol and octanol); and strong surfactants such as Triton® X-100 (simplified as Triton X-100 in the text), Brij® 30 and dodecylamine, which are often employed in surface chemistry studies.

Most of the velocity profile measurements were done with Triton X-100 as it is stable and the relevant physical property data are available. Triton X-100 [p-(1,1,3,3-tetramethylbutyl)phenoxypoly-(oxyethylene)$_n$ glycol], was obtained from Sigma-Aldrich

Canada Ltd. It is a nonionic surfactant containing an average number of 9.5 oxyethylene units per molecule with the following structure:

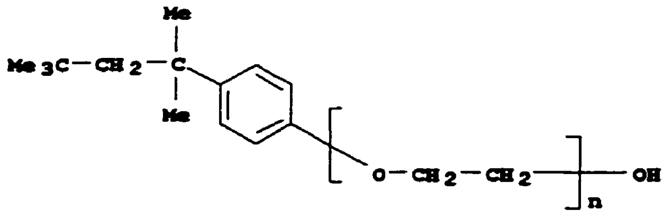

It has a critical micellar concentration less than 1.0 mol/m$^3$ (Ray and Nemeth, 1971, gave 0.25 mol/m$^3$, and Streletzky and Phillies, 1995, 0.93 mol/m$^3$). The molar weight and volume of Triton X-100 are 624 and 811, respectively.

Among nonionic surfactants, diffusion of Triton X-100 in aqueous solution has been most thoroughly studied (Corti and Degiorgio, 1975; Weinheimer et al., 1981; Van et al. 1986; Leaist, 1988; Lin et al., 1990). Lin et al. (1990) using a pendent drop digitization method studied dynamic surface tension of Triton X-100 solutions. The diffusion coefficient was determined to be $2.6\pm0.3\times10^{-10}$ m$^2$/s at 22 ± 0.5 °C by minimizing the difference between the theoretical diffusional relaxation profiles and the experimental profiles. The concentration range was from $9.89\times10^{-3}$ mol/m$^3$ to $2.32\times10^{-2}$ mol/m$^3$. Van et al. (1986) obtained $D=1.9\text{-}2.3\times10^{-10}$ m$^2$/s using the drop volume method for a similar concentration range as in Lin et al.'s work. Leaist (1988) predicted the diffusion coefficient of Triton X-100 at infinite dilution to be $3.5\times10^{-10}$ m$^2$/s at 25 °C. The diffusion coefficient is $3.5\times10^{-10}$ m$^2$/s calculated by the Stokes-Einstein equation and $3.01\times10^{-10}$ m$^2$/s by the Wilke-Chang equation at 25 °C ($2.79\times10^{-10}$ m$^2$/s at 22 °C).

The literature value of diffusion coefficient for Triton X-100 ranges from 1.9 to $3.5\times10^{-10}$ $m^2/s$. The value from Lin et al. is in the middle of the range. Lin et al. also correlated other thermodynamic parameters. In the simulation of velocity profile, the physical parameters from Lin et al. were selected (Table 4.1).

Table 4.1 Physical parameters of Triton X-100

| | |
|---|---|
| **Diffusion coefficient D, $m^2/s$** | $2.6\pm0.3\times10^{-10}$ |
| **Maximum surface coverage $\Gamma_\infty$, $mol/m^2$** | $2.91\times10^{-6}$ |
| **Langmuir Von Szyskowski constant $\alpha/\beta$, $mol/m^3$** | $6.62\times10^{-4}$ |
| **Lower bound of desorption constant $\alpha$, $s^{-1}$** | $3.3\times10^{-2}$ |

## 4.3 Measurements

### 4.3.1 Bubble size

The bubble was photographed with a stationary camera (Canon, EOS-1000F). The size was measured using an image analyser with, from repeat experiments, a 95% confidence interval of ± 0.05 mm. Three capillary sizes were employed, 14, 64 and 125 μm. The measured bubble sizes at the point of generation were 0.8, 1.4 and 1.8 mm, respectively.

As the bubble rises it will expand. However, the size change was not obvious from the photographs because of the limitation imposed by measurement precision. The bubble size increases calculated from the decrease in hydrostatic pressure from bottom to top of the 4 m column at 25 °C are listed in Table 4.2.

Table 4.2 Bubble sizes expansion along the column at 25 °C

| **Capillary size, μm** | **14** | **64** | **125** |
|---|---|---|---|
| **Bubble size at bottom, mm** | 0.8 | 1.4 | 1.8 |
| **Bubble size at top, mm** | 0.9 | 1.6 | 2.0 |

### 4.3.2 Bubble velocity profile

The vertical velocity of the bubble was calculated from readings of the displacement of the bubble and corresponding time interval on the videotape. The procedure is illustrated in Fig. 4.2, which shows a sequence of two video images. Suppose image 1 is obtained at time t, and after five frames, image 2 is obtained. The time interval between these two is 5×(1/30 s)=1/6 s. Therefore the velocity of the bubble between these two positions (7.1 and 13.2 cm) is: 6.1/(1/6)=36.6 cm/s.

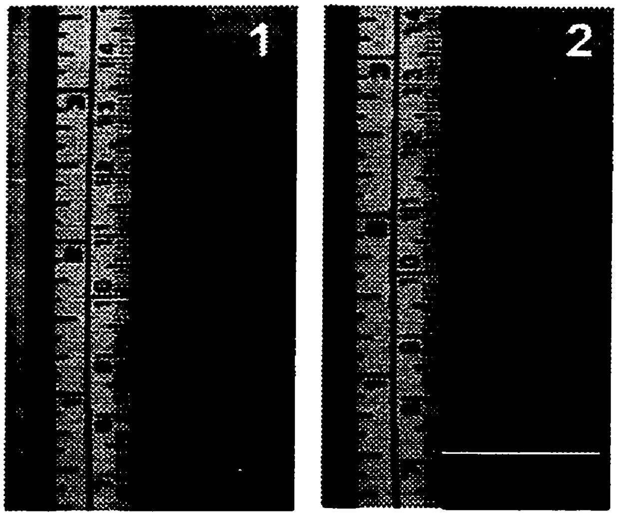

Fig. 4.2 Measurement of bubble velocity
(line on RH image represents position in LH image)

### 4.4 Establishment of the repeatability of velocity profile measurement

In the experiments, bubbles are produced in a chain from the capillary. When the bubble generation frequency is less than ca. 80/min, the bubbles do not influence each other (Sam, 1995). Because interaction between succeeding bubbles can be ignored, the single bubble velocity profile is solely determined by the dynamic adsorption process of surfactant (if the bubble expansion along the column is neglected).

The first requirement is to establish experimental repeatability. To begin, the velocity profiles of a single bubble were compared in tap and distilled water. The bubble decelerated in both and no significant improvement was achieved by using distilled water. In addition, the volume of solution needed is more than 40 litres, which makes the choice of distilled water impractical.

Next, bubble velocity profiles were measured in the same batch of tap water after letting it sit in the column for different times. The quality of the water does change when retained for prolonged times (Fig. 4.3), which may have been caused by the inevitable dissolution of some impurities from the equipment (i.e., Plexiglas column wall). It is mandatory to use fresh water for each experiment.

Initially three flotation frothers, DF 250, MIBC and pine oil were selected as surfactants. Of these three, DF 250 is the most surface active (reduces surface tension most as shown in Fig. 4.4). In Fig. 4.4 the data for MIBC, DF 250 and pine oil are from Sam (1995) and for Triton X-100 and Brij 30 from Göbel and Joppien (1997), and Lucassen and Giles (1974), respectively. Given its high surface activity and wide industrial applications DF 250 was the first choice for the velocity profile study. Using samples from a given batch repeatable profiles were possible (Fig. 4.5) as found by Sam. However, it proved difficult to obtain repeatable profiles for different batches. A reason for this poor repeatability between batches was sought. Properties from the MSDS supplied by the frother manufacturers are listed in Table 4.3. The instability of DF 250 may have caused the poor repeatability. A similar problem was found with MIBC and pine oil. The low surface activity (small surface tension change with concentration, Fig. 4.4) makes them susceptible to impurities, which probably accounts for their poor repeatability. After a paper study of the possible candidates for a stable surfactant, Triton X-100 was selected for the experiments intended to test models of the velocity profiles.

Table 4.3 Properties of surfactants

| **Surfactants** | **Formula** | **Stability** |
|---|---|---|
| **DF 250** | $CH_3\text{-}(OC_3H_6)_4\text{-}OH$ | Prolonged storage in contact with air may form peroxides |
| **MIBC** | $C_6H_{13}OH$ | stable |
| **Pine oil** | $C_{10}H_{17}OH$ | Polymerization may occur. |
| **Triton® X-100** | $C_{14}H_{21}(OC_2H_4)_{9.5}OH$ | stable |
| **Brij® 30** | $C_{12}H_{25}(OC_2H_4)_4OH$ | stable |

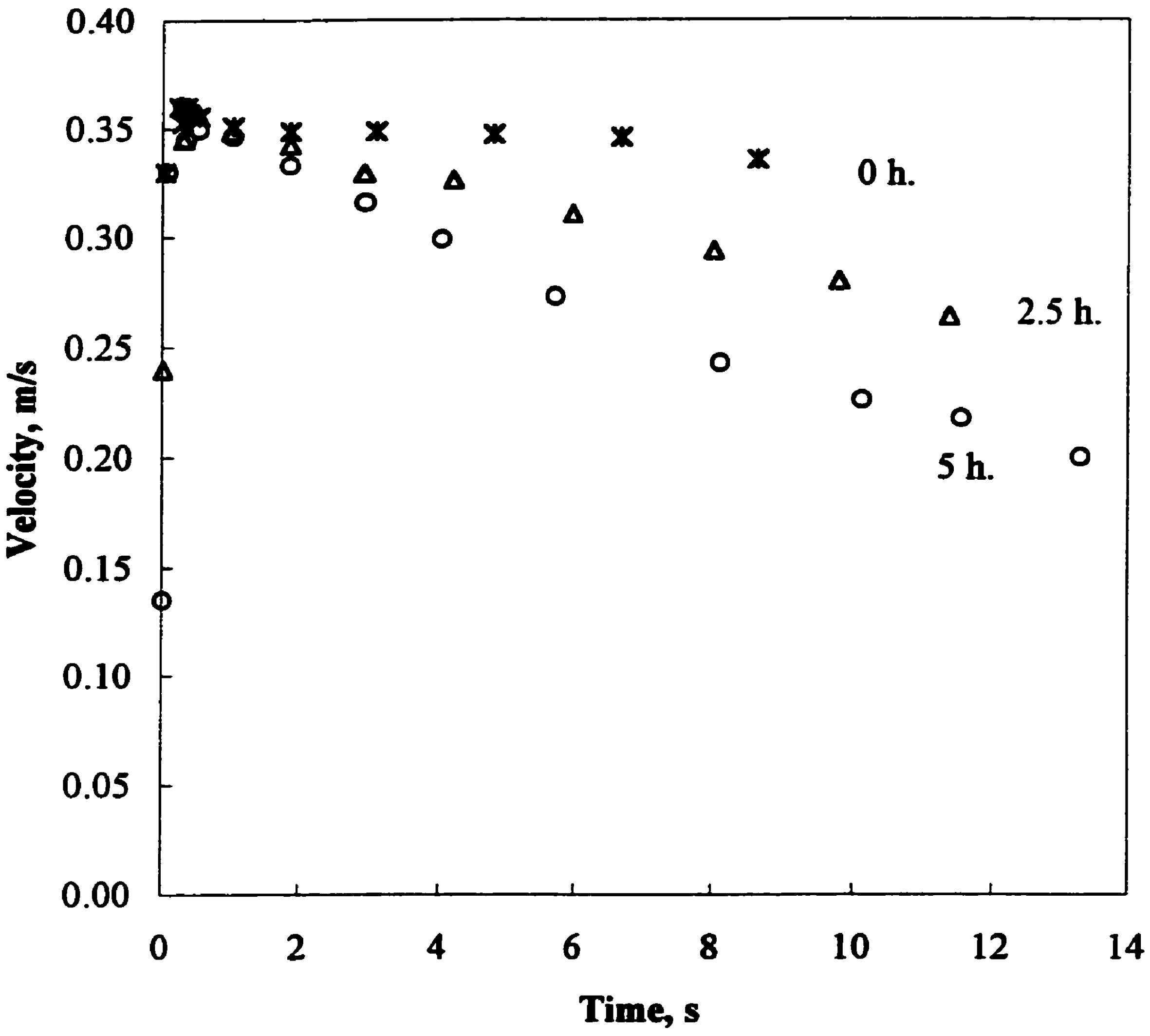

Fig. 4.3 Velocity profiles of a single bubble (1.4 mm) in tap water: effect of time retained in equipment

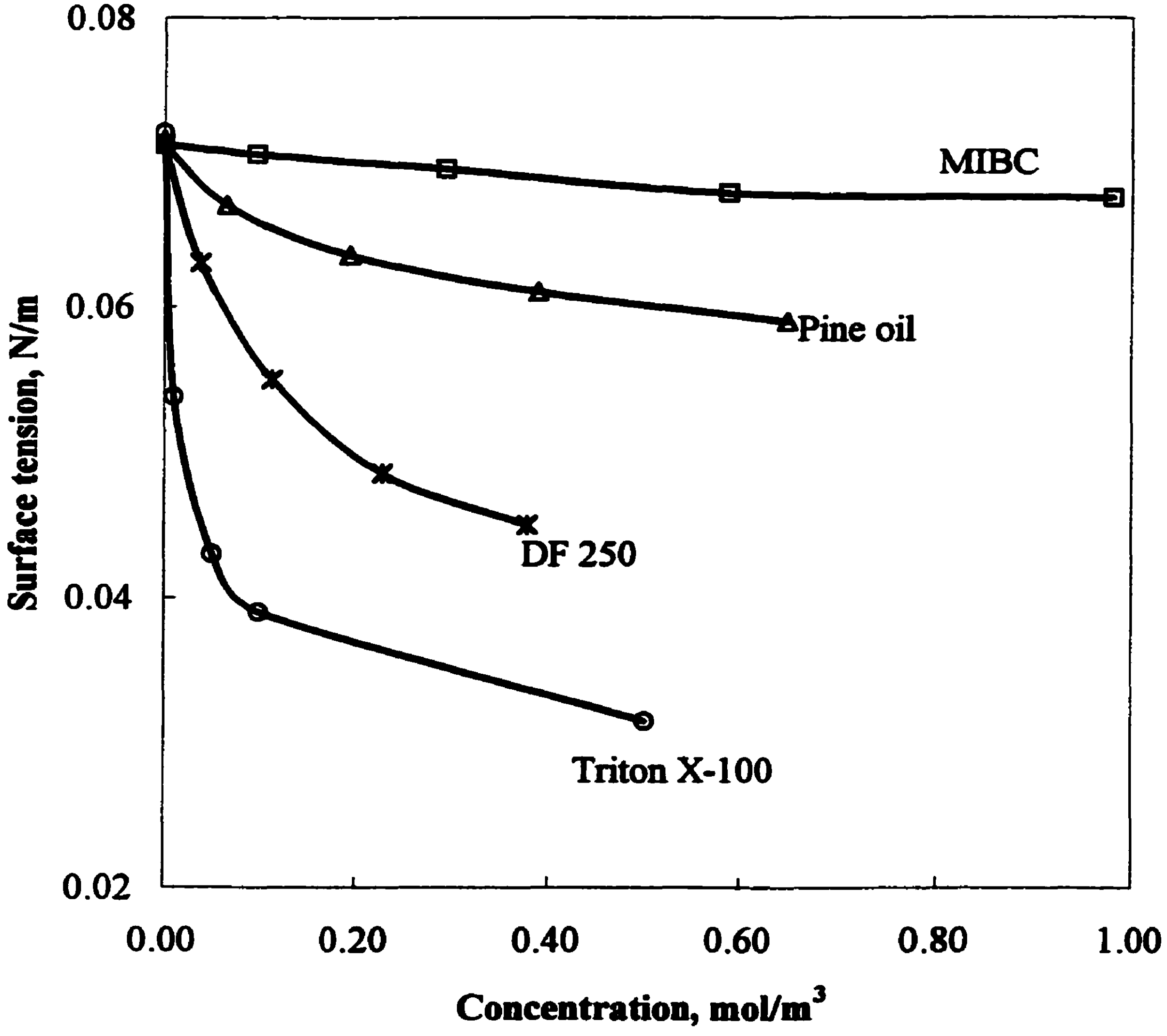

Fig. 4.4 Equilibrium surface tension of surfactant solutions

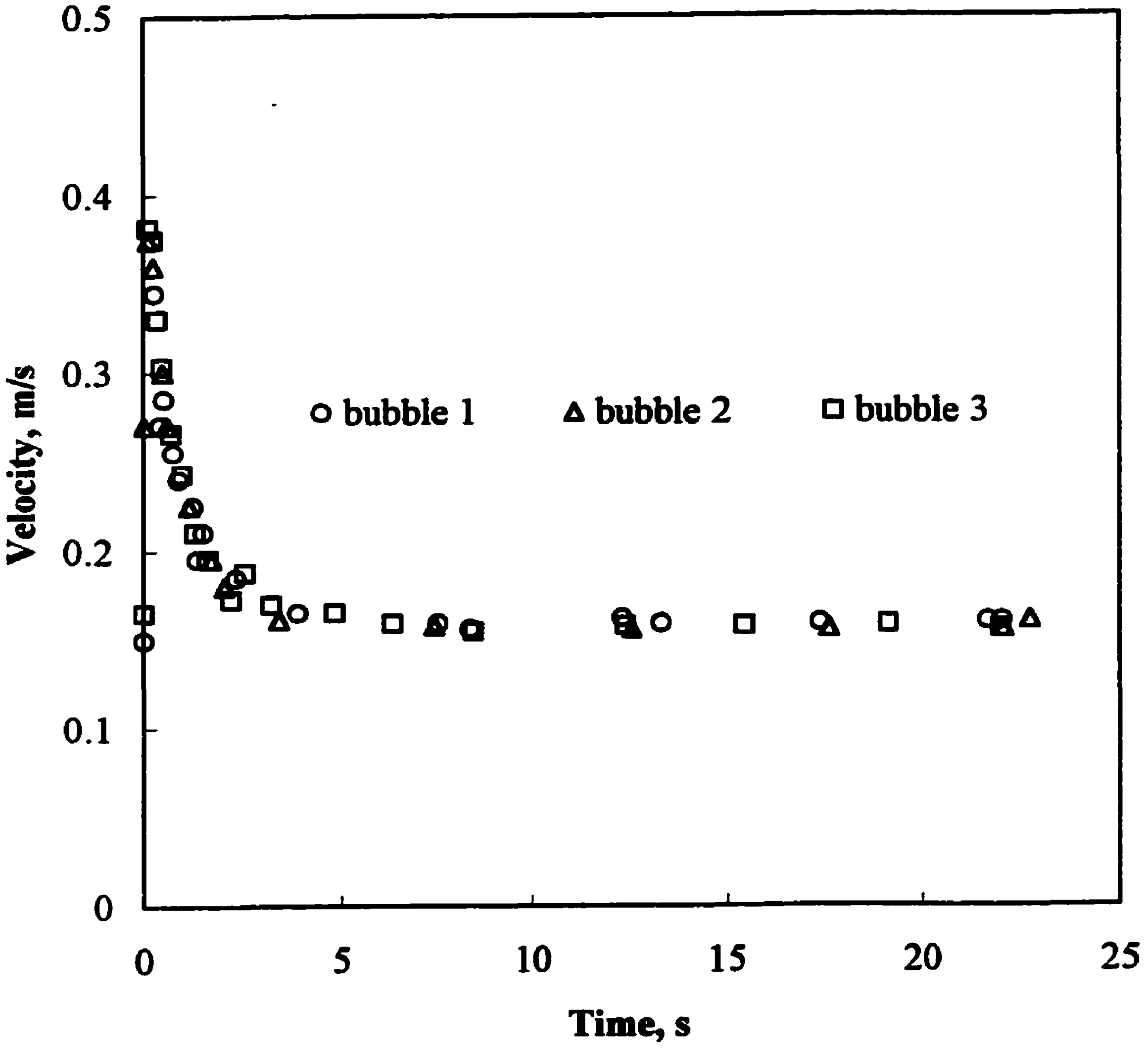

Fig. 4.5 Velocity profiles for 3 randomly selected bubbles (1.4 mm) at room temperature from one batch of DF 250 solution

The sensitivity of the measurement to the surfactant concentration was investigated in Triton X-100 solutions. The lowest concentration was $1.3\times10^{-7}$ mol/m$^3$. When the concentration is below ca. $1.3\times10^{-6}$ mol/m$^3$ the velocity profile for a 1.5 mm bubble showed no significant difference from that in tap water, as shown in Fig. 4.6.

Velocity profiles were obtained next in both tap water and different batches of the same concentration of Triton X-100. The results for the solutions showed satisfactory repeatability (Fig. 4.7), even though there is some variation in the tap water (compare day 1 with the other two days). The contribution due to variations in tap water quality is judged to be negligible for the solutions $\geq 2.5\times10^{-5}$ mol/m$^3$ which was a restriction respected in later modeling of the velocity profile.

### 4.5 Effect of humidity on bubble velocity

It was suspected that the humidity of the air might affect the bubble velocity. Humidity will add mass to the bubble and mass transfer of water into the air phase may change the force balance. However, the results (Fig. 4.8) for 1.5 mm bubbles in both water and DF 250 solution did not reveal any obvious difference in the velocity profiles for "dry" bubbles and water saturated bubbles. It is concluded that for bubbles moving with a high Re, the effects of flow and adsorption of surface active agents are far larger than the effect of humidity.

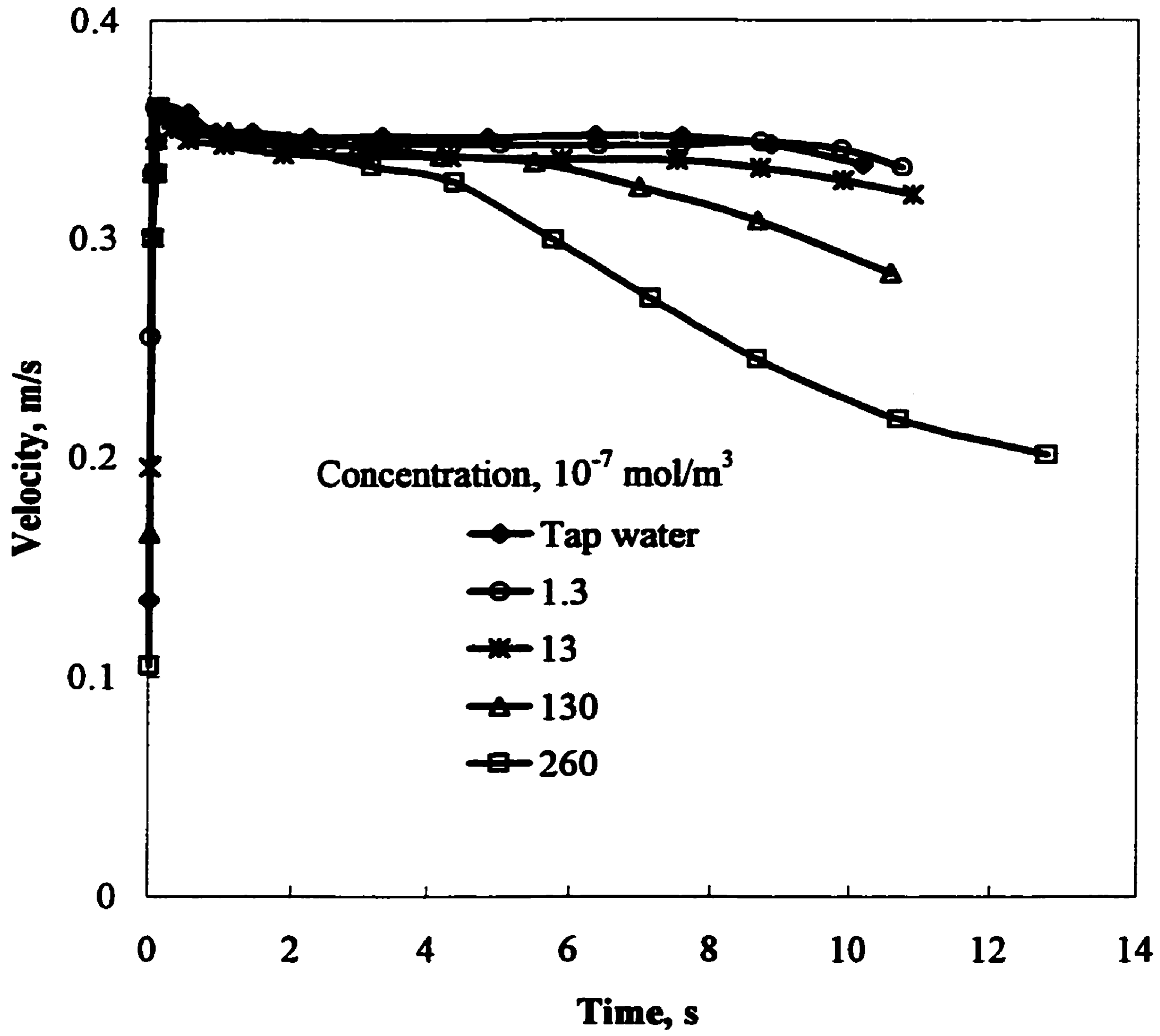

Fig. 4.6 Velocity profiles of bubbles (1.4 mm) in tap water and Triton X-100 solutions: establishing sensitivity, i.e., lower concentration limit.

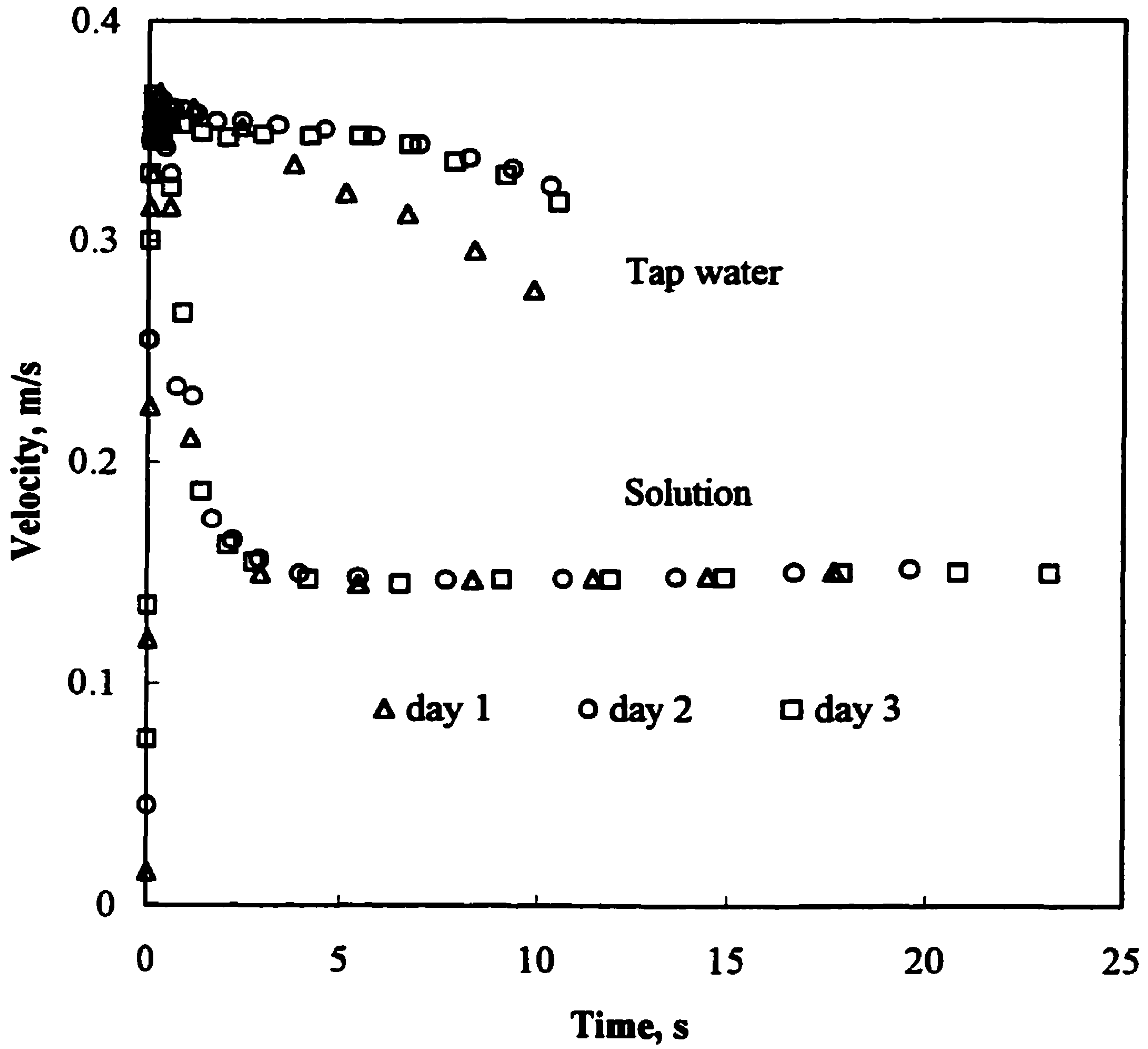

Fig. 4.7 Velocity profiles of bubbles (1.4 mm) in tap water and Triton X-100 solution at 30 °C on different days

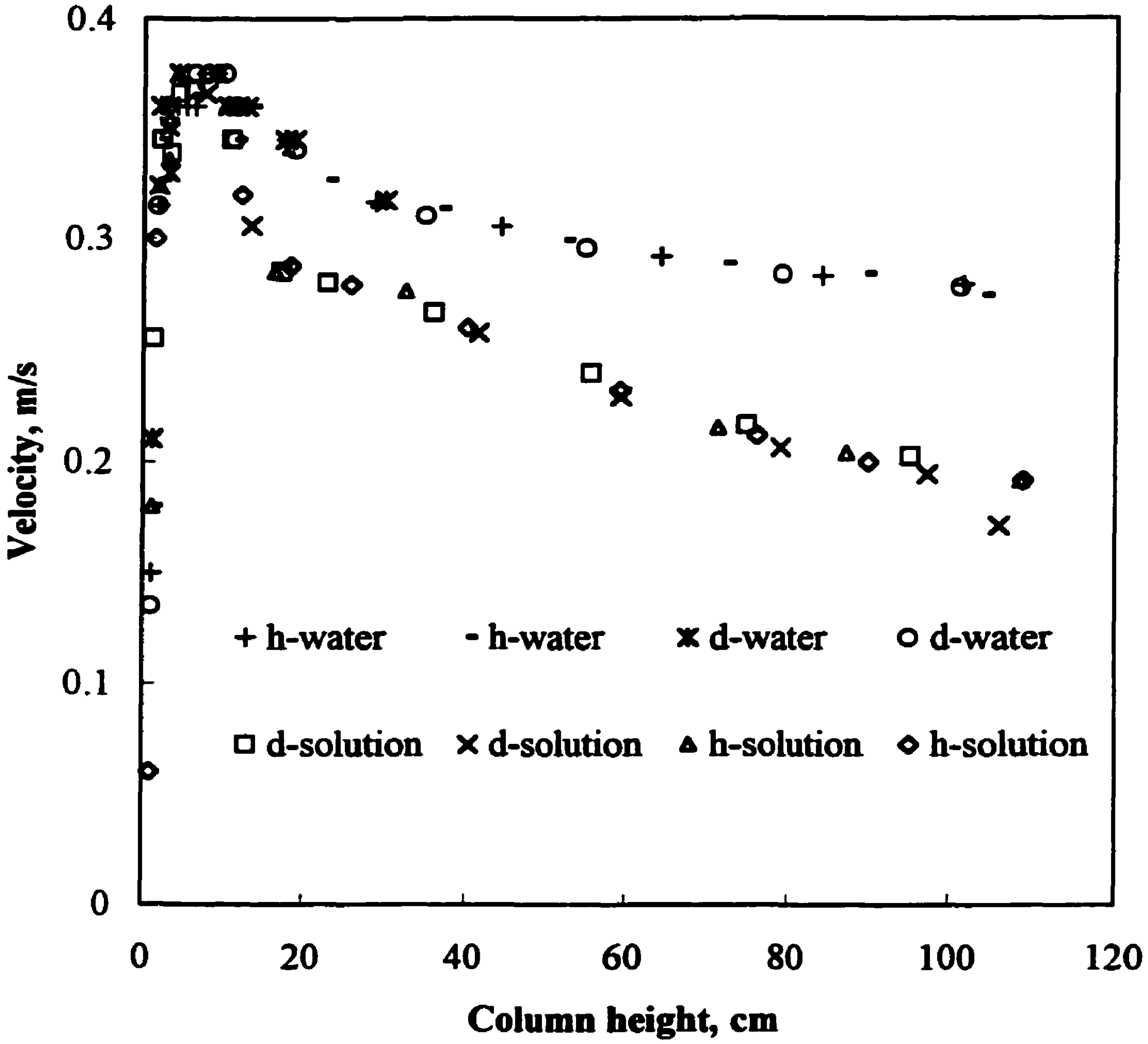

Fig. 4.8 Effect of humidity on single bubble velocity profiles
h-: saturated bubble, d-: dry bubble

### 4.6 Conclusions

The experimental setup is suitable for the objectives of this study. The measurements are repeatable provided solutions are prepared fresh and a stable surfactant is used, in this case Triton X-100. The variation of tap water quality does not affect the velocity profiles in Triton X-100 solutions provided the concentration is greater than ca. $2.5\times10^{-5}$ mol/m$^3$. The suspicion of a humidity effect has been eliminated.

# CHAPTER 5

# SINGLE BUBBLE TERMINAL VELOCITY

## 5.1 Introduction

Predicting the bubble terminal velocity is a key test of fundamental models of the velocity profile. There have been numerous experimental studies to determine the terminal velocity of a single bubble. However, because of restrictions imposed by the experimental set-up, most studies usually report an average velocity of a bubble over a given distance, e.g., the height of a column of liquid. As a result the measurements of terminal velocity can be in error. Further, the measurement of terminal velocity in water alone is bedeviled by the effect of even minute traces of impurities. It is, therefore, necessary to measure the velocity profile in order to obtain the terminal velocity. Typical single bubble velocity profiles are summarised in Fig. 5.1.

In theoretically pure water, the velocity of a single bubble should have only two stages, acceleration followed by a constant rising velocity (ignoring expansion of the bubble as it rises for now). In actual waters, the bubble velocity decreases after the maximum velocity is reached because of the impurities present. In a 4 m high column, the constant velocity stage is not reached. If the impurity level is sufficiently small, the terminal velocity in pure water can be approximated by taking the maximum velocity in the profile which represents the closest approach to the terminal velocity the bubble would achieve in truly pure water.

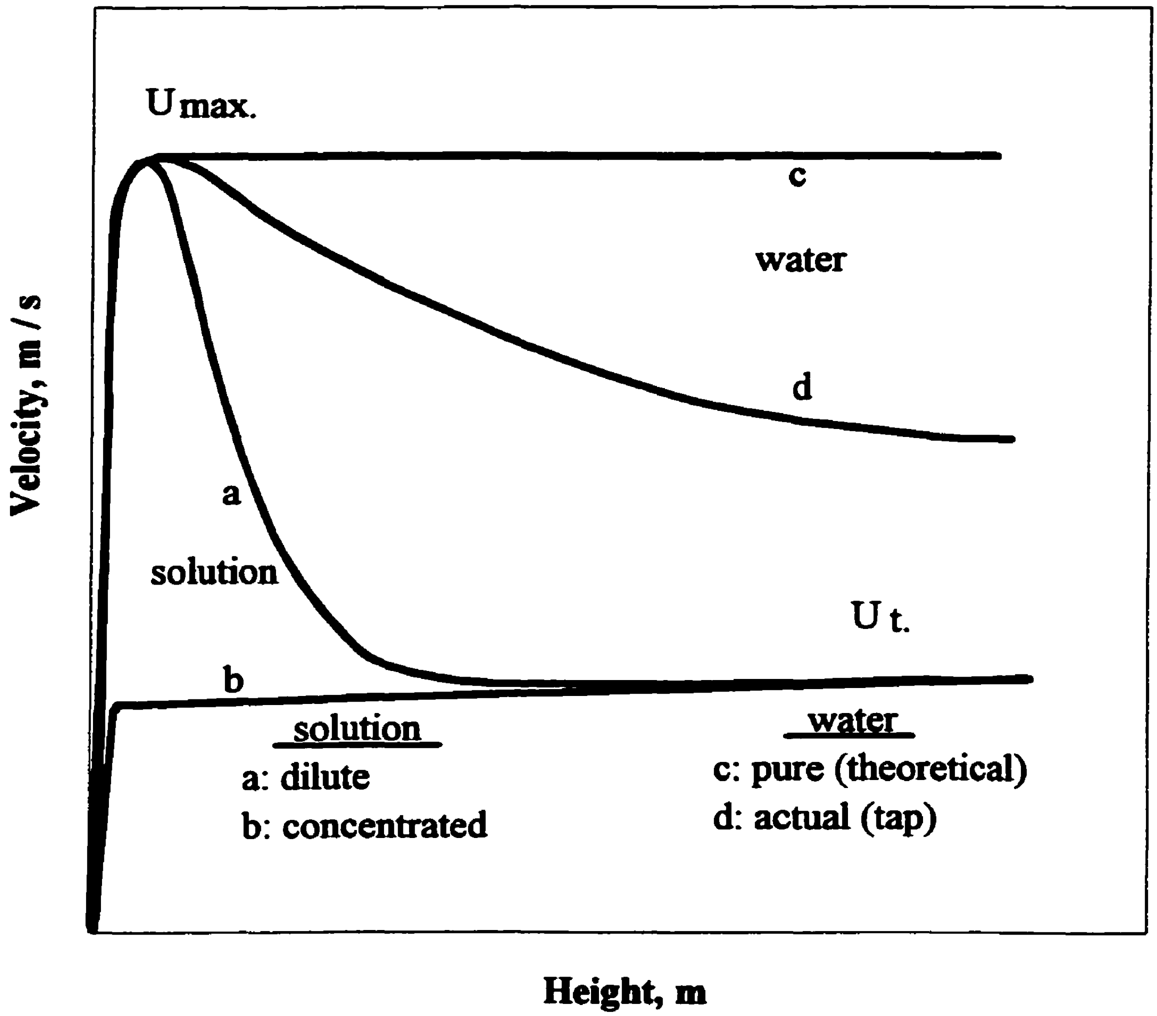

Fig. 5.1 Typical velocity profiles in water alone and surfactant solution

The situation is different in surfactant solutions. With sufficient concentration, the velocity profile has three stages as the constant velocity is reached in the 4 m column. The terminal velocity should be equated to this constant velocity as suggested by Sam et al. (1996).

This chapter reports terminal velocity as a function of surfactant type and concentration. The results are compared with existing models.

## 5.2 Results and discussion

### 5.2.1 Water alone

Tap water was used rather than attempting to obtain "pure" water as discussed in chapter 4. The terminal velocities for a 1.4 mm (diameter) bubble obtained by taking the maximum in the profile are shown in Table 5.1. The data are reproducible (the standard deviations are given). Included also are results for the maximum velocity from profiles obtained in dilute salt and surfactant solutions at 30 °C in order to compare the results from Sam (1995). The maximum velocities measured in dilute solutions were indistinguishable from those in tap water. The reason that small quantities of impurity are not a major factor in determining the maximum velocity is probably because the time for surfactant to adsorb is large compared to the acceleration time.

The terminal velocity of different size bubbles was also measured at 25 °C. The velocities predicted from Moore's theory, Sawi and Moore's theory, and Clift et al.'s correlation are compared with the experimental values in Fig. 5.2. Sawi and Moore's theory considers the bubble deformation.

Table 5.1 Maximum velocity in tap water and dilute solutions for 1.4 mm bubble at 30 °C

| **Media** | **$U_{max}$, cm/s** | **Standard deviation** |
|---|---|---|
| Tap water | 37.7 | 1.7 |
| DF 250 (0.06 ppm) | 37.6 | 0.2 |
| Ethanol (17 ppm) | 38.4 | 0.7 |
| KCl (10 ppm) | 37.6 | 0.1 |
| Average | 37.8 | 0.33 |

For the small bubble (0.8 mm), the predicted value from Moore's theory is close to the experimental. The closeness of Moore's theory and Sawi and Moore's theory for the small bubble shows that deformation is negligible for this size bubble. Therefore, the 0.8 mm bubble can be regarded as spherical in the simulation discussed in the next chapter. For bigger bubbles (1.4 and 1.8 mm), the experimental velocities are larger than the value predicted from Clift el al.'s correlation. Experimental results from Sam et al. (1996) and Duineveld (1995) show the same trend. In the case of Duineveld, a special purification system was built to produce water of extremely high quality. It was said to have no electrolyte and less than 10 ppb organic particles. His measurements represented the average velocity over the distance of 10 to 12 cm above the orifice. From our experience, the maximum velocity is reached at distances less than 10 cm. For example, the terminal velocity is reached at about 8 cm for a 1.4 mm bubble. Smaller bubbles need shorter

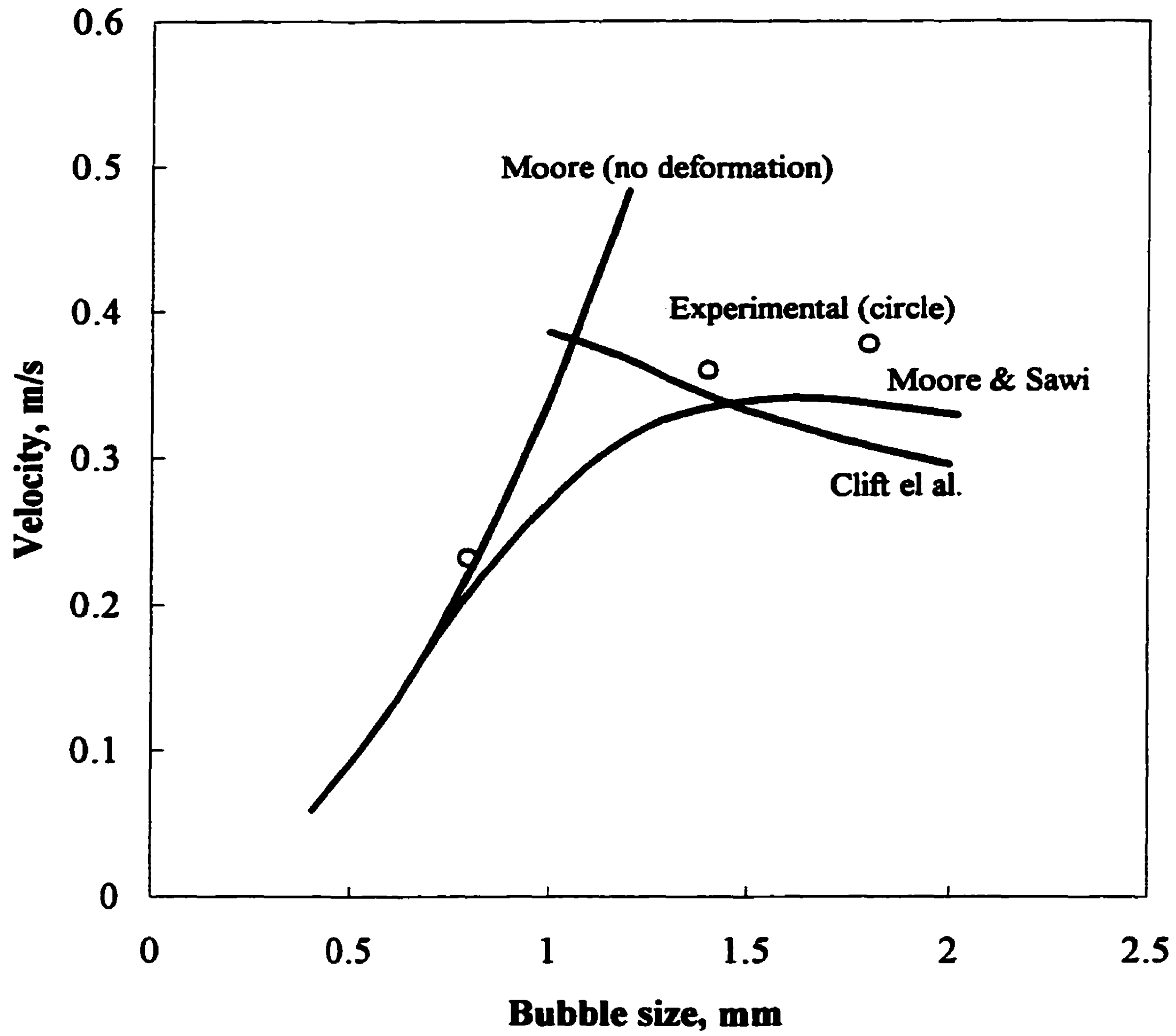

Fig. 5.2 The comparison of experimental terminal bubble velocity in water at 25 °C and model predictions

distance to reach the maximum velocity. A comparison of the data from Duineveld with the data obtained here shows the latter is consistently higher by 1-2 cm/s. The measure of the terminal velocity using the maximum in the velocity profile gave the highest values compared to any in the literature. At this juncture it is considered that the study of bubble terminal velocity in pure water can be done by equating it with the maximum in the profile in tap water (or even dilute solutions). This is useful since it means that the need to purify water for these measurements can be relaxed.

### 5.2.2 Surfactant solutions

#### 5.2.2.1 Effect of concentration

The velocity of free rising single bubbles in surfactant solution is time, surfactant type and surfactant concentration dependent. The velocity profile of a 1.4 mm bubble in Triton X-100 solution is shown in Fig. 5.3. The findings mirror those of Sam et al.: as concentration increases the time to reach constant velocity (adsorption time) decreases but the actual terminal velocity is not greatly affected. It is also supported by the results from Zhou et al. (1991). However, on close inspection it is seen that the velocity in the case of high concentration increases with height which suggests bubble expansion due to the reducing hydrostatic pressure. The distance travelled before terminal velocity is reached depends on bubble size and surfactant concentration (Table 5.2).

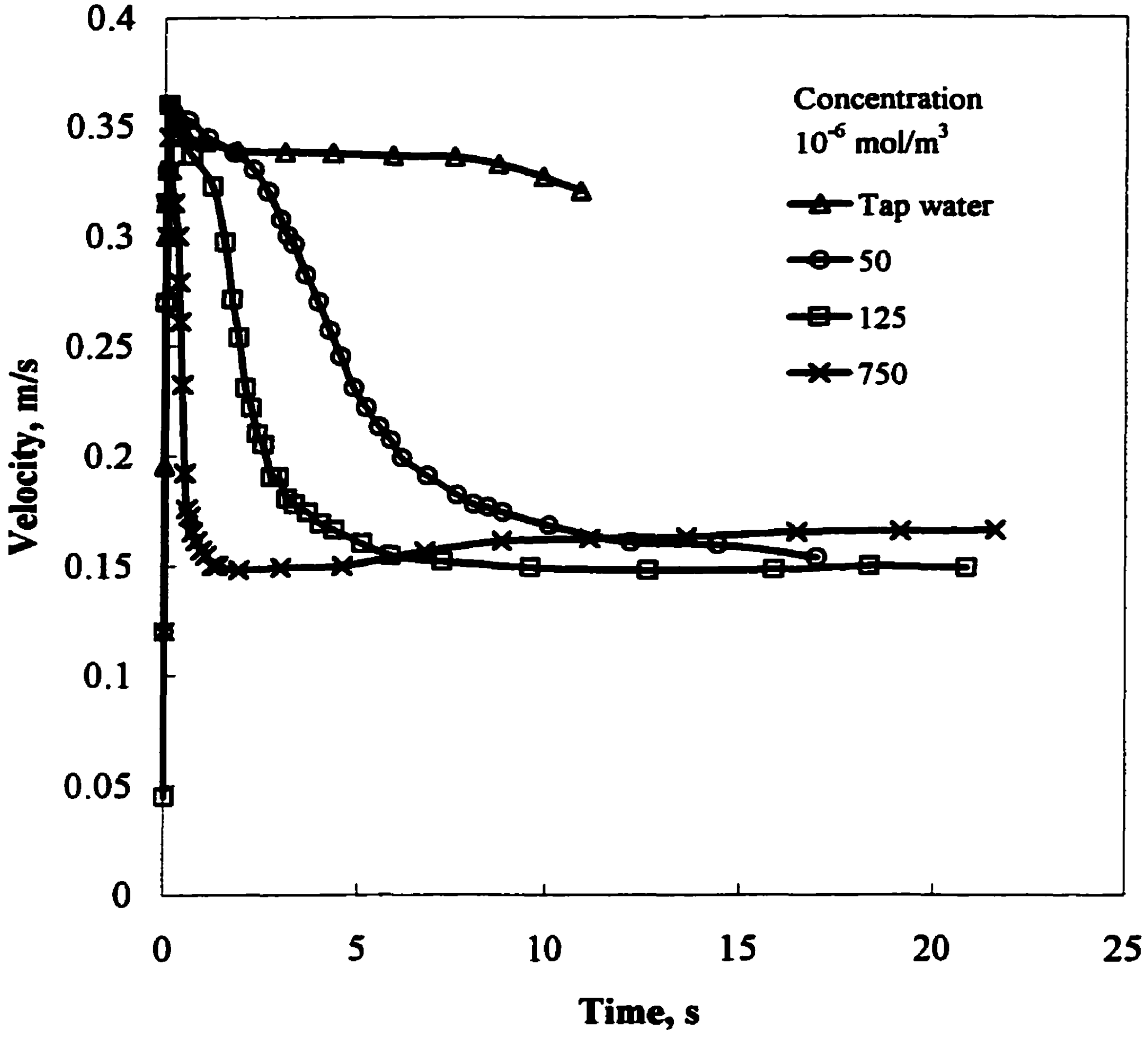

Fig. 5.3 Velocity profiles for 1.4 mm bubble in Triton X-100 solution

Table 5.2 Distance (cm) to reach terminal velocity in Triton X-100 solution

| **0.8 mm bubble** | | **1.4 mm bubble** | | **1.8 mm bubble** | |
|---|---|---|---|---|---|
| **C[#]** | **Distance*** | **C** | **Distance** | **C** | **Distance** |
| ≤2.5 | Not reached | | | | |
| 5.0 | 314 | ≤12.5 | Not reached | | |
| 12.5 | 133 | 12.5 | 265 | ≤12.5 | Not reached |
| 25.0 | 97 | 49.9 | 99 | 25.0 | 164 |
| 74.9 | 42 | 74.9 | 44 | 74.9 | 87 |

[#]Concentration in the unit of $\times 10^{-3}$ mol/m$^3$

*Distance in the unit of cm (±5)

From the distance required for a bubble to reach terminal velocity it is evident that the surface of a small bubble is more easily retarded by surfactant than that of larger bubbles. According to the stagnant cap model, the amount of surfactant needed to retard the bubble surface is related to the tangential stress. A large bubble rises fast, which induces a large shear force and hence a greater distance is needed for the bubble to accumulate the surfactant necessary to fully retard the bubble surface. To measure the terminal velocity, the distance must be sufficient for the bubble to reach this state. From the discussion of the concentration effect, it can be deduced that the surfactant type also affects the distance needed for a bubble to reach terminal velocity.

### 5.2.2.2 Effect of surfactant type

The terminal velocity of a 1.6 mm bubble[1] at 30 °C in the presence of a variety of surfactants of interest primarily in flotation is summarized in Table 5.3. The predicted velocity from Karamanev for a 1.6 mm bubble is 14.8 cm/s. The immediate observation is that the values are quite similar, ranging from 14.8 to 16.6 cm/s. The global average, 15.7 cm/s with a standard deviation of 0.8, at the 90% confidence level is greater than 14.8 cm/s. Nevertheless for most practical purpose the experimental values agree with the predicted.

Table 5.3 Terminal velocity for $d_b$=1.6 mm in surfactant solutions at 30 °C

| Surfactant | Terminal velocity ($U_t$), cm/s | |
|---|---|---|
| | **This work, (±0.5 )** | **Sam et al.** |
| DF 250 (≤30 ppm) | 16.1 | 15.6 (0.5) |
| MIBC (≤30 ppm) | 16.6 | 16.5 (0.3) |
| Pine oil (≤30 ppm) | 14.8 | 14.8 (0.2) |
| DF 1263 (≤30 ppm) | 16.8 | |
| Ethanol (≤460 ppm) | 15.1 | |
| Octanol (≤30 ppm) | 15.8 | |
| Dodecylamine (≤0.55 ppm) | 15.0 | |
| Triton X-100 (≤0.5 ppm) | 15.0 | |

---

[1] This is the size at top of the 4 m high column for a 1.4 mm bubble starting at the bottom; the size at the top is the one relevant here.

### 5.3 Conclusions

The velocity profile was used to determine the terminal velocity for a single bubble in tap water and surfactant solutions. The former was taken as the maximum in the profile, i.e., at the end of stage 1, the latter as the constant velocity attained, i.e., stage 3. The following conclusions were drawn from the study:

- The terminal velocity in pure water was larger than previous experimental values and higher than predicted from existing models.
- For 0.8 mm bubble in water, the similar terminal velocity predicted from models for both spherical bubble and deformed bubble establishes that it can be treated as spherical for subsequent modeling work (see chapters 6 and 7).
- The distance to reach terminal velocity in surfactant solutions is bubble size, surfactant type and surfactant concentration dependent.

# CHAPTER 6

# NUMERICAL MODELING OF SINGLE BUBBLE TERMINAL VELOCITY

## 6.1 Introduction

A single bubble released into dilute surfactant solution first accelerates to a maximum velocity then decelerates to reach a terminal velocity. Bubble deceleration is caused by the accumulation of surfactant at the surface. There are two extreme conditions governing bubble rise: the surface is free of surfactant resulting in a mobile surface and hence a maximum in velocity is reached; or the surface is totally covered by surfactant resulting in a retarded surface and hence a constant or terminal velocity is reached. In this chapter, modeling of the terminal velocity in pure water or surfactant solution is considered to test the fluid flow model and the numerical method, which lays the foundation of modeling the velocity profile.

There are a number of models of single bubble velocity in surfactant solution (Cuenot et al., 1997). When the surfactant transport from bulk solution to bubble surface is far slower than the adsorption kinetics and the surface convection, an immobile cap (stagnant cap) forms on the rear of the bubble. Cuenot et al. suggested that the surfactant distribution on a moving bubble in most situations of practical interest corresponds to the stagnant cap configuration. Fainerman (1998) suggested that for most surfactants non-diffusional adsorption kinetics can be expected only when $\alpha/\beta$ is larger than ca. 1 $\mathrm{mol{\cdot}m^{-3}}$. In the case of Triton X-100, the value of $\alpha/\beta$ is $6.62\times10^{-4}$ $\mathrm{mol{\cdot}m^{-3}}$ which is far less than the above criterion. The available information about Triton X-100 suggests the stagnant cap model is applicable. However, because of the lack of experimental data, it is hard to validate the claim. Karamanev (1994) reviewed the work on bubbles rising in contaminated liquids (i.e., the bubble surface is rigid), The results were in good agreement with the conclusion obtained for free rising rigid particles. The results on bubble terminal velocity in surfactant solution presented by Zhang et al. (1996) support Karamanev's model. The agreement between the drag coefficient for rigid buoyant particles and air bubbles in surfactant solution suggests the same boundary conditions apply at terminal velocity, that is, the surface is immobile. Therefore, the stagnant cap model is a logical choice.

### 6.2 Establishment of numerical method

The physical model and numerical method employed were presented in chapter 3. The governing equations are solved in a boundary fitted coordinate system which allows for deformation of the bubble.

The parameters used in the simulation are first tested for the range in Re of concern here. First the grid number in the discretization needs to be determined. McLaughlin (1996) used three grid numbers in both $\xi$ and $\eta$ directions, 61, 81 and 101. Two grid numbers were tested here for a mid sized (1.5 mm) bubble. The results are shown in Table 6.1. The grid number chosen was 61 rather than 81 because the difference was minimal but computer time was reduced.

Table 6.1 Test of grid number for 1.5 mm bubble

| **Grid No.** | **Re** |
|---|---|
| 61 | 293 |
| 81 | 292 |
| difference | <0.4% |

The effect of the bubble shape on the simulation results was also tested for 1.5 mm bubble. The shape of the bubble is shown in Fig. 6.1, the axis ratio (y/x) is 1.057 with the boundary fitted coordinates. The difference in Re is not significant as shown in Table 6.2. However, the computing time shows a large difference.

Table 6.2 Test of boundary fitting algorithm

| **Algorithm** | **Re** | **Time, hr** |
|---|---|---|
| **Boundary fitting** | 290 | 168 |
| **No boundary fitting** | 295 | 40 |

Therefore, for bubble size ≤ 1.5 mm, the conditions of the numerical simulation can be relaxed to save computing time. The parameters used in the simulation are listed in Table 6.3.

Table 6.3 Parameters used in the program

| $\Delta t$ | $\beta_h$ | $\beta_\omega$ | $N_\eta$ | $N_\xi$ | Iteration No. |
|---|---|---|---|---|---|
| 0.05 | $10^{-2}$ | $5\times10^{-4}$ | 61 | 61 | $2\times10^{4}$ |

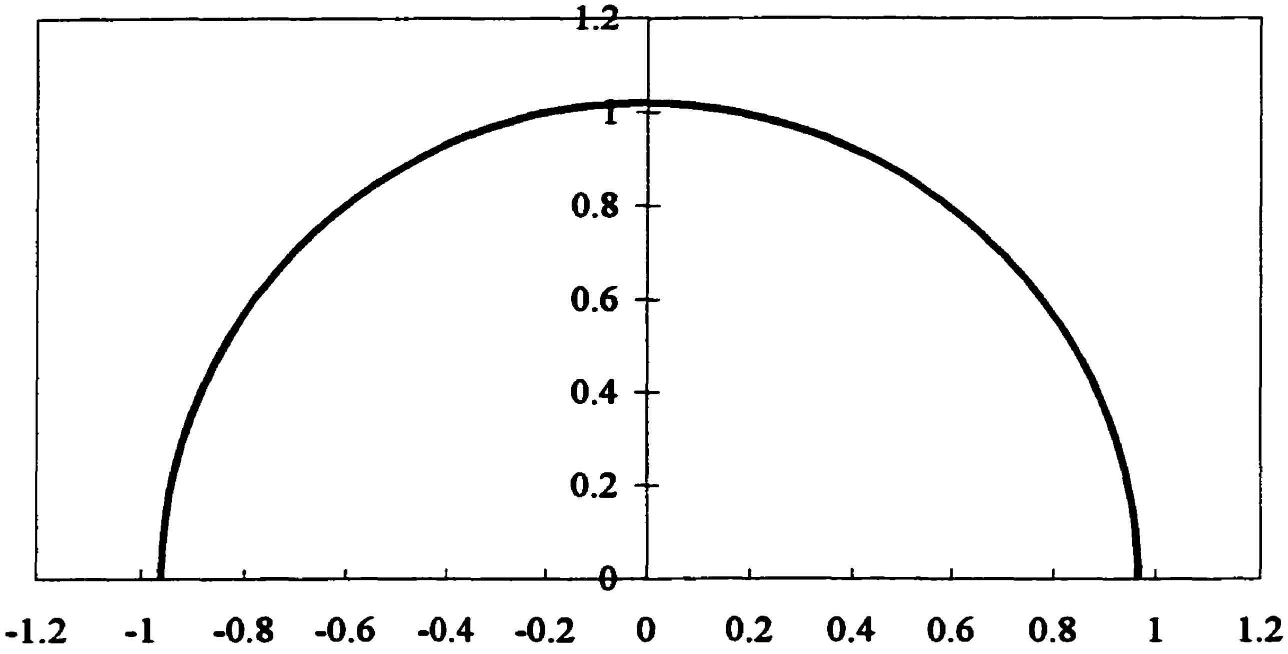

Fig. 6.1 Bubble shape from simulation of a 1.5 mm bubble

### 6.3 Simulation results for terminal velocity in water and surfactant solution

In chapter 5, the terminal velocity of 1.4 mm bubble in different surfactant solutions was investigated. The experimental results showed that the empirical model of Karamanev gave a good estimation of the terminal velocity as long as the Re>130. For Re<130, the drag coefficient of an air bubble is considered to be the same as that of a free falling sphere. The empirical correlation from Schiller and Naumann (1933) for the drag coefficient of a falling sphere can be substituted into the general equation for terminal velocity, which was employed by Finch and Dobby (1990). From Table 6.4 we can see the simulated results are in good agreement with the experimental data and the velocity calculated from the empirical correlations. For the 1.4 mm (1.6 mm at top) bubble in surfactant solution the simulated terminal velocity is higher than the experimental, which may reflect that the assumption of the flow remaining symmetric up to this Re (= 249) is not valid. Visually, the path was slightly zigzag for the 1.4 mm bubble. In general, however, the stagnant cap model and the numerical method adequately predict single bubble terminal velocity. The simulation results also conform to the results of Duineveld (1996). Predicting the terminal velocity is an essential first step in simulation of the velocity profile.

The discrepancy between the experiment and the simulated velocity for the large bubble suggests that at high Re only modifying bubble deformation is not enough. The asymmetric flow should be considered in the model. Further work needs to be done in this regard for large bubbles.

Table 6.4 Comparison of the experimental, simulation and empirical velocity (cm/s) results (25 °C)

a) Water

| $d_e$, mm[1] (±0.05) | Experiment | Simulation | Empirical models | |
|---|---|---|---|---|
| | | | **Clift et al.** | **Moore & Sawi** |
| 1.4 | 36.0 | 32.8 | 34.3 | 33.6 |
| 0.8 | 23.2 | 22.2 | NA | 22.0 ($\chi$=0) |

NA, not applicable.

[1] diameter near bottom, i.e., close to position of maximum velocity.

b) Surfactant solution

| $d_e$, mm[2] (±0.05) | Experiment | Simulation | Empirical models | |
|---|---|---|---|---|
| | | | **Karamanev** | **Finch/Dobby** |
| 2.0 | 16.4 | NA | 16.6 | 21.3 |
| 1.6 | 14.8 | 16.7 | 14.8 | 17.6 |
| 0.9 | 10.9 | 10.5 | 11.1 | 10.5 |

[2] diameter at top, relevant in this case.

## 6.4 Effect of frother type on single bubble velocity

According to the stagnant cap model of adsorption and the mechanism of deceleration, the bubble surface is immobile as long as the bubble surface is totally covered by surfactant. Therefore, surfactant type should have no effect on the terminal velocity as long as the stagnant cap model holds. According to the experimental data discussed in the previous chapters, while surfactant type affects the dynamic adsorption part of the profile, the terminal velocity is not much affected by the frother type as evident in Table 5.3. The stagnant cap model is applicable when the surface activity is strong as compared to diffusivity. The data in Table 5.3 do reveal certain variations. Further work is needed to investigate surfactant types resulting in larger terminal velocities to establish quantitative criterion for the stagnant cap model.

### 6.5 Bubble velocity with stagnant cap ($0< \theta <180$)

The velocity of a small bubble (0.8 mm) was simulated as a function of stagnant cap angle. The drag on the bubble as a function of angle for this size bubble is shown in Fig. 6.2. As the angle (i.e., size) of stagnant cap increases the drag increases. The drag coefficient increased from 0.21 for a clean bubble to 1.2 for a fully covered bubble. McLaughlin (1996) studied the effect of stagnant cap angle on the drag coefficient at fixed Re and We. The representation here shows the sole effect of the build-up of surfactant. From the physical model, i.e., stagnant cap model, the bubble velocity is only dependent on the size of stagnant cap.

### 6.6 Surfactant coverage on bubble surface

The surface tension on the bubble changes with the angle. The Marangoni force balances the tangential stress (eq. 3-26). For a fully covered bubble, the surface tension at the top of the bubble (cap angle $180^{\circ}$) is assumed to be that of the solution (in dilute solution, it is the same as that of water). The surface tension is the lowest at the bottom of the bubble. The concentration of surfactant on the bubble surface was calculated from the Langmuir isotherm (eq. 3-27). The average surface coverage on the bubble surface increases with the size of stagnant cap (Fig. 6.3).

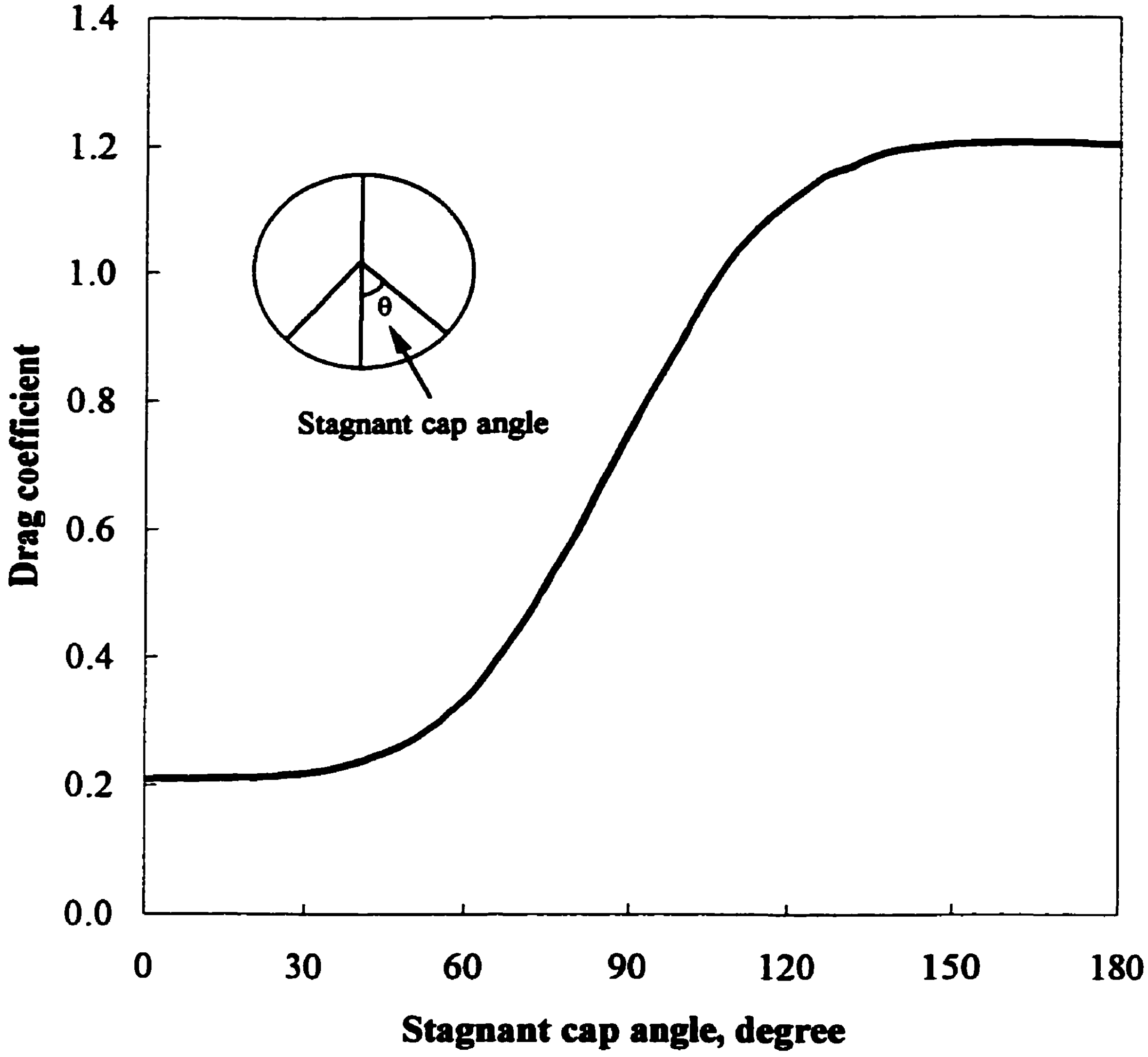

Fig. 6.2 Drag coefficient vs. stagnant cap angle

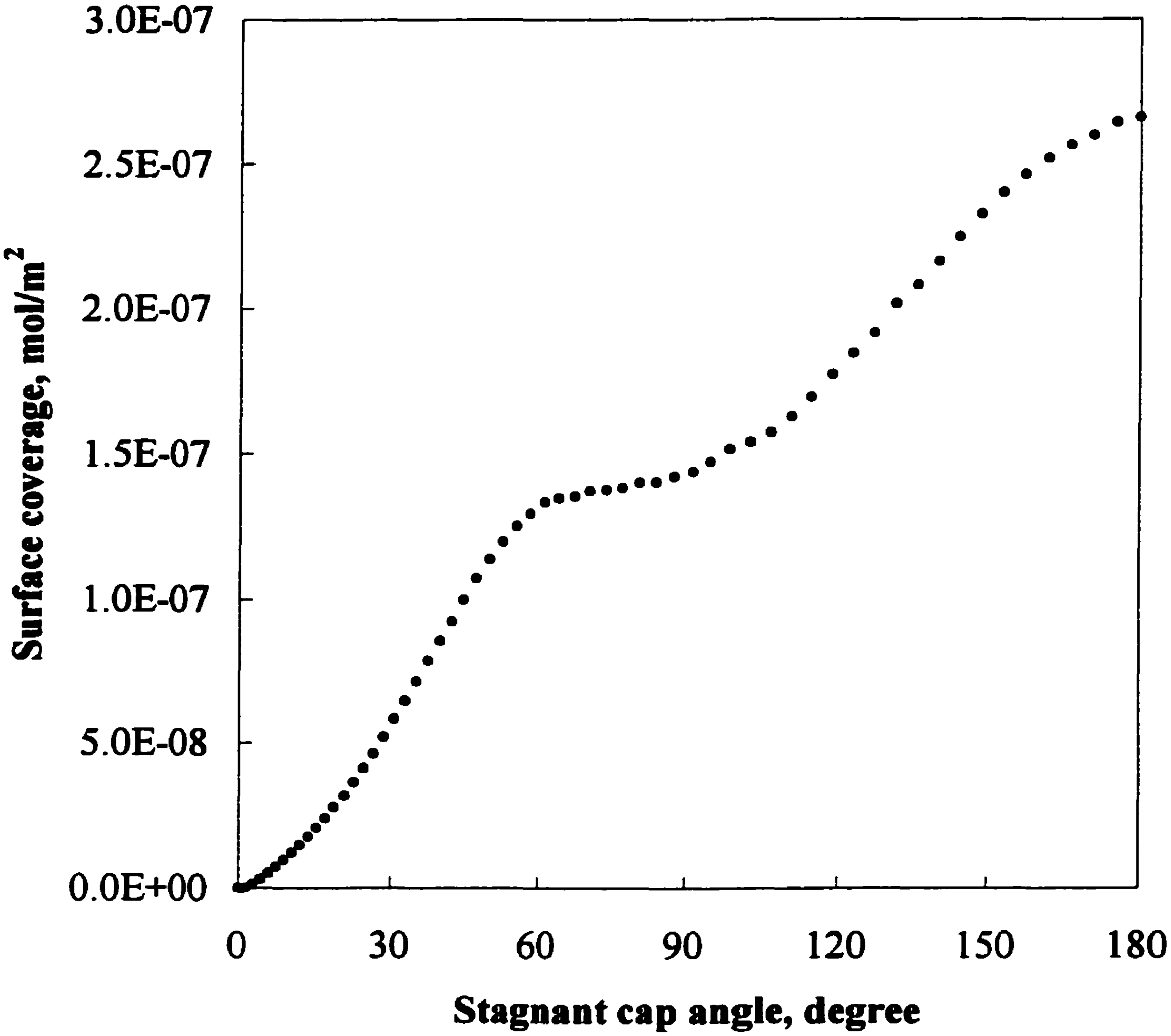

Fig. 6.3 Average surfactant coverage vs. stagnant cap angle

The surface coverage is bubble size dependent when the bubble surface is fully covered by surfactant. This is because the surfactant layer is more compressed on a larger bubble due to its higher rise velocity. To illustrate, the amount of surfactant on a 0.8, 1.0 and 1.5 mm bubble is shown in Table 6.5; the average surface coverage on the 0.8 mm bubble is about 3/8 that on the 1.5 mm bubble.

Table 6.5 Average surfactant on different size bubbles

| **Bubble size, mm** | **Average $\Gamma$, mol/m$^2$** | **Relative carrying capacity** |
|---|---|---|
| 0.8 | $2.7\times10^{-7}$ | 1 |
| 1.0 | $3.8\times10^{-7}$ | 1.3 |
| 1.5 | $8.0\times10^{-7}$ | 1.6 |

In flotation, micro bubbles are often considered necessary to collect small particles because of the high surface area supplied. Equipment developments continuously try to produce small bubbles (down to10 μm) (Owen et al., 1999). From the simulation results, it is clear that the average surfactant coverage decreases as bubble size decreases under the stagnant cap constraint. This higher bubble surface area per unit volume of gas of small bubbles is therefore offset by a decreased surfactant loading per bubble. Taking this into account the relative carrying capacity for the different size bubbles was calculated (Table 6.5) which shows that larger bubbles actually have a higher capacity

### 6.7 Conclusions

The terminal velocity of single bubble was simulated using the stagnant cap model. The good agreement between experimental and simulated values in pure water and in surfactant solutions showed that the physical model and numerical solution are valid. Simulation showed the average surfactant coverage is bubble size dependent.

# CHAPTER 7

# MODEL OF VELOCITY PROFILE

## 7.1 Introduction

In chapter 6, the stagnant cap model and the numerical method were used to simulate the bubble terminal velocity. The good agreement between simulation and experimental data validated the numerical method. The results show that the stagnant cap model satisfactorily represents the terminal velocity in both pure water and dilute surfactant solutions at least for the small bubbles (< 2 mm) of interest to flotation.

The surfactant distribution over the bubble surface is determined by the fluid flow around the bubble and the mass transfer of surfactant from bulk solution to the bubble surface. The mass transfer is controlled by one or a combination of the following three rate limiting steps: boundary layer mass transfer in the continuous phase, adsorption-desorption kinetics at the interface, and mass transfer on the interface.

The adsorbed surfactant layer on a moving bubble, termed the dynamic adsorption layer, differs from the equilibrium absorbed surfactant layer at a stationary air/water interface in both its angular dependence and the average amount adsorbed (Sadhal and Johnson, 1983; Dukhin et al., 1995; Warszynski et al., 1996). However, there are no experimental data to confirm the theoretical work concerning the existence and the effect of the dynamic adsorption layer on bubble motion.

In this chapter, the single bubble velocity profile is simulated by a combination of numerical simulation of the quasi-steady state bubble velocity employing the stagnant cap model and empirical mass transfer models. The results from simulation are compared with the experimental velocity profile for a 0.8 mm (size at the bottom of column) bubble to determine the suitable mass transfer mechanisms.

## 7.2 Physical models for mass transfer

According to the theoretical analysis in chapter 3, the bubble surface can be regarded as having two distinct parts: the bare leading surface free of surfactant and the stagnant cap on the trailing (lower) part of the bubble. The mass transfer at each part of the surface is treated differently.

### 7.2.1 Boundary layer mass transfer control at bare surface with simulated surface coverage

For the 0.8 mm diameter bubble of concern here, fluid flow around the bubble separates as the stagnant cap angle becomes larger than 35° (Fig. 7.1). Therefore the flow boundary layer and mass transfer boundary layer at the rear of the bubble are much thicker than those at the front. The adsorption and desorption at the rear part of the bubble can be ignored because of the thick diffusion boundary layer and small diffusion coefficient ($D=2.6\times10^{-10}$ $m^2/s$, Lin et al., 1990). The mass transfer coefficient is $3.05\times10^{-5}$ m/s for a 0.8 mm rigid sphere calculated from eq. (2-27) using the experimental terminal velocity. The mass transfer coefficient for the same size mobile bubble calculated from eq. (2-26) is in the range $16.2\times10^{-5}$ to $27.1\times10^{-5}$ m/s corresponding to a velocity ranging from the terminal velocity to the maximum velocity, respectively.

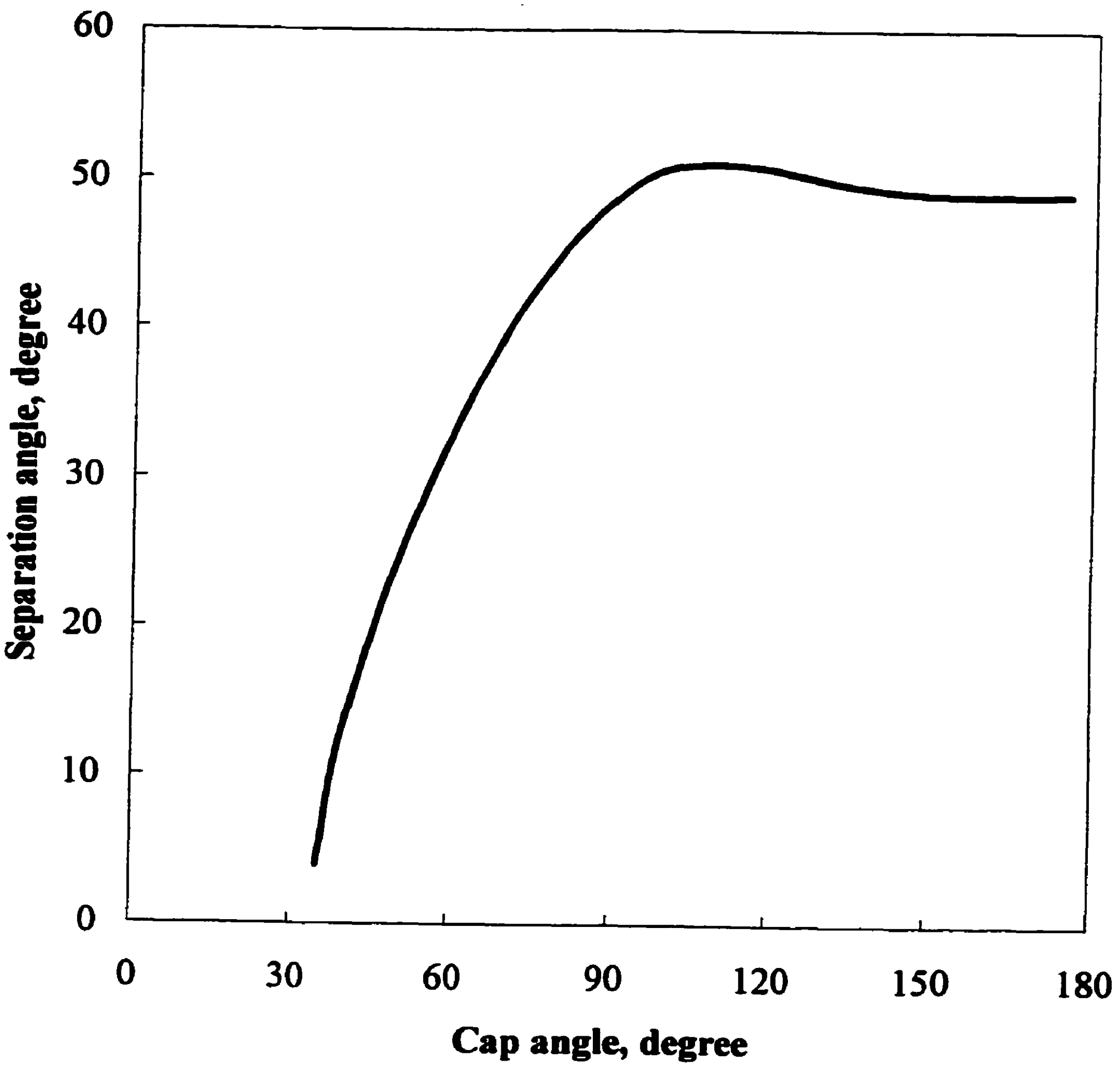

Fig. 7.1 Separation angle vs. stagnant cap angle for a 0.8 mm bubble

The relatively small mass transfer coefficient at the stagnant cap allows the surfactant to accumulate, which supports the choice of the stagnant cap model. If the mass transfer at the stagnant cap is ignored, the approximation of eq. (3-14) results in:

$$S_b k\Delta c|_{S_b} = \frac{d(S_{sc}\Gamma)}{dt} \tag{7-1}$$

$$dt = \frac{d_e}{Sh}\frac{1}{(1+\cos\theta)}\frac{1}{c_\infty}\frac{1}{D}d[\Gamma(1-\cos\theta)] \tag{7-2}$$

### 7.2.2 Boundary layer mass transfer control at the entire bubble surface with simulated surface coverage

Considering mass transfer at both the bare surface and the stagnant cap, the integration of the mass balance equation over the whole surface yields:

$$dt = \frac{d[\Gamma(1-\cos\theta)]}{\left[D(1+\cos\theta)c_\infty \dfrac{Sh}{d_e} + (1-\cos\theta)(c_\infty - c_s)k\right]} \tag{7-3}$$

### 7.2.3. Adsorption kinetic control at the entire bubble surface with simulated surface coverage

Suppose that surface adsorption kinetics is the mass transfer control step, and that surface coverage is the same as the simulated result from the stagnant cap model, then the integration of the mass balance equation over the whole surface becomes:

$$S_b \beta c_\infty \Gamma_\infty + S_{sc} \beta c_\infty (\Gamma_\infty - \Gamma) - S_{sc} \alpha \Gamma = \frac{d(S_{sc}\Gamma)}{dt} \tag{7-4}$$

$$dt = \frac{1}{\beta} \frac{d[\Gamma(1-\cos\theta)]}{2c_\infty \Gamma_\infty - (1-\cos\theta)(\frac{\alpha}{\beta} + c_\infty)\Gamma} \tag{7-5}$$

### 7.2.4 Boundary layer mass transfer control at the entire bubble surface with maximum surface coverage ($\Gamma_\infty$)

The simulated surface coverage is obtained by the force balance on the bubble surface. For a moving bubble, it is believed to be different from both the equilibrium and maximum surface coverage at steady state (Dukhin et al., 1995). The actual surface coverage on a moving bubble may be solved by matching the simulated velocity profile to the experimental data. On the other hand, the comparison of experimental data and the simulated results could validate the model. Supposing the average surface coverage on the stagnant cap is the maximum surface concentration, the integration of the mass balance equation over the whole surface is then:

$$dt = \frac{\Gamma_\infty d(1-\cos\theta)}{\left[D(1+\cos\theta)c_\infty \frac{Sh}{d_e} + (1-\cos\theta)(c_\infty - c_s)k\right]} \tag{7-6}$$

### 7.2.5 Boundary layer mass transfer control at the entire bubble surface with equilibrium surface coverage ($\Gamma_e$)

If the average surface coverage over the stagnant cap part of the bubble is identical to the equilibrium surface coverage at steady state, the integration of the mass balance equation with boundary layer mass transfer over the whole surface will be:

$$dt = \frac{\Gamma_e d(1-\cos\theta)}{\left[D(1+\cos\theta)c_\infty \frac{Sh}{d_e} + (1-\cos\theta)(c_\infty - c_s)k\right]} \tag{7-7}$$

The equilibrium surface coverage can be obtained by solving the Langmuir kinetic equation at equilibrium:

$$\Gamma_e = \frac{\beta c_\infty}{\beta c_\infty + \alpha}\Gamma_\infty \tag{7-8}$$

### 7.2.6 Adsorption kinetic control at the entire bubble surface with equilibrium surface coverage

If surface adsorption is the mass transfer control step, the mass transfer boundary layer can be ignored. The concentration in the sublayer should then be the same as the bulk concentration. The surface coverage on the bubble will be at equilibrium with the bulk solution, which is close to the completely stagnant surface model proposed by Cuenot et al. (1997). Integration of the mass balance equation over the whole surface yields:

$$S_b \beta c_\infty \Gamma_\infty = \frac{d(S_{stc}\Gamma_e)}{dt} \tag{7-9}$$

$$dt = \frac{1}{\beta}\frac{\Gamma_e d(1-\cos\theta)}{c_\infty \Gamma_\infty (1+\cos\theta)} \tag{7-10}$$

### 7.3 Results

Simulations for the six physical models were performed. The simulated profiles are compared with the experimental data for a 0.8 mm diameter bubble at three concentrations of Triton X-100, $2.5\times10^{-5}$, $12.5\times10^{-5}$ and $74.9\times10^{-5}$ mol/m$^3$. The physical parameters for Triton X-100 used in the simulation are from Lin et al. (1990) listed in Table 4.1.

#### 7.3.1 Boundary layer mass transfer control at bare surface with simulated surface coverage

Fig. 7.2 shows the simulated velocity profiles are close to the experimental profiles for the higher two concentrations. The maximum velocities agree with the experimental. However, the simulated terminal velocities are smaller than the experimental values. This may reflect the need to modify bubble size along the column by taking into account expansion in the simulation. At low surface coverage (short time) the simulated time is larger than the experimental result while at a higher coverage (stagnant cap angle about 68°) the simulated value is less than the experimental. This discrepancy may be caused by the simplifications in the simulation, such as ignoring the adsorption during the acceleration stage and the bubble expansion along the rise path.

Generally, the simulation results are a satisfactory fit to the experimental.

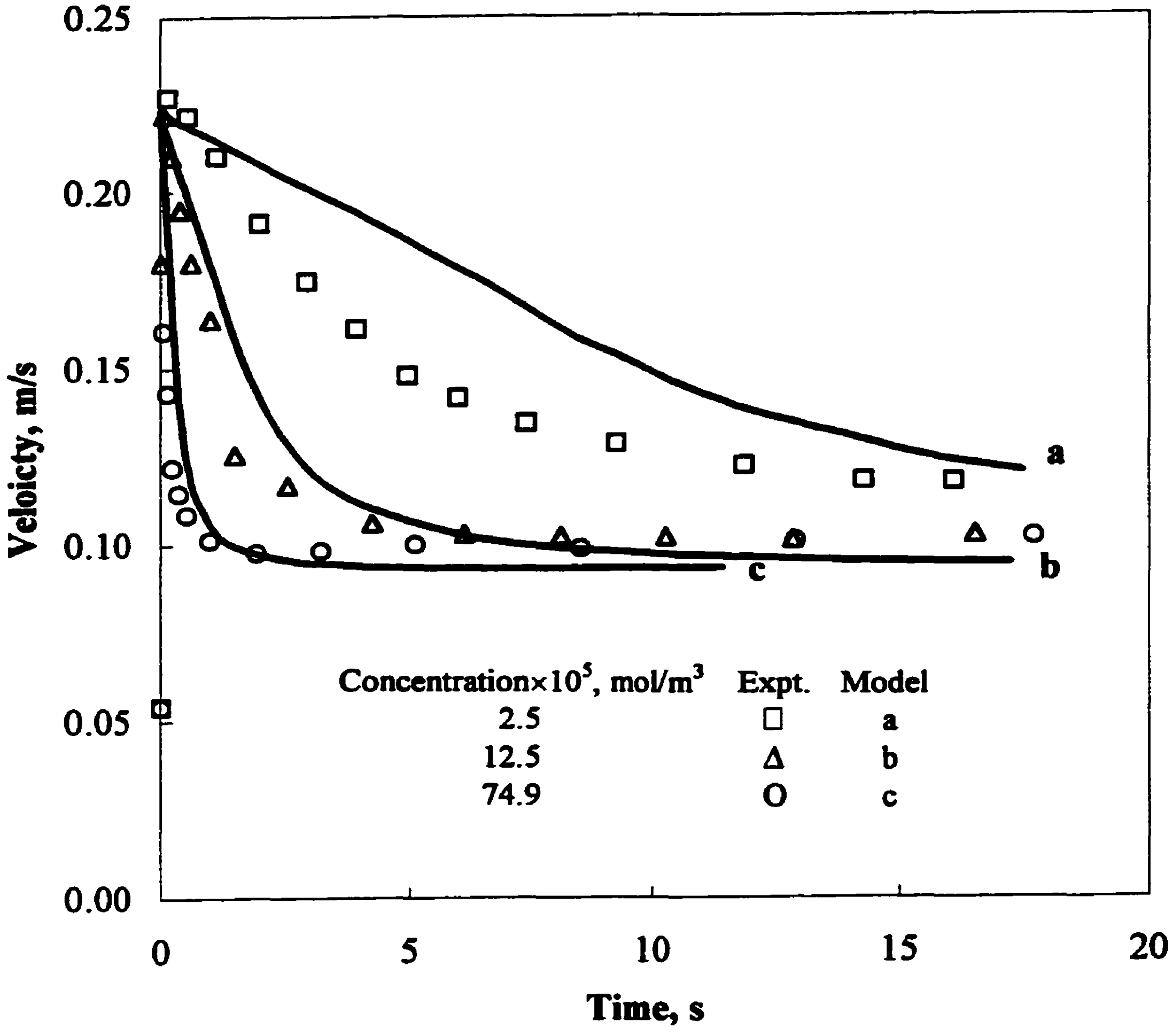

Fig. 7.2 Test of model of boundary layer mass transfer control at bare surface with simulated surface coverage. The lines are the simulation results, points experimental data.

### 7.3.2 Boundary layer mass transfer control at the entire bubble surface with simulated surface coverage

In Fig. 7.2 mass transfer at the stagnant cap was ignored. Fig. 7.3 shows the result when the mass transfer is considered. Comparison of Fig. 7.2 and Fig. 7.3 shows little difference, which supports the approximation to the mass transfer used in Fig. 7.2. The low mass transfer rate at the stagnant cap further supports the stagnant cap model as reasonable.

### 7.3.3 Adsorption kinetic control at the entire bubble surface with simulated surface coverage

The simulation results with adsorption kinetic control on the entire bubble surface (Fig. 7.4) show the times needed to reach a specified velocity (i.e., specified stagnant cap angle) at different concentrations are all larger than the experimental values and larger than the simulated times with the boundary layer mass transfer control assumption. By comparison with the first two cases it can be concluded that the boundary layer mass transfer is more likely the rate controlling process than adsorption kinetics. This conclusion also supports employing the stagnant cap model for the retardation of 0.8 mm bubble by Triton X-100.

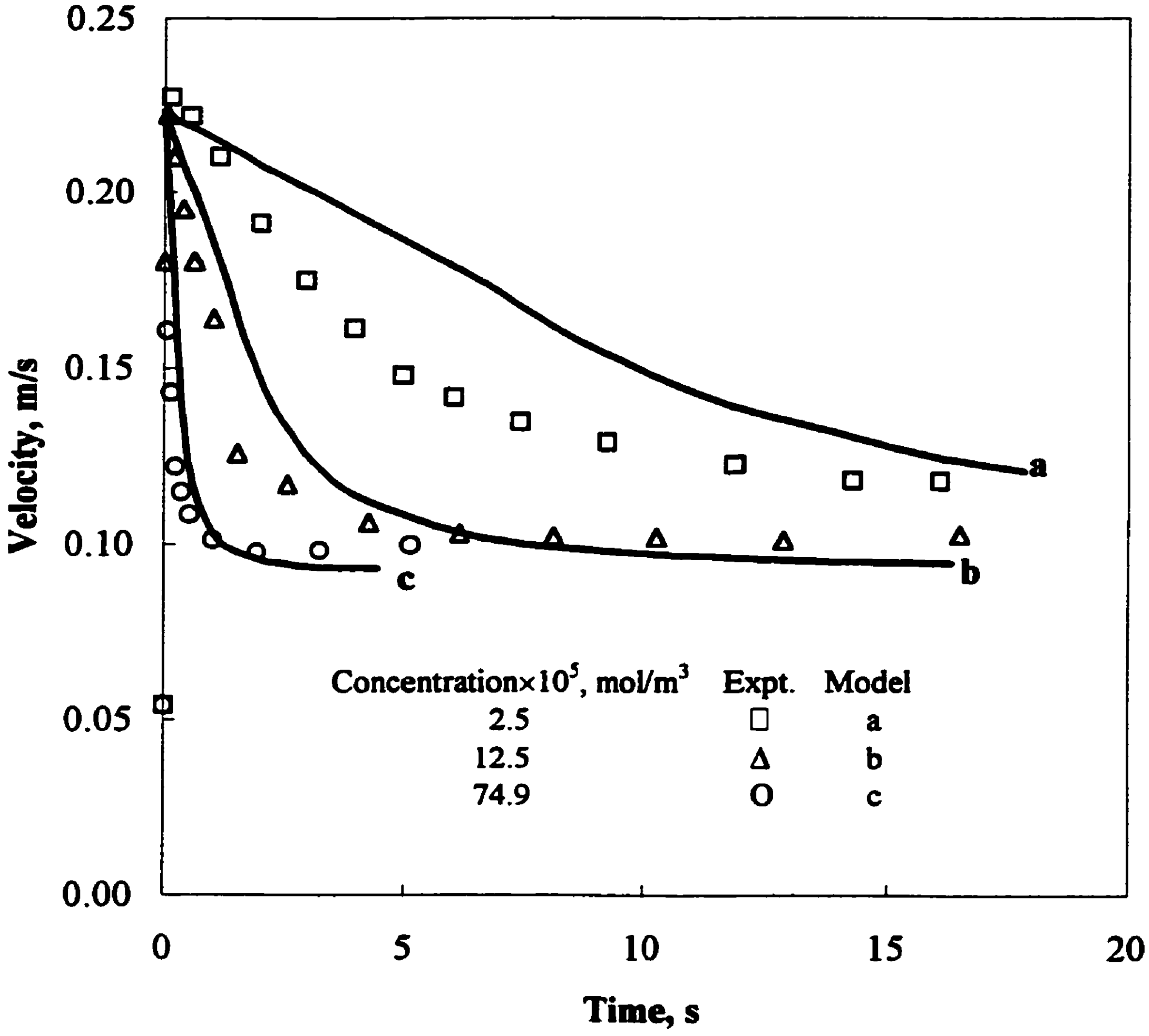

Fig. 7.3 Test of model of boundary layer mass transfer control at the entire bubble surface

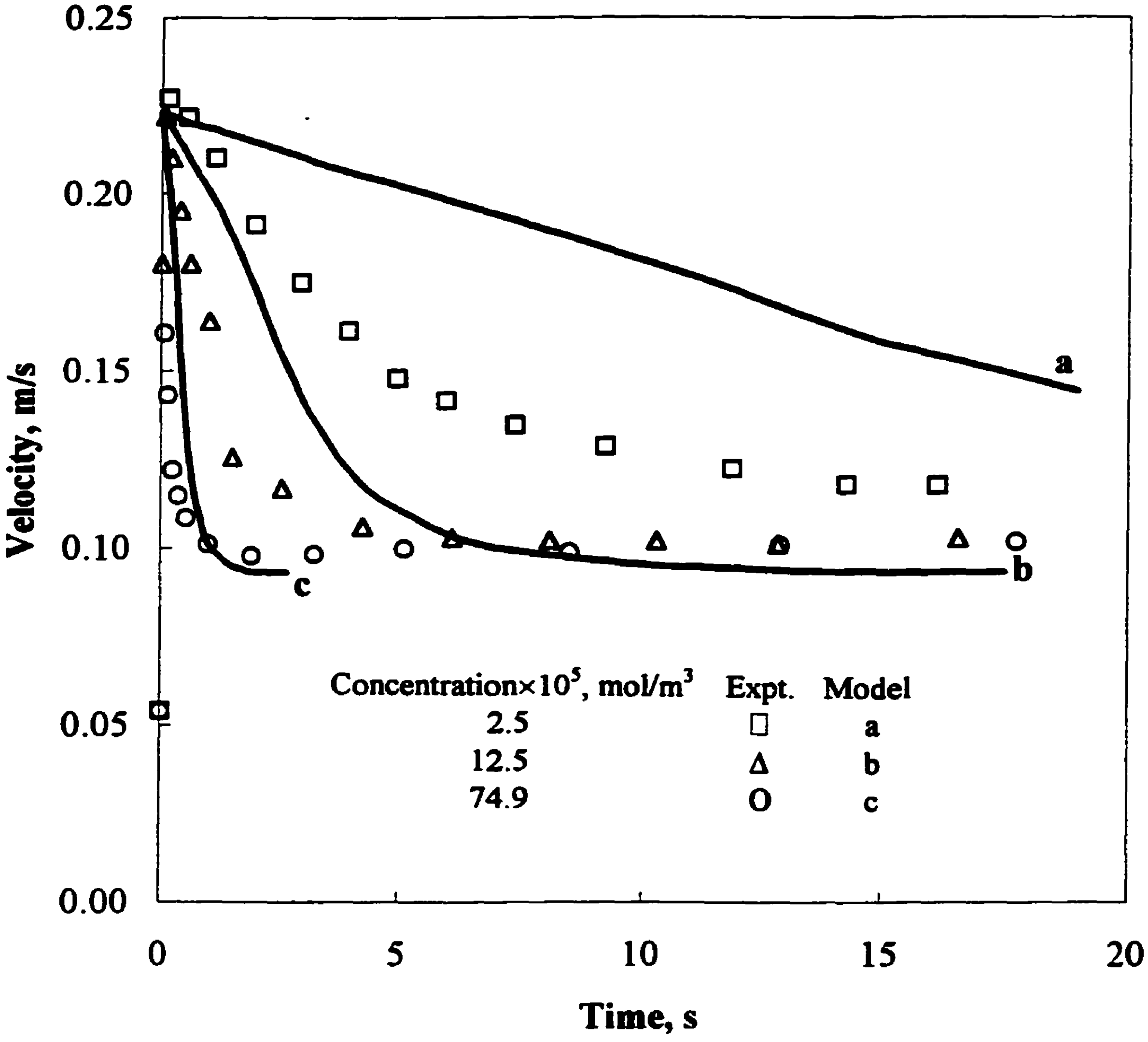

Fig. 7.4 Test of model of adsorption kinetic control at the entire bubble surface with $\beta$=50 $m^3 \cdot mol^{-1} \cdot s^{-1}$

In the above simulation, the Langmuir constant ($\alpha/\beta$) was set as $6.63\times10^{-4}$ mol·m$^{-3}$ (Lin et al., 1990). The value of $\beta$ was chosen as 50 m$^{3}$·mol$^{-1}$·s$^{-1}$, which corresponds to the lower bound of $\alpha$ given by Lin et al. The value of the adsorption rate constant could be larger. The velocity profiles, therefore, are also simulated for values of $\beta$ equal to 100 and 200 m$^{3}$·mol$^{-1}$·s$^{-1}$. The results are shown in Fig. 7.5 and Fig. 7.6.

Modifying the adsorption rate constant does result in a better fit to the experimental data as shown in Fig. 7.5. However, there is an inconsistency with the stagnant cap model, which will be discussed in section 7.4.

### 7.3.4 Boundary layer mass transfer control at the entire bubble surface with maximum surface coverage ($\Gamma_\infty$)

The surface coverage on the bubble is affected by the shear force. It may be suspected that under shear compression the amount of surfactant in the dynamic adsorption layer reaches the maximum surface coverage for the stationary state. The profiles in Fig. 7.7 show the time needed to reach maximum surface coverage (for stationary state) is much larger than the experimental measurement. Therefore, maximum surface coverage is not reached in the concentration range studied, which shows the two-phase surfactant isotherm proposed by Andrews et al. (1988) is not applicable here.

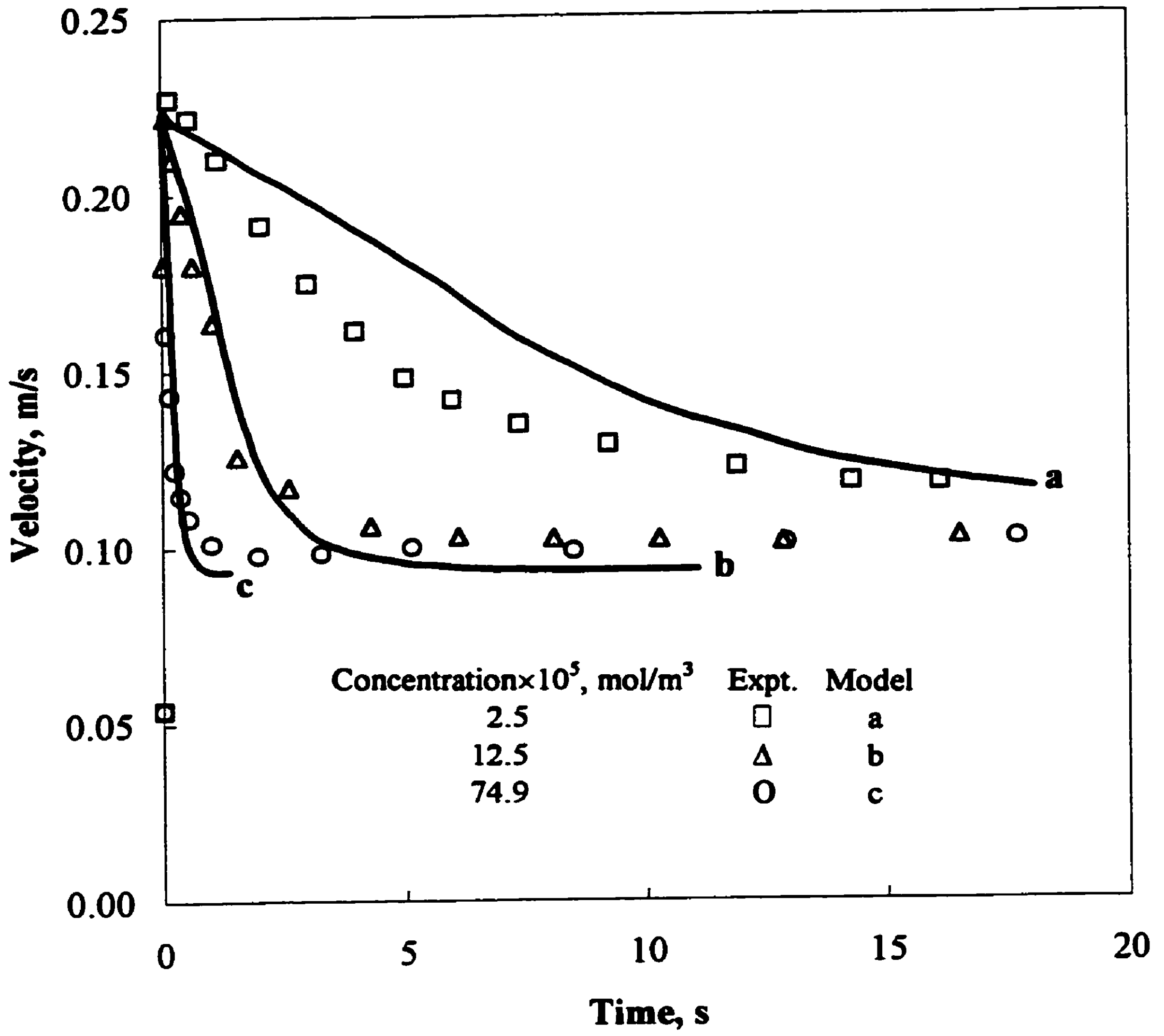

Fig. 7.5 Test of model of adsorption kinetic control at the entire bubble surface with $\beta$=100 $m^3 \cdot mol^{-1} \cdot s^{-1}$

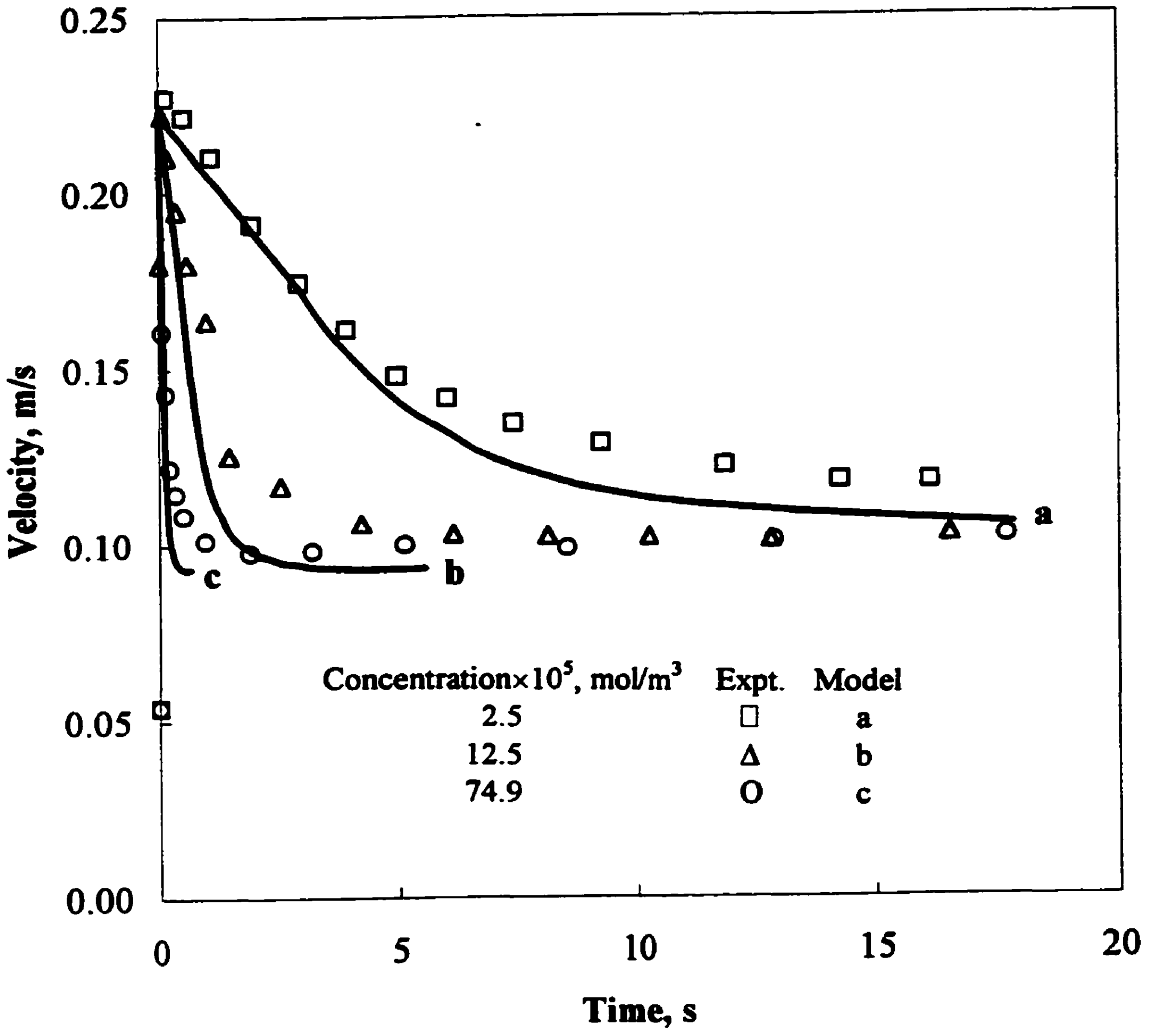

Fig. 7.6 Test of model of adsorption kinetic control at the entire bubble surface with $\beta$=200 m$^3$·mol$^{-1}$·s$^{-1}$

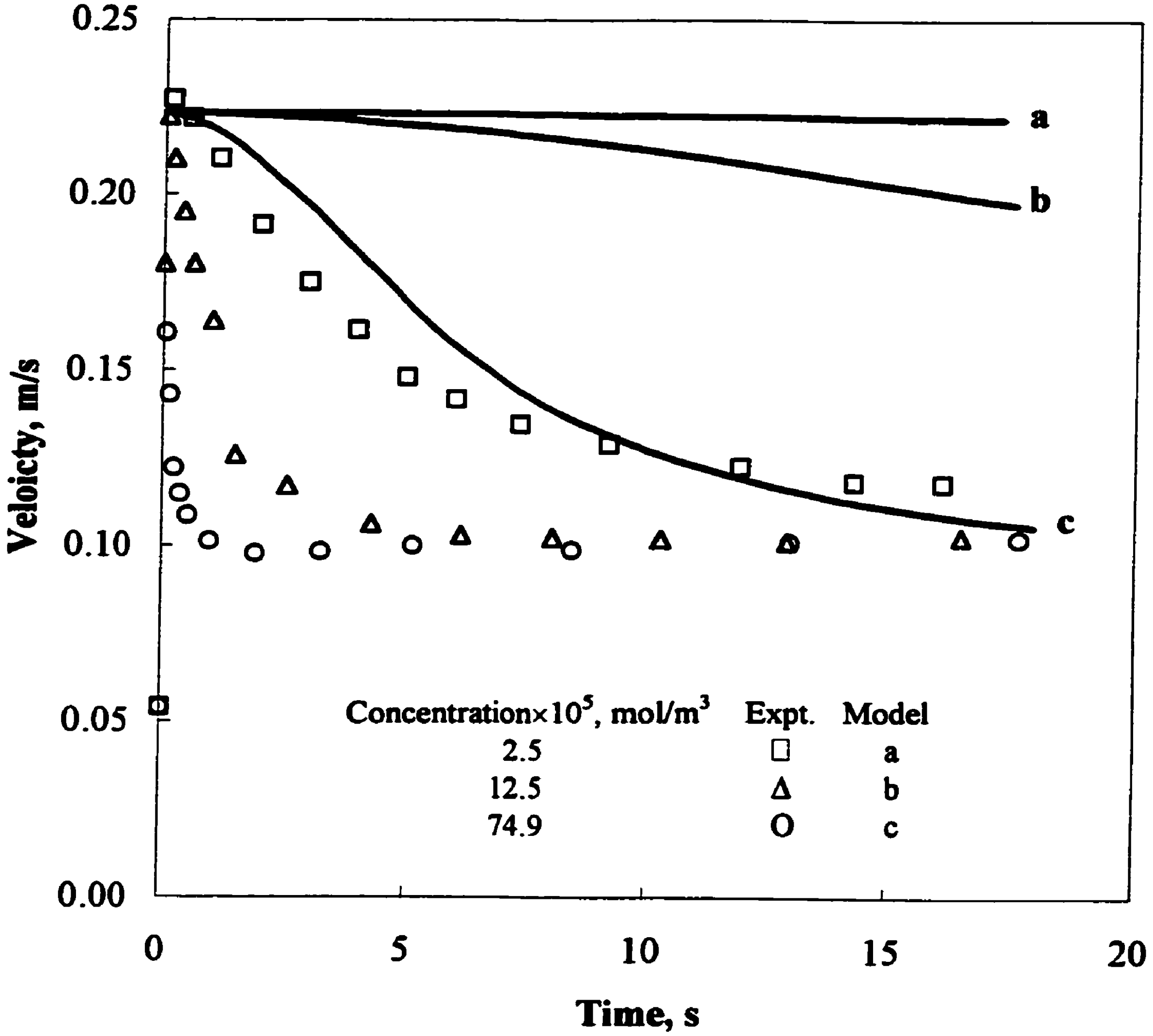

Fig. 7.7 Test of model of boundary layer mass transfer control at the entire bubble surface with maximum surface coverage

### 7.3.5 Boundary layer mass transfer control at the entire bubble surface with equilibrium surface coverage ($\Gamma_e$)

Assuming the surface coverage in the dynamic adsorption layer is the same as the stationary equilibrium state value the simulated results show much weaker concentration dependence for the velocity profiles (Fig. 7.8). Therefore, the surface coverage on a moving bubble is not the same as the equilibrium surface coverage reached in the stationary state.

### 7.3.6 Adsorption kinetic control at the entire bubble surface with equilibrium surface coverage

In the completely stagnant surface model proposed by Cuenot et al. (1997) surface coverage on the bubble is very close to the equilibrium surface coverage. Under this assumption, the adsorption of surfactant is the mass transfer control step. The simulation results, Fig. 7.9, show the simulated profiles have relatively little concentration dependency compared to the experimental data. This signifies that equilibrium surface coverage and adsorption control are not applicable.

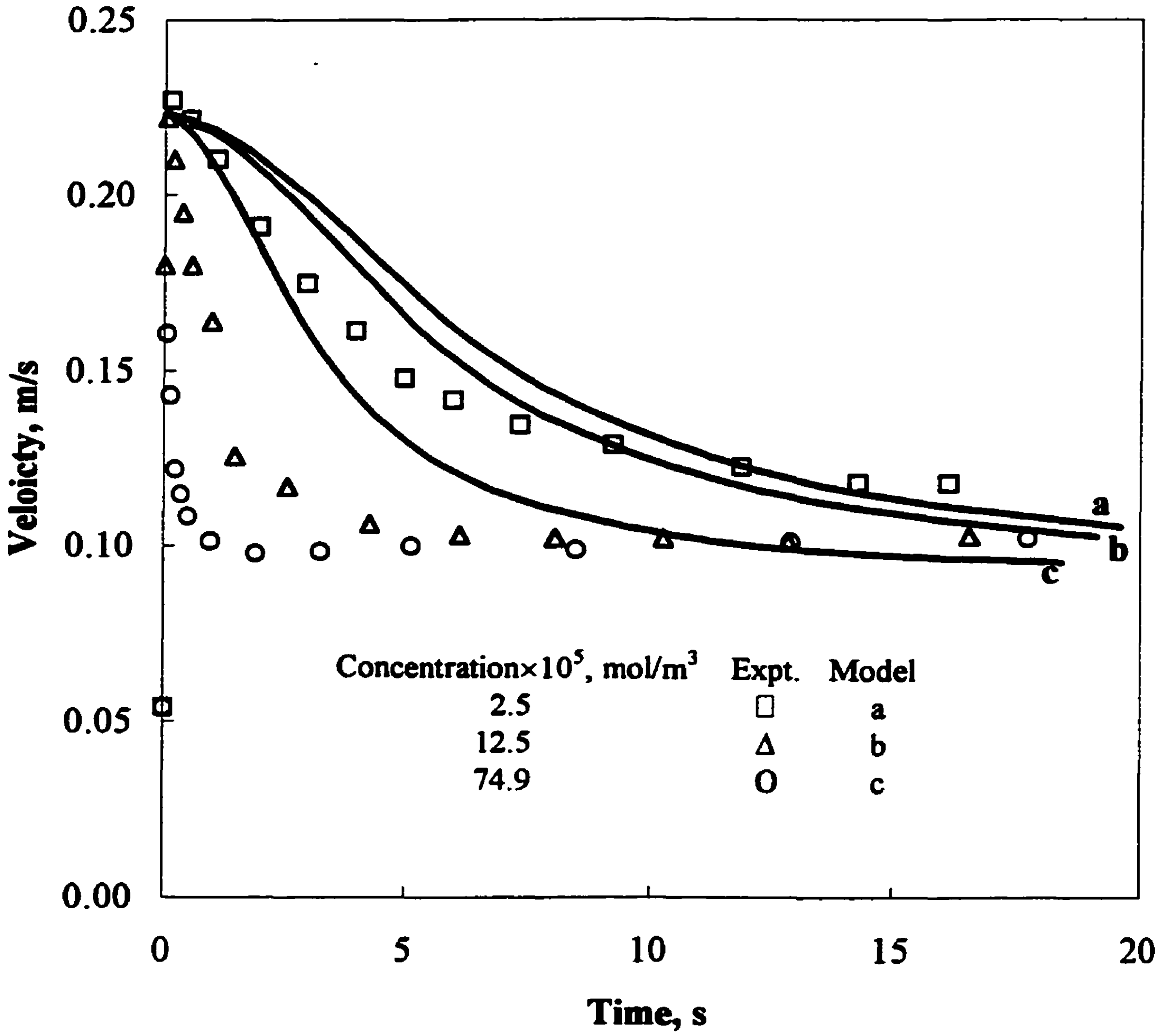

Fig. 7.8 Test of model of boundary layer mass transfer control with equilibrium surface coverage at the entire bubble surface

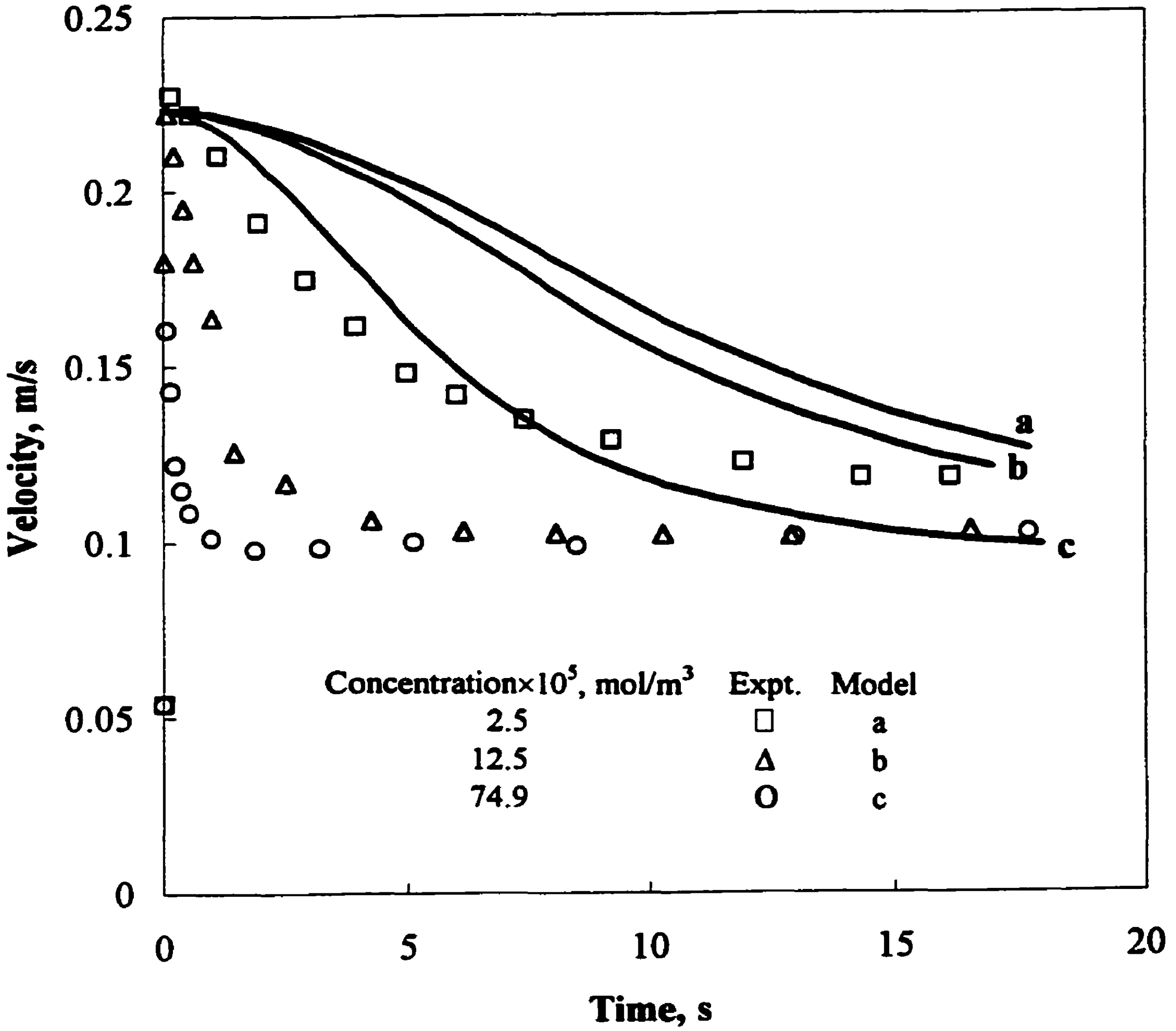

Fig. 7.9 Test of model of adsorption kinetic control at the entire bubble surface with equilibrium surface coverage, $\beta$=50 $m^3 \cdot mol^{-1} \cdot s^{-1}$

### 7.4 Identifying the best model

The square root of the mean squared difference between the simulated value and experimental data (Δ) can be used to compare the models. The definition of Δ is shown in eq. (7-11), where n is the number of experimental data sets.

$$\Delta = \sqrt{\frac{(U_{exp} - U_{simulated})^2}{n-1}} \tag{7-11}$$

Table 7.1 The value of Δ for the 6 models discussed

| **Model** | **Δ, m/s** |
|---|---|
| 1 | 0.03 |
| 2 | 0.02 |
| 3 | 0.06 (β=50) |
|  | 0.02 (β=100) |
|  | 0.02 (β=200) |
| 4 | 0.07 |
| 5 | 0.05 |
| 6 | 0.12 |

Comparison of the Δ value for the 6 models shows that model 7.3.2, which assumes boundary layer mass transfer to the whole bubble surface is the rate controlling step, has the best fit to the experimental data. The difference between model 7.3.1 and 7.3.2 is that the mass transfer on the stagnant cap is ignored in model 7.3.1. The value of Δ increased from 0.02 to 0.03 (m/s) as a consequence, which confirms the mass transfer at the stagnant cap is much smaller than that at the front, bare surface.

The assumption of adsorption kinetic control can give a better fit by changing the value of adsorption rate constant from the literature value of 50 to 100 or 200 $m^3 \cdot mol^{-1} \cdot s^{-1}$. However, the assumption of adsorption kinetic control would result in the surfactant concentration on the surface being in equilibrium with the bulk concentration and that violates the stagnant cap model.

The combination of two assumptions, adsorption control and equilibrium surface coverage in model 7.3.6, represents the worst case. The combination of boundary layer mass transfer control with possible equilibrium or maximum surface coverage (model 7.3.4 and 7.3.5) also produced larger deviations than models 7.3.1 and 7.3.2.

## 7.5 Conclusions

The comparison of the simulated velocity profiles with the experimental data under different possible model assumptions shows that the stagnant cap model and the boundary layer mass transfer control step are valid for Triton X-100 adsorption onto a small buoyant bubble. The work is the first test and validation of the theory of the dynamic adsorption layer. This approach lays the foundation for the simultaneous solution of fluid flow and mass transfer.

# CHAPTER 8

# TEMPERATURE EFFECTS ON VELOCITY PROFILE

## 8.1 Introduction

In chapter 7 the velocity profiles in Triton X-100 solutions at 25 °C were simulated by a stagnant cap model assuming various mass transfer mechanisms. It was concluded that boundary layer mass transfer is the mass transfer control process rather than adsorption kinetic control.

Since temperature affects the physical properties of the surfactant, i.e., diffusion coefficient, adsorption kinetics and thermodynamics (including adsorption and desorption coefficients, maximum surface coverage and equilibrium surface coverage) and of the solution, i.e., the properties of water as shown in Table 8.1, varying temperature was selected to further test the models.

Table 8.1 Physical properties of water*

| **Temperature, °C** | **Density, kg/m$^3$** | **Viscosity$\times 10^4$, Pa·s** | **Surface tension$\times 10^2$, N/m** |
|---|---|---|---|
| 6 | 999.8 | 15.01 | 7.48 |
| 25 | 996.9 | 9.00 | 7.18 |
| 45 | 990.1 | 6.00 | 6.86 |

*CRC Handbook of Chemistry and Physics, 80th edition.

## 8.2 Fundamentals

### 8.2.1 The diffusion coefficient of Triton X-100

The studies on diffusion coefficient of Triton X-100 have been mostly at a fixed ambient temperature as shown in chapter 4 (Corti and Degiorgio, 1975; Weinheimer et al., 1981; Van et al., 1986; Leaist, 1988; Lin et al., 1990). No experimental data are available at the temperatures employed in this work, viz. 6 and 45 °C. The diffusion coefficient at different temperatures will be calculated from the Wilke-Chang equation (eq. 2-21).

### 8.2.2 Maximum surface coverage and dependence on temperature

Maximum surface coverage ($\Gamma_\infty$) is the maximum adsorption that can be attained at the air/water interface. The available data for Triton X-100 and for surfactants of similar structure are summarized in Table 8.2.

If the molecules can be regarded as analogous to an ideal gas, the force between the molecules has no effect on the surface coverage and therefore the maximum surface coverage should not be affected by temperature. Although there are no data for maximum surface coverage as a function of temperature for Triton X-100, data of the maximum surface coverage for similar surfactants have been reported (Table 8.2).

Table 8.2 Maximum surface coverage at different temperatures

| **Surfactant** | **T, °C** | **$\Gamma_\infty \times 10^6$, mol/m$^2$** | **Reference** |
|---|---|---|---|
| $C_{12}H_{25}(OC_2H_4)_8OH$ | 10 | 2.5 | Rosen, 1989 |
| | 25 | 2.5 | |
| | 40 | 2.4 | |
| Triton X-100 | 22 | 2.91 | Lin et al., 1990 |
| p-t-$C_8H_{17}C_6H_4(OC_2H_4)_9OH$ | 25 | 2.5 | Crook et al., 1963, 1964 |
| p-t-$C_8H_{17}C_6H_4(OC_2H_4)_{10}OH$ | 25 | 2.2 | |
| | 55 | 2.1 | |
| | 85 | 2.1 | |

Table 8.2 shows that the maximum surface coverage changes little with temperature for both $C_{12}H_{25}(OC_2H_4)_8OH$ and p-t-$C_8H_{17}C_6H_4(OC_2H_4)_{10}OH$. The later in particular has a similar molecule structure to Triton X-100 (only 0.5 more oxyethylene units). It is reasonable to assume the maximum surface coverage of Triton X-100 is constant over the present experimental temperature range of 6 to 45 °C.

### 8.2.3 Bubble size and path

The bubble size generated by a capillary at sufficiently low gas rate can be predicted by the force balance between the buoyancy and surface tension on the bubble, so-called Tate's law (Blanchard and Syzdek, 1977):

$$d_e = 2\left(\frac{3r_c\gamma\cos\theta}{2\Delta\rho g}\right)^{\frac{1}{3}} \tag{8-1}$$

The contact angle θ between the glass capillary and water is usually assumed to be zero. Sam (1995) established the validity of eq. (8-1) for bubbles generated by capillaries in the present setup at 30 °C. The temperature effect on the bubble size is represented by the corresponding physical property changes in eq. (8-1).

As a bubble rises, it expands because of the decrease in the static pressure according to the ideal gas law. Experimental measurement of bubble size to differentiate the impact on size caused by a change in temperature or hydrostatic pressure is difficult. The comparison of velocity from experiment and numerical simulation offers a better way to resolve size changes.

The path of a 0.9 mm bubble at 30 °C is rectilinear (Sam et al., 1996), which supports the conclusion given by Hartunian and Sears (1957). They proposed two criteria for rectilinear motion: in impure liquids $Re<202$; in pure liquids $We<1.26$.

### 8.2.4 Temperature effect on bubble terminal velocity

The effect of temperature on the velocity of a single bubble differs in the different regions of the velocity profile. In the first stage, the bubble accelerates to the maximum velocity. Because the time to reach the maximum velocity is very short (<0.25 s), in tap water (and other dilute solutions) adsorption of surface active species on the bubble surface can be ignored. (The maximum velocity can be regarded as the bubble terminal velocity in pure water as discussed in chapter 5.)

Many attempts have been made to predict bubble terminal velocity in water (Levich, 1962; Moore, 1959, 1963, 1965; Sawi, 1974; Mendelson, 1967; Clift et al., 1978; Duniveld, 1996). In chapter 5, the experimental maximum velocity in tap water was compared to the predicted value from the different models. The results show that Moore and Sawi's model is valid for a 0.8 mm bubble in pure water, and Clift et al.'s correlation gives a close prediction for a 1.4 mm bubble although the predicted values are consistently lower than the experimental ones. Most of the models were developed from experimental conditions at a single temperature (20 to 25 °C). Experimental results over a larger temperature range will reveal more precisely the dependence of terminal velocity on the physical properties of the medium.

For the terminal velocity of a single bubble in surfactant solution, the experimental data support Karamanev's (1994) conclusion. That is, when $Re<130$ and the density of the particle is larger than 300 kg/m$^3$ the velocity conforms to the standard drag curve. When $Re>130$ and the density of the particle is less than 300 kg/m$^3$ the drag coefficient is constant at ~0.95. Under these circumstances the temperature should not affect the terminal velocity. The temperature effect on a single bubble terminal velocity should be represented by the Reynolds number.

## 8.3 Results and discussion

### 8.3.1 Bubble size and path

Three capillary sizes were used in the experiments, 14, 64 and 125 μm in diameter. Bubble size was measured photographically at different temperatures for each capillary. The bubble size as a function of temperature measured and predicted from Tate's Law is shown in Fig. 8.1. The 95% confidence interval on the bubble size measurement was ±0.05 mm. The bubble size changes caused by temperature (i.e., 0.04, 0.03 and 0.02 mm for the three capillaries, respectively) are smaller than the measurement error. Therefore, it is reasonable to regard the bubble size as constant over this temperature range.

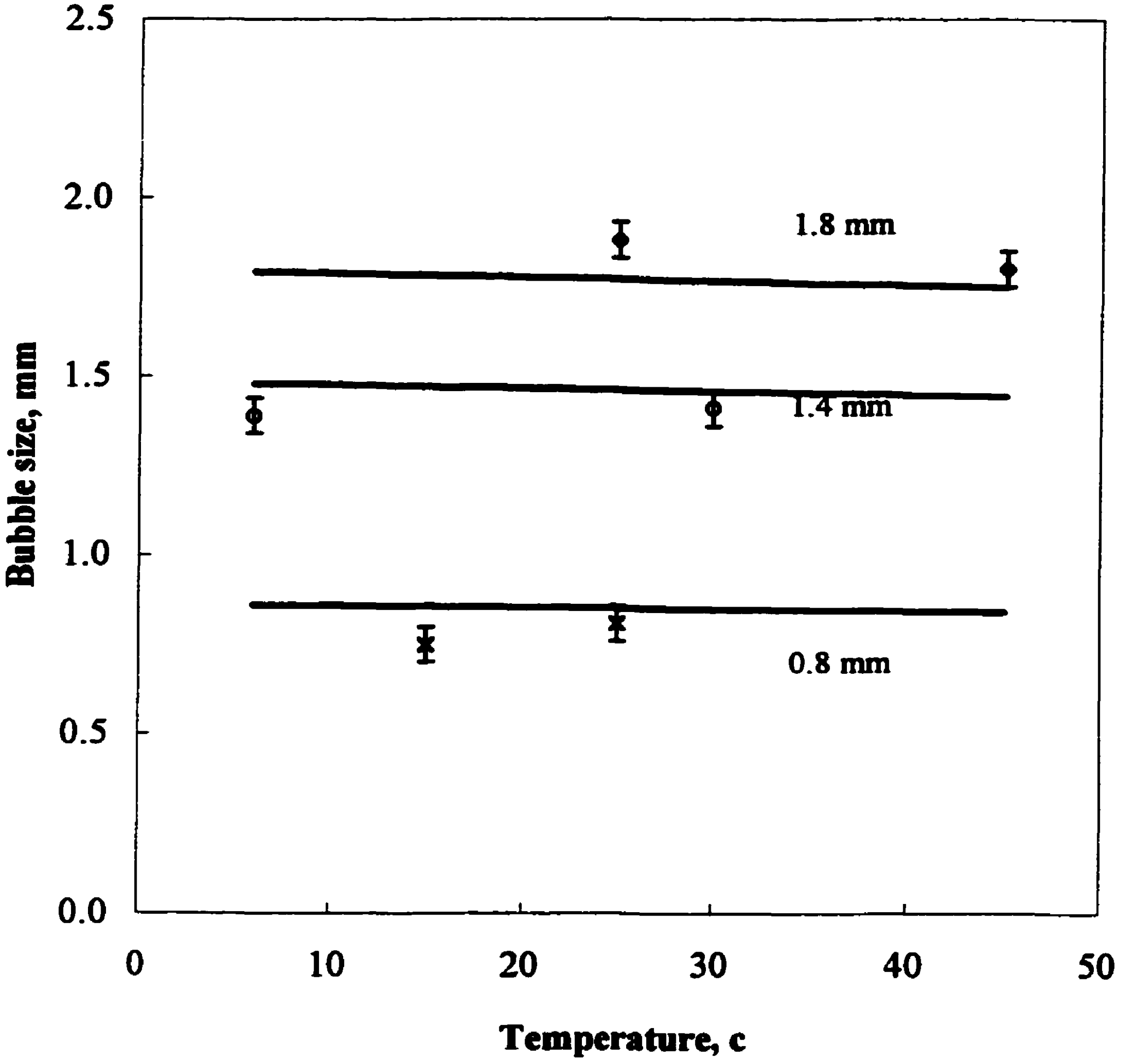

Fig. 8.1 Bubble size measurement as a function of temperature and values from Tate's Law (straight line)

The rising path of a 0.8 mm bubble in tap water and Triton X-100 solutions at 45 °C is linear from inspection of the tapes. The maximum Re in tap water is 396 with a We of 1.04 (assuming the surface tension is the same as pure water). In surfactant solutions the path is still linear at Re above 202, which is in the deceleration region. The criterion given by Hartunian and Sears (1957) is hard to apply here because the bubble is not in equilibrium with the solution. The system does not behave like either "pure liquid" or "impure liquid".

### 8.3.2 Velocity profiles in tap water

The physical properties of water, especially viscosity, strongly depend on temperature as shown in Table 8.1. The viscosity of water more than doubles as temperature is lowered from 45 °C to 6 °C. In addition to the change in physical properties of water, the surface activity of unidentified impurities in tap water may also vary with temperature.

Velocity profiles were measured for 0.8 and 1.4 mm bubbles in tap water at different temperatures. The profiles in Fig. 8.2 are for a 1.4 mm bubble at 6, 25 and 40 °C, and those in Fig. 8.3 are for the 0.8 mm bubble at 6, 25 and 45 °C.

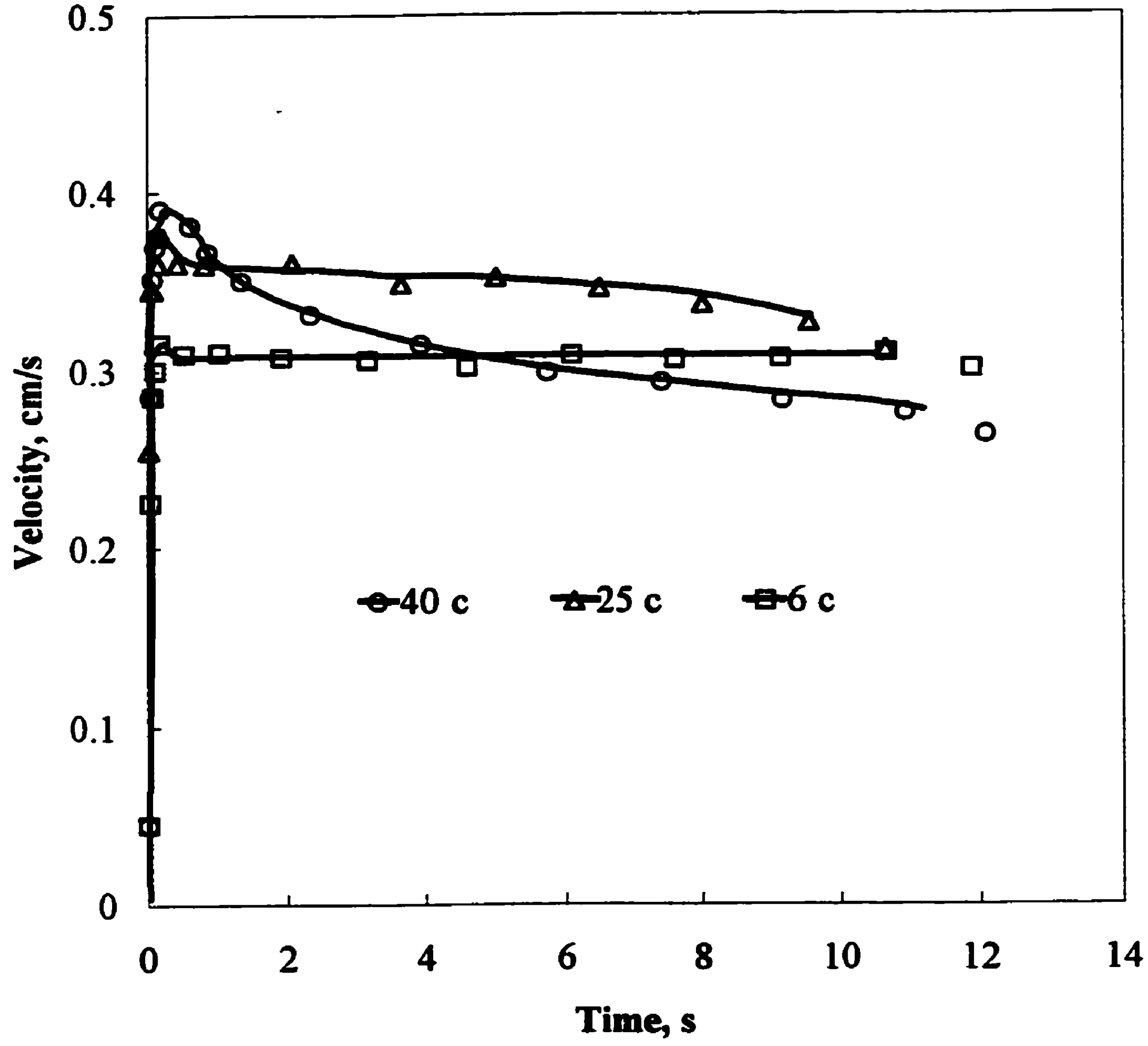

Fig. 8.2 Velocity profiles for a 1.4 mm bubble in tap water at three temperatures

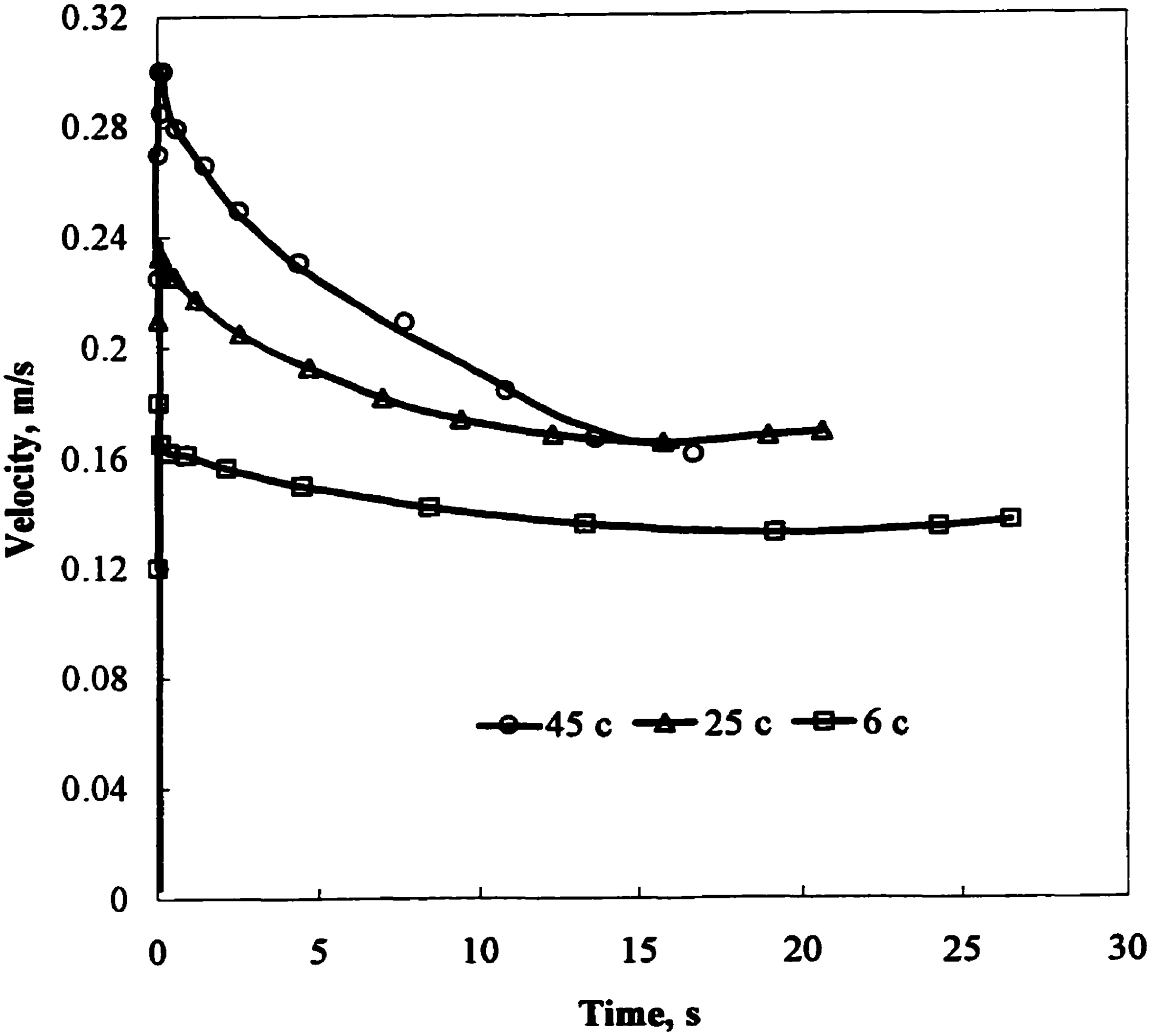

Fig. 8.3 Velocity profiles for a 0.8 mm bubble in tap water at three temperatures

The extent of bubble deceleration at high temperatures (40 and 45 °C) is greater than at low temperatures. For the 1.4 mm bubble, the velocity profile at 6 °C is very close to the theoretical profile in pure water (rapid acceleration to a constant, terminal velocity). There is essentially no deceleration, which implies that the effect of impurity in tap water at low temperature is negligible for bubbles of this size. (The reduced surface activity of impurities in tap water at low temperature may mean water at low temperature can be used as pseudo-pure water for application and research where very high purity water is required.)

The small bubble (0.8 mm) still decelerated slightly at 6 °C. This further supports previous observation that the effect of surface active impurities is stronger on a small bubble than on a large bubble (see page 73 and 77).

### 8.3.3 Terminal velocity in surfactant solution

Bubbles of the same size rising in different surfactant solutions regardless of type or concentration will reach the same terminal velocity at the same temperature (Zhang et al., 1996). If the variation of bubble size with temperature can be ignored, the difference between the terminal velocities at different temperatures could be solely attributable to the change in physical properties of water. As discussed in chapter 5, the experimental terminal velocity for a 1.4 mm bubble is in good agreement with the predicted value from Karamanev (1994). The data in Table 8.3 include the experimental terminal velocities at different temperatures, the values of terminal velocity from numerical simulation and the terminal velocity calculated by Karamenev's correlation (except for the case noted).

The calculated values of terminal velocity for bubbles at different temperatures with Re>130 are in good agreement with experimental with a maximum deviation < 8%. The results show that Karamanev's correlation for the drag of a rigid bubble is applicable. The agreement with the experimental results shows that the correlation correctly accounts for the effect of fluid properties on bubble velocity. For 0.9 mm bubble at 6 °C, Re<130 which is outside the application range of Karamanev's correlation. The drag for bubbles in this region is the same as that for rigid falling spheres.

Table 8.3 Terminal velocity $U_t$ (cm/s) in Triton X-100 solutions at different temperatures

| $d_e$*, mm | T, °C | Experiment | Simulated | Calculated |
|---|---|---|---|---|
| 0.9 | 6 | 8.7 | 9.05 | 8.8** |
| | 25 | 10.9 | 10.5 | 10.5** |
| | 45 | 11.8 | 12.2 | 11.1 |
| 1.6 | 10 | 15.4 | 15.9 | 14.8 |
| | 25 | 14.8 | 16.7 | |
| | 40 | 14.8 | 17.9 | |
| 2.0 | 15 | 16.7 | 21.7 | 16.6 |
| | 25 | 16.4 | NA | |
| | 45 | 16.1 | NA | |

*values at top of column when terminal velocity is known to be reached
**from standard drag curve as Re<130
NA: not available

When the bubble size and temperature increase, the terminal velocity increases and the bubble tends to deform (Clift et al., 1978). The deformation of the bubble increases the drag. Furthermore, the path of the bubble becomes more zigzag as the bubble size increases and viscosity decreases. In numerical simulation, the assumption of symmetric flow is applied. The data in Table 8.3 show that as the bubble size exceeds 1.6 mm and temperature is higher than 25 °C, i.e., Re increases to larger than 250, the simulated velocity becomes larger than the experimental value. A non-linear bubble path should be considered in order to apply the numerical solution to high Re. For the 2.0 mm bubble, the numerical method fails to converge at 25 and 45 °C.

### 8.3.4 Terminal velocity in pure water

Table 8.4 shows the results for the terminal velocity in pure water (experimentally determined from the maximum velocity in the profile for tap water as described in chapter 5). The velocity of the small bubble (0.8 mm) at 25 °C is close to the predicted value from Moore's theory as indicated in Table 6.4, where the bubble was regarded as spherical. For larger bubbles deformation must be considered. Moore's theory as modified by Sawi can be used to calculate the axis ratio of the bubble directly from We. The equation to correlate We with the axis ratio $\chi$ given by Sawi is:

$$We = \frac{2(h\chi^2 - g)^2[g\chi(3\chi^2 - g^2) - (3\chi^2 + g^2)\tanh^{-1}(g/\chi)]}{g^4(3h\chi^2 - 2hg^2 3g)\chi^{\frac{7}{3}}} \tag{8-2}$$

where

$$\begin{aligned} g &= (\chi^2 - 1)^{\frac{1}{2}} \\ h &= \sec^{-1}\chi \end{aligned} \tag{8-3}$$

Moore's theory with Sawi's modification (Moore and Sawi's model) gives a lower velocity than the experimental value (Table 8.4) because of the overestimation of the bubble deformation as was found by Duineveld (1995) with Moore's theory. However, the model does include the temperature dependency revealed by experiments. The comparison of the measured terminal velocity and that predicted from Moore and Sawi's model shows a linear relationship (Fig. 8.4) in the size range 0.9 to 2.0 mm, and temperature range 6 to 45 °C. The combination of this linear relationship and Moore and Sawi's model can serve as an estimation of the bubble velocity in pure water. The following correlation results (with $U_t$ in cm/s):

$$U_t = 1.0488\frac{g d_e^2 \Delta\rho}{36\mu G(\chi)\left(1+\frac{H(\chi)}{\mathrm{Re}^{1/2}}\right)} + 1.6851 \tag{8-4}$$

Table 8.4 Terminal velocity $U_t$ (cm/s) in water at different temperatures

| $d_e$,[a] mm | T, °C | Experiment | Simulated | Mendelson | Moore & Sawi |
|---|---|---|---|---|---|
| 0.8 | 6 | 17.0 | 17.3 | NA | 14.9 |
| | 25 | 23.2 | 22.3 | NA | 20.7 |
| | 45 | 30.0 | 31.2 | NA | 26.4 |
| 1.4 | 6 | 31.5 | 32.1 | 34.8 | 28.3 |
| | 25 | 36.0 | 38.7 | 34.3 | 33.6 |
| | 40 | 38.3 | 38.1 | 33.9 | 35.9 |
| 1.8 | 15 | 37.0 | 35.0 | 31.3 | 32.7 |
| | 25 | 37.8 | 37.0 | 30.8 | 33.8 |
| | 45 | 38.0 | 43.7 | 30.2 | 34.6 |

[a] values at bottom of column as this is close to where maximum (i.e., terminal) velocity for water is reached

NA: not applicable

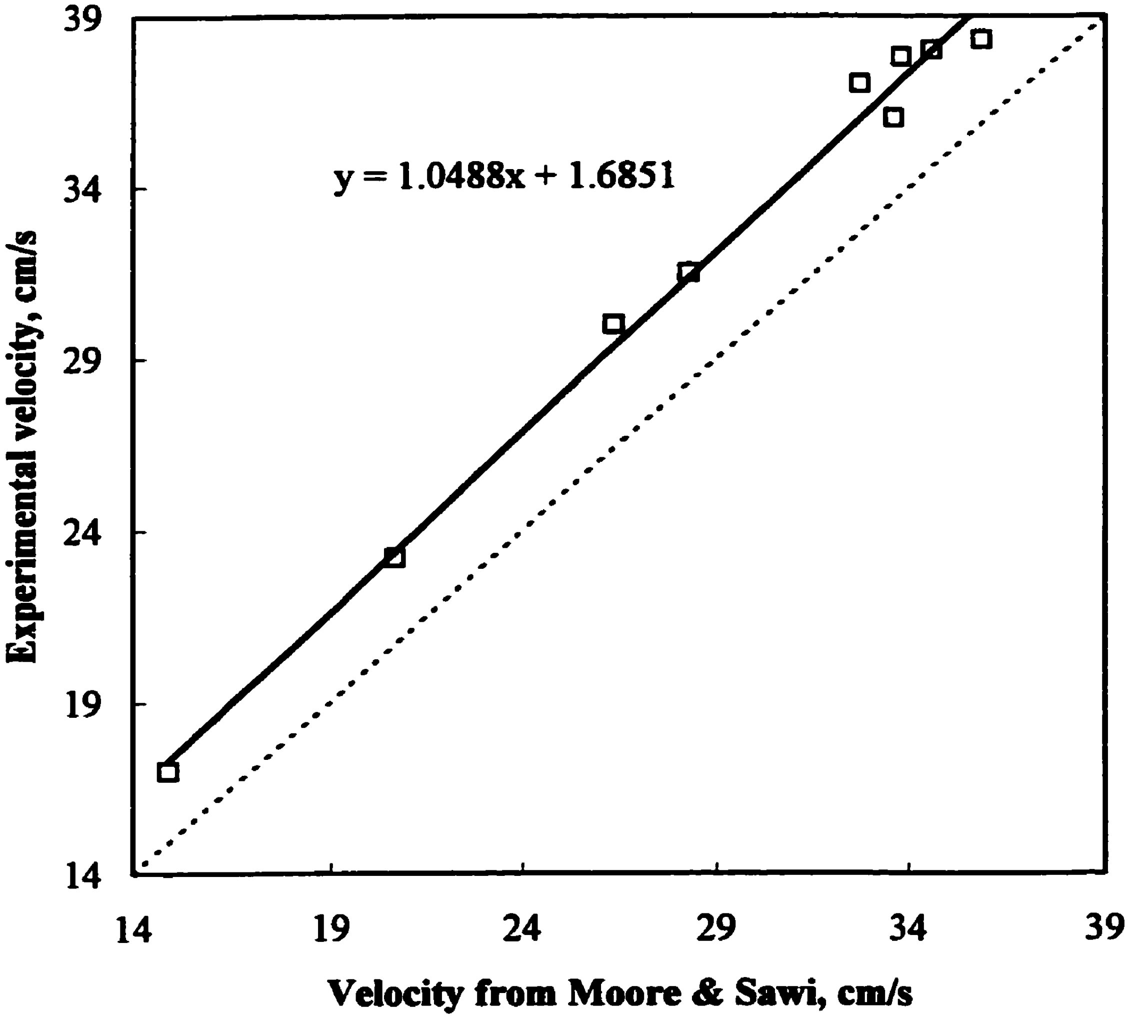

Fig. 8.4 Correlation between experimental terminal velocity in pure water and Moore & Sawi's model

For $d_e$ = 1.4 mm at 25 °C, Clift et al.'s correlation was considered appropriate for the terminal velocity in water (Zhang and Finch, 1999). However, as the bubble size and temperature increase, the values of experimental terminal velocity are much larger than the predicted values from the correlation as shown in Table 8.4. The numerical simulation gives closer agreement than the empirical correlation.

Referring to the empirical correlation given by Mendelson (1967) (eq. 8-5), the terminal velocity in pure water was supposed to have the form suggested by analogy with wave theory:

$$U_t = \sqrt{2\frac{\gamma}{\rho d_e} + 0.5 g d_e} \qquad (8\text{-}5)$$

The deviation of the experimental data in this work from the data collected by Clift et al. may lie in an inappropriate velocity measurement. Generally, the velocity is measured as an average over a certain distance, which will always give a value less than the maximum. The discrepancy between the present experimental velocity for pure water and the predicted values from Mendelson's and Clift et al.'s expressions could also be attributed to inadequate representation of some of the physical properties, e.g. the viscosity, in the equations. The equations are based on the form suggested by wave theory, in which the wavelength (i.e., velocity) depends on the surface tension of liquid. However, the effect of surface tension is much lower than that of viscosity after the bubble is formed in the case of single bubble motion. The experimental data from this work cover a large range of physical properties, in particular of viscosity. The expressions need refinement to reflect more precisely the dependence on the physical properties.

### 8.3.5 Velocity profile in surfactant solution

Temperature affects velocity profiles of the small bubble (0.8 mm) and the mid-size bubble (1.4 mm) differently. From the discussion of the temperature effect on terminal velocity, it is known that the temperature change has little effect on the terminal velocity for 1.4 mm (1.6 mm at top of 4 m column) bubble as the bubble Re exceeds 130 (Table 8.3). The temperature change only affects the dynamic part of the bubble velocity profile. However, temperature does affect both the dynamic part and terminal velocity in the case of the small bubble (0.8 mm). The experimental results are shown in Fig. 8.5.

The change in dynamic part of the profiles may be attributed to the thinner boundary layer and higher diffusion coefficient at high temperature, as long as the stagnant cap model holds. There is no information available on the temperature dependence of the surface activity ($\alpha/\beta$) of Triton X-100. A change of $\alpha/\beta$ from $6.62\times10^{-4}$ to 1 $\mathrm{mol{\cdot}m^{-3}}$ over the temperature range 6 to 45 °C is highly improbable. The value of $\alpha/\beta$ has to exceed 1 $\mathrm{mol{\cdot}m^{-3}}$ to change the mass transfer mechanism from diffusion control to adsorption control (Fainerman 1998). This supports the use of the stagnant cap model at temperatures from 6 to 45 °C.

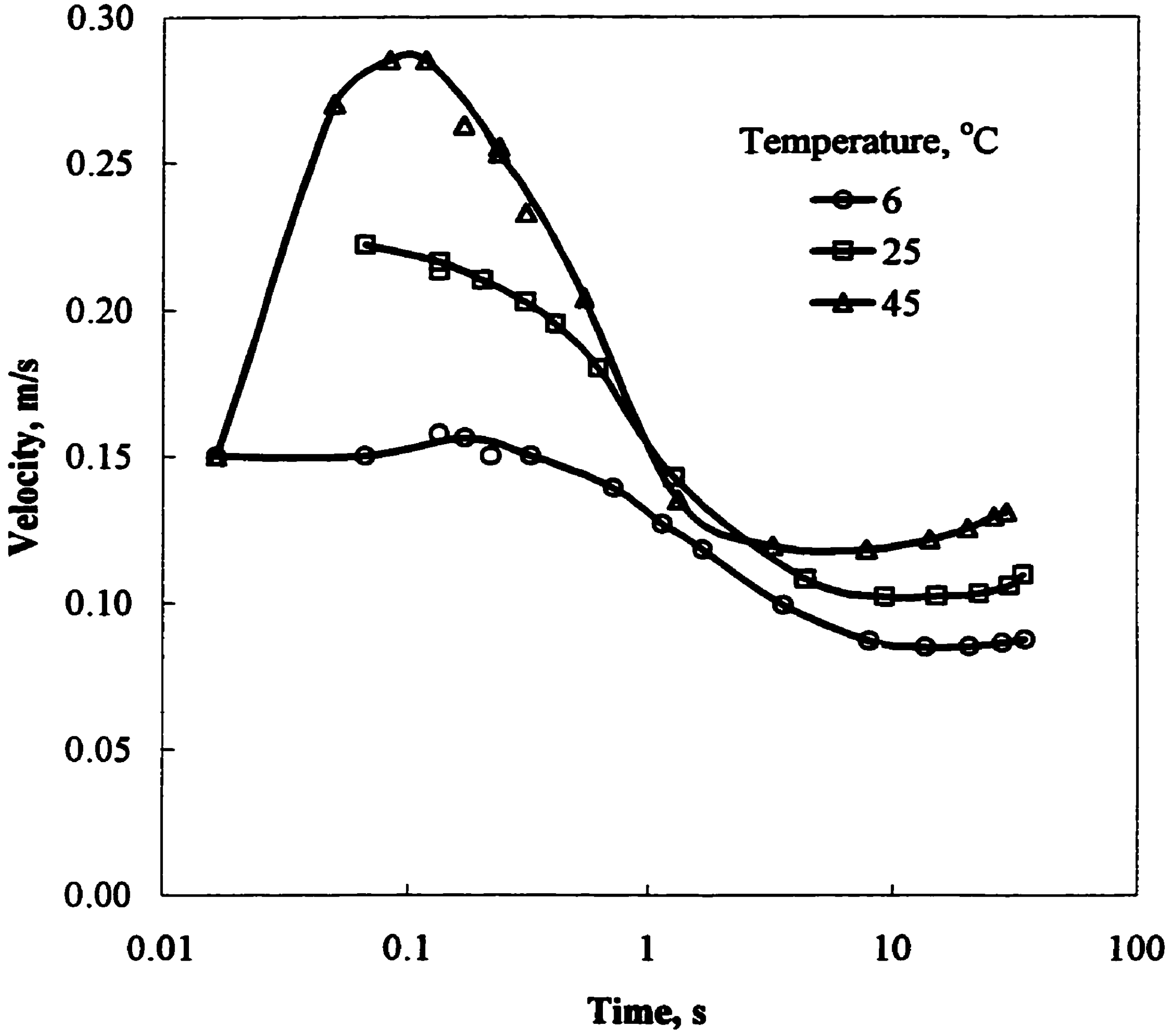

Fig. 8.5 Velocity profile of 0.8 mm bubble at different temperatures in $12.5\times10^{-5}$ mol/m$^3$ Triton X-100 solution

Although the adsorption kinetic parameters are not available at 6 °C, the combination of different $\beta$ values in testing adsorption kinetic control model (as discussed in chapter 7) covered the likely range.

Simulation of the velocity profile of a 0.8 mm bubble in chapter 7 indicated that a boundary layer mass transfer control mechanism fitted the experimental data better than an adsorption kinetic control mechanism. As the temperature changes, the diffusion coefficient of surfactant in liquid will change proportionally according to the Stokes-Einstein equation. The values of diffusion coefficient at different temperatures are listed in Table 8.5.

Table 8.5 Diffusion coefficient for Triton X-100 at different temperatures according to Stokes-Einstein equation

| **T, °C** | **6** | **25** | **45** |
|---|---|---|---|
| **$D \times 10^{10}$, $m^2/s$** | 1.6 | 2.8 | 4.5 |

The velocity profiles were simulated at 6 °C using the same models as for 25 °C. The results showed the same trends presented in chapter 7. The results from the best-fitting model, that of boundary layer mass transfer control, at 6 °C are shown in Fig. 8.6.

Compared with the results at 25 °C (Fig. 7.3), the model fits the data even better at 6 °C especially at the lowest concentration. The small deviation between simulated and experimental data at low concentration may suggest that the poorer fit at 25 °C attributable to surface active impurities in water. At low temperature, the profile shows more clearly the effect of Triton X-100 on the bubble retardation with less interference from the background water (as shown in Fig. 8.3).

The situation was different at 45 °C. The simulation over the cap angle range ~24 to 91 degrees diverged at high temperature. It was suspected that the low viscosity of water at 45 °C may promote added turbulence causing the bubble rise path to be more zigzag, which would demand modification of the symmetric flow assumption in the physical model. However, inspection of the tapes eliminated this possibility. More numerical experiments need to be done.

In the tests of the model in chapter 7 and chapter 8, the diffusion coefficient was known, and the successful simulation can be taken as confirmation of the literature values. On the other hand, if the physical parameters of a surfactant are not known, simulation of the experimental velocity profile as a function of concentration and temperature could be used to back calculate the physical properties. Usually, the mass transfer coefficient of surfactant in water is measured via the surface tension. According to the definition of diffusion coefficient, the measurement should be done in an infinite dilute solution. However, the accuracy of the surface tension measurement is questionable at low surfactant concentration (Lin et al., 1990). The velocity profile remains very sensitive to trace amount of surfactant, and provides a better way to determine the diffusion coefficient of surfactant.

### 8.3.6 Temperature effect on average surfactant surface coverage

The bubble size effect on the average surface coverage was discussed in chapter 6. Similarly, the temperature also affects the surface coverage because of the decreased drag at high temperature. Data in Table 8.6 shows that the average Triton X-100 coverage on a 0.8 mm bubble surface almost doubled as the temperature increased from 6 to 25 °C. However, the surface coverage dropped a little when the temperature increased from 25 to 45 °C. This implies the change of surface coverage is a balance between the changes in viscosity and surface tension. Temperature, as a consequence, is an important operational parameter for the adsorptive bubble separation process.

Table 8.6 Surfactant coverage vs. temperature

| **T, °C** | **6** | **25** | **45** |
|---|---|---|---|
| **$\Gamma \times 10^7$, mol/m$^2$** | 1.4 | 2.7 | 2.4 |

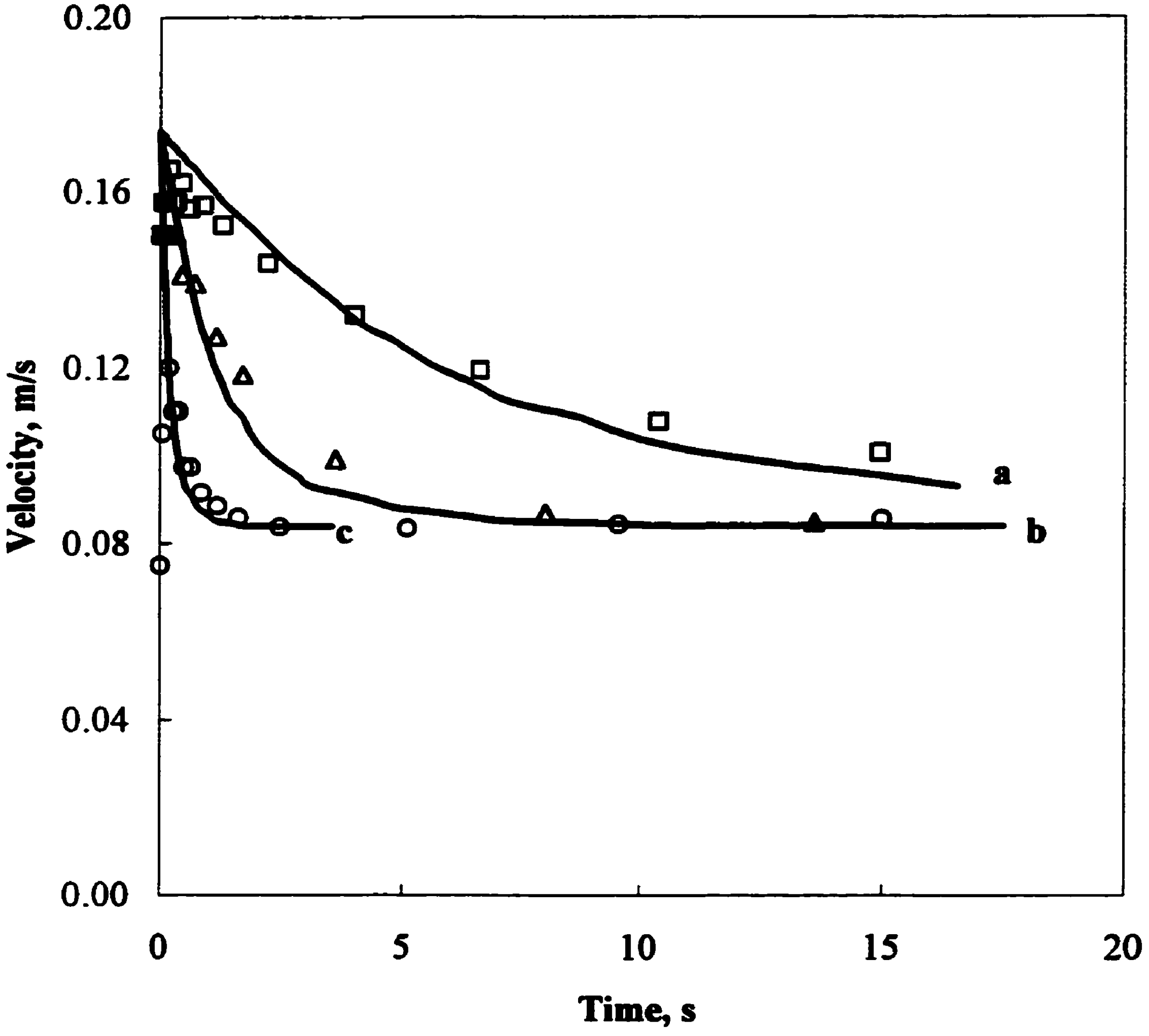

Fig. 8.6 Experimental and simulated velocity profiles with boundary layer mass transfer control at 6 °C

## 8.4 Conclusions

From the discussion of temperature effects on the single bubble velocity profile, the following conclusions are obtained:

- Temperature affects the velocity of a single bubble in tap water. At low temperature the effect of impurities in tap water is limited.
- The temperature effect on the terminal velocity in surfactant solution is well represented by Re.
- The terminal velocity in pure water can be estimated by a combination of an empirical linear relationship and Moore & Sawi's model.
- The simulation of velocity profile for a small bubble (0.8 mm) shows the mass transfer of Triton X-100 from bulk solution to bubble surface is the controlling step at both 6 and 25 °C.
- The simulation of experimental velocity profiles could be used as a method to determine the physical parameters of mass transfer and adsorption.
- Temperature affects the amount of Triton X-100 adsorbed on a bubble surface.
- Temperature is an important parameter in the design of adsorptive bubble separation units.

# CHAPTER 9

# SUMMARY

## 9.1 Conclusions

Study of the single bubble velocity profile in surfactant solutions is vital to the understanding of the mechanism of bubble motion and modeling of surfactant adsorption in adsorptive bubble separation processes. The thesis has established the experimental and theoretical foundation for a new approach to the study of dynamic adsorption in the field of physico-chemical hydrodynamics. For the first time the experimental velocity profile has been modeled, in this case using a numerical simulation. The confusion regarding the definition and measurement of bubble terminal velocity is resolved. The highlights of the work are listed.

### 9.1.1 Experimental bubble velocity profiles

The experimental procedure and repeatability appropriate to the objectives of the study were established.

- The measurements are repeatable provided a stable surfactant is used.
- Humidity is not a factor for the size of bubble of interest here.
- The quality of tap water does not affect the measurement as long as the surfactant concentration exceeds a certain value (which is surfactant type and bubble size dependent).
- Solutions must be prepared fresh to maximize repeatability.

### 9.1.2 Physical model and numerical simulation

Based on the experimental evidence, a stagnant cap model for bubble surface retardation and boundary layer mass transfer of surfactant was developed.

- A pseudo-steady state approach was adopted which considers the mass transfer and fluid flow interactively. The solution is physically meaningful.
- The program (generously provided by J. McLaughlin) was modified to improve simulation of the fluid flow for a given bubble size and random input of Re. It runs more automatically than the original version.

### 9.1.3 The terminal velocity in water and surfactant solutions

The maximum velocity in the profile in tap water was justified as the measure of terminal velocity in pure water. The constant velocity i.e., stage 3 in the profile was justified as the terminal velocity in surfactant solutions. Both terminal velocities were compared to available models and previous experimental data in order to validate the measurement technique and establish the basis for modeling the full profile.

Water:

- The maximum value reached in the profile in tap water is an estimate of bubble terminal velocity in pure water.
- This measure of terminal velocity in pure water gives values larger than previous experimental values and larger than those predicted from existing models.
- Small amounts of impurity do not affect the maximum velocity. Thus, the requirement for high purity in the measurement of terminal velocity in water can be relaxed

- For a 0.8 mm bubble, the prediction of maximum velocity from models for spherical and deformed bubbles proves that it can be treated as spherical.

Surfactant solutions:

- The distance to reach terminal velocity is bubble size, surfactant type and concentration dependent.
- Surfactant type (especially those of high surface activity) does not affect the terminal velocity, which established that the boundary condition for a bubble moving at terminal velocity in different surfactant solutions is the same.
- The agreement between measured terminal velocity in surfactant solution and Karamanev's prediction for Re>130 and that predicted using the standard drag correlation for Re<130 proved that at the terminal velocity, the bubble surface can be reasonably set as a no-slip boundary condition.

### 9.1.4 Simulation of terminal velocity in water and surfactant solutions

- For the 0.8 mm bubble, the simulated velocity values are very close to the experimental value.
- The simulation of surfactant surface coverage showed that the average surface coverage is bubble size dependent.

### 9.1.5 Velocity profile simulation

The velocity profile is simulated by testing various combinations of possible physical models. Comparison of the simulated profiles with the experimental data under different model assumptions showed that:

- The stagnant cap model and the boundary layer mass transfer control step are valid for adsorption of Triton X-100 onto a small buoyant bubble.
- The experimental results confirmed the theory of dynamic adsorption layer for the first time.
- The work lays the foundation for the simultaneous solution of fluid flow and mass transfer.

### 9.1.6 Temperature effect

- The simulation of velocity profile for a small bubble (0.8 mm) at two temperatures further confirmed that mass transfer of Triton X-100 from bulk to bubble surface is the controlling step.
- The temperature effect on the terminal velocity in a surfactant solution is well represented by Re.
- Empirical correlation of bubble terminal velocity in pure water is established by correlation of the experimental data with the value predicted from Moore and Sawi's model.
- The surfactant surface coverage is temperature dependent.

*"The measurement of buoyant bubble velocity is not suitable for solving these problems and attention must be paid to other experimental techniques."*

——Excerpt from "Dynamics of Adsorption at Liquid Interfaces" by S.S. Dukhin, G. Kretzschmar and R. Miller, 1995, (p. 321)

This research work has shown that a variation in the experimental approach, namely determining the *single bubble velocity profile*, can serve the needs in the study of dynamics of adsorption at the gas liquid interface, which is a breakthrough in experimental technique.

### 9.2 Contributions to knowledge

- Established a new experimental method for dynamic adsorption studies.
- Refined measurement techniques in the study of single bubble velocity.
- Provided reliable experimental data for dynamic adsorption studies.
- Terminal velocity established as independent of temperature in addition to independent of the type and concentration of surfactant provided Re>130.
- Concluded that the viscosity effect is much stronger than a surface tension effect on bubble velocity in pure water.
- Improved and validated the numerical method at moderate Re (≤200).
- Confirmed that the stagnant cap model and the boundary layer mass transfer control step is applicable for Triton X-100 adsorption onto a small buoyant bubble.

- Experimentally demonstrated the theory of dynamic adsorption layer for the first time.
- Laid the foundation for the simultaneous solution of fluid flow and mass transfer.
- Suggested that the simulation of experimental velocity profiles could be used to determine the physical parameters of mass transfer and adsorption.

### 9.3 Suggestions for future work

- Refine the physical model for bubble motion at high Re to consider the path of the bubble.
- Exploit the simulation of experimental velocity profiles to determine the physical parameters of mass transfer and adsorption.
- Investigate surfactant types resulting in larger terminal velocities to establish a quantitative criterion for the stagnant cap model.
- Investigate effect on bubble velocity of interaction between multiple bubbles.
- Experiment on liquids other than water to reveal the dependence on physical properties of the media, particularly viscosity.
- Develop simultaneous numerical solution of mass transfer and fluid flow around the bubble.
- Correlate the adsorption time to column configuration (bubble retention time).
- Integrate single bubble velocity profile with adsorptive bubble column design.

# REFERENCES

Andrews, G. F., Fike, R., and Wong, S. (1988). Bubble hydrodynamics and mass transfer at high Reynolds number and surfactant concentration. *Chem. Eng. Sci.*, 43(7), 1467-1477.

Aybers, N. M., and Tapucu, A. (1969). The motion of gas bubbles rising through stagnant liquids. *Wärme-und Stoffübertragung* 2, 118-128.

Beitel, A., and Heideger, W. (1971). Surfactant effects on mass transfer form drops subject to interfacial instability. *Chem. Eng. Sci.*, 26, 711-717.

Blanchard, D. C., and Syzdek, L. D. (1977). Production of air bubbles of a specified size, *Chem. Eng. Sci.*, 32, 1109-1112.

Bleys, G. and Joos, P. (1985). Adsorption kinetics of bolaform surfactants at the air/water interface. *J. Phys. Chem.*, 89(6), 1027-1032.

Calderbank, P. H., and Lochiel, A. C. (1964). Mass Transfer Coefficients, Velocities, and Shapes of Carbon Dioxide Bubbles in Free Rise through Distilled Water. *Chem. Eng. Sci.*, 19, 485-506.

Campbell, J. A, and Hanratty, T. J. (1982). Mass transfer between a turbulent fluid and a solid boundary: linear theory. *AIChE J.*, 28(6), 988-993.

Chen, J., and Stebe, K. J. (1996). Marangoni retardation of the terminal velocity of settling droplet: The role of surfactant Physico-chemistry. *J. Colloid Interface Sci.*, 178, 144-155.

Chen, S. (1994). Modelling surfactant removal in foam fractionation: I-Theoretical development. *Aquacultural Engineering*, 13, 163-181.

Clarke, A. N., and Wilson, D. J. (1983). *Foam Flotation, Theory and applications*. Marcel Dekker, Inc. New York and Basel.

Clift, R., Grace, J. R., and Weber, M. E. (1978). *Bubbles, Drops, and Particles*. Academic press.

Corti, M., and Degiorgio, V. (1975). Light-scattering study on the micellar properties of a no-ionic surfactant. *Optics Commun.*, 14, 358-362.

Crook, E. H., Fordyce, D. B., and Trebbi, G. F. (1963). Molecular weight distribution of nonionic surfactants. I. Surface and interfacial tension of normal distribution and homogeneous p,t-Octylphenoxyethoxyethanols (OPE'S). *J. Phys. Chem.* 67, 1987-1994.

Crook, E. H., Trebbi, G. F., and Fordyce, D. B. (1964). Thermodynamic properties of solutions of homogeneous p,t-Octylphenoxyethoxyethanols ($OPE_{1-10}$). *J. Phys. Chem.* 68, 3592-3599.

Cuenot, B., Magnaudet, J., and Spennato, B. (1997). Effects of slightly soluble surfactants on the flow around a spherical bubble. *J. Fluid Mech.*, 339, 25-53.

Dankwerts, P. V. (1951). *Industrial and Engineering Chemistry*, 43, 1460.

Davis, R. E., and Acrivos, A. (1966). The influence of surfactants on the creeping motion of bubbles. *Chem. Eng. Sci.*, 21, 681-685.

Dewsbury, K., Karamanev, D., and Margaritis, A. (1999). Hydeodynamic characteristics of free rise of light solid particles and gas bubbles in on-Newtonian liquids. *Chem. Eng. Sci.*, 54, 4825-4830.

Duineveld, P.C. (1995). The rise velocity and shape of bubbles in pure water at high Reynolds number. *J. Fluid Mech.*, 292, 325-332.

Dukhin, S. S. (1987) in Goddard, E. G., and Rusanov, A. T. (Eds.). *Modern Theory of Capillarity*, Academic verlag, Berlin, 83.

Dukhin, S. S., Kretzschmar, G., and Miller, R. (1995). *Dynamics of adsorption at liquid interfaces: theory, experiment, application*. Elsevier, Amsterdam.

Fainerman, V. B., Zholob, S. A., Miller, R., and Joos, P. (1998). Non-diffusional adsorption dynamics of surfactants at the air/water interface: adsorption barrier or non-equilibrium surface layer. *Colloids and Surfaces, A: Physicochemical and Engineering Aspects* 143, 243-249.

Fdhila, R. B., and Duineveld, P. C. (1996). The effect of surfactant on the rise of a spherical bubble at high Reynolds and Peclet numbers. *Phys. Fluids*, 8(2), 310-320

Elzinga, E., and Banchero, J. (1961). Some observations on the mechanics of drops in liquid-liquid systems. *AIChE J.*, 7, 394-399.

Feinerman, V. B. (1985). Kinetics of formation of adsorption layers at a solution-air interface. *VNIPIChermetenergoochistka, Donetsk, USSR. Usp. Khim.*, 54(10), 1613-1631.

Finch, J. A., and Dobby, G. S. (1990). *Column Flotation*. Pergamon Press, 180.

Frumkin, A. (1925). *Phys. Chem.*, 116, 466.

Frumkin, A., and Levich, V. G. (1947). On surfactants and interfacial motion. *Zh. Fiz. Khim.*, 21, 1183-1204.

Garner, F. H., and Skelland, A. H. P. (1955). Some factors affecting droplet behaviour in liquid - liquid systems. *Chem. Eng. Sci.*, 4, 149-158.

Göbel, J. G., and Joppien, G. R. (1997). "Dynamic interfacial tensions of aqueous Triton X-100 solutions in contact with air, cyclohexane, n-heptane, and n-hexadecane", *J. Colloid Interface Sci.*, 191, 30-37.

Griffith, R. (1962). The effect of surfactants on the terminal velocity of drops and bubbles. *Chem. Eng. Sci.*, 17, 1057-1070.

Hadamard, J. (1911). Mouvement Permanent Lens d'une sphere liquide et visqueuse dans un liquide visqueux. *Comptes Rendus*, 152, 1735-1738.

Harper, J. F., (1972). The motion of bubbles and drops through liquids, *Advance Applied Mechanics*, 12, 59-129.

Harper, J. F. (1973). On bubbles with small immobile adsorbed films rising in liquids at low Reynolds numbers. *J. Fluid Mech.*, 58, 539-545.

Harper, J. F. (1974). On spherical bubbles rising steadily in dilute surfactant solutions. *Q. J. Mech. Appl. Math.*, 27, 87.

Harper, J. F. (1988). The near stagnantion region of bubble rising steadily in dilute surfactant solution. *Q. J. Mech. Appl. Math.*, 41, 203.

Hartunian, R. A., and Sears, W. R. (1957). On the instability of small gas bubbles moving uniformly in various liquids. *J. Fluid Mech.*, 3, 27-47.

He, Z., Dagan, Z., and Maldarelli, C. (1991a). The influence of surfactant adsorption on the motion of a fluid sphere in a tube. Part. 1. Uniform retardation controlled by sorption kinetics. *J. Fluid Mech.*, 222, 1-32.

He, Z., Maldarelli, C., and Dagan, Z. (1991b). The size of stagnant caps of bulk soluble surfactant on the interfaces of translating fluid droplets. *J. Colloid Interface Sci.*, 146(2), 442-451.

Higbie, R. (1935). The rate of absorption of a pure gas into a still liquid during short periods of exposure. *Transactions American Institute of Chemical Engineers*, 31, 365-388.

Holbrook, J. A., and Levan. M. D. (1983a). The retardation of droplet motion by surfactant. Part 1. Theoretical development and asymptotic solutions. *Chem. Eng. Commun.*, 20, 191-207.

Holbrook, J. A., and Levan, M. D. (1983b). The retardation of droplet motion by surfactant. Part 2. Numerical solutions for exterior diffusion, surface diffusion and adsorption kinetics. *Chem. Eng. Commun.*, 20, 273-290.

Huang, W., and Kintner, R. C. (1969). Effects of surfactants on mass transfer inside drops. *AIChE J.*, 15, 735-744.

Horton, Y. J., Fritsch, I. R., and Kintner, R. (1965). Experimental determination of circulation velocities inside drops. *Can. J. Chem. Eng.*, 43, 143-146.

Jordan, M., Sucker, H., Einsele, A., Widmer, F., and Eppenberger, H. M. (1994). Interactions between animal cells and gas bubbles: The influence of serum and Pluronic F68 on the physical properties of the bubble surface. *Biotechnology and Bioengineering*, 43, 446-454.

Karamanev, D. G., and Nikolov, L. N. (1992). Free rising spheres do not obey Newton's law for free settling. *AIChE J.*, 38(11), 1843-1846.

Karamanev, D. G. (1994). Rise of gas bubbles in quiescent liquids. *AIChE J.*, 40(8), 1418-1421.

Keyser, P. M., McKay, J. K., Walker, C. D., and Foot, D. G. Jr. (1996). Application of column flotation for the removal of organic material from aqueous streams. *Column 96*, 119-133.

Kown, B. T. (1971). The effects of column height and diameter on the effectiveness of a continuous bubble fractionation system. *Water Research*, 5, 93-102.

Leaist, D. G. (1988). Diffusion in associating nonelectrolyte mixtures: stepwise aggregation and micelle formation. *Can. J. Chem. Eng.*, 66, 1129-1134

LeClair, B. P., and Hamielec, A. E. (1971). Viscous flow through particle assemblages at intermediate Reynolds numbers - A cell model for transport in bubble swarms. *Can. J. Chem. Eng.*, 49, 713-720.

Lemlich, R. (1972). *Adsorptive bubble separation techniques*. Academic Press, New York.

Lin, S., McKeigue, K., and Maldarelli, C. (1990). Mass transfer-Controlled surfactant adsorption studied by pendant drop digitization. *AIChE J.*, 36 (12), 1785-1795.

Lochiel, A. C., and Calderbank, P. H. (1964). Mass transfer in the continuous phase around axisymmetric bodies of revolution. *Chem. Eng. Sci.* 19. 471-484.

Levich, V. G. (1962). *Physicochemical Hydrodynamics*, Prentice-Hall, Englewood Cliffs, NJ.

Lide, D. R. (1999). *CRC handbook of chemistry and physics*, 80th edition. CRC press.

Lucassen, J., and Giles, D. (1975). Dynamic surface properties of Nonionic surfactant solutions. *J. Chem. Soc. Faraday*, 71(2), 217-232.

Mendelson, H. D. (1967). The prediction of bubble terminal velocities from wave theory, *AIChE J.*, 13, 250-252.

McLaughlin, J. B. (1996). Numerical simulation of bubble motion in water. *J. Colloid Interface Sci.*, 184, 614-625.

Moore, D. W. (1959). The rise of distorted gas bubbles in a viscous liquid. *J. Fluid Mech.*, 6, 113-130.

Moore, D. W. (1963). The boundary layer on a spherical gas bubble. *J. Fluid Mech.*, 16, 161-176.

Moore, D. W. (1965). The velocity of rise of distorted gas bubbles in a liquid of small viscosity. *J. Fluid Mech.*, 23, 749-766.

Nernst, W. (1904). Zeitschrift für physikalische Chemie, 47, 52.

Newman, J. (1967). Retardation of falling drops. *Chem. Eng. Sci.*, 22, 83-85.

Oellrich, L., Schmidt-Traub, H., and Brauer, H. (1973). Theoretiche Berechnung des stofftransports in der umgebung einer einzelblase. *Chem. Eng. Sci.*, 28, 711-721.

Owen, J. J., Morse, D., E., Morse, W. O., and Jovine R. (1999). New developments in flotation equipment for water treatment systems. *Advances in Flotation Technology*, Edited by Parekh, B. K., and Miller, J. D., 381-389.

Ray, A., and Nemethy, G. (1971). A difference spectrophotometric method for the determination of critical micelle concentrations. *J. Phys. Chem.*, 75, 804-808.

Reid, R. C., Prausnitz, J. M., and Sherwood, T. K. (1977). The properties of gases and liquids, 3rd ed., Chap. 11. McGraw-Hill, New York.

Richards, R. H. (1909). *Ore Dressing*. McGraw-Hill Book Company, New York.

Rosen, M. J. (1989). *Surfactants and interfacial phenomena*, 2nd edition. John Wiley & Sons. Inc., p225.

Rousseau, R. W. (1987). *Handbook of separation process technology*. John Wiley & Sons

Rubin, E. (1981). Foam Fractionation – Some Recent Studies, in Theory, Practice, and Process Principles for Physical Separations. Freeman, M. P., and FitzPatrick, J. A. (editors). *Proceedings of the Engineering Foundation Conference*, Asilomar Conference Grounds, Pacific Grove, California, Oct. 30-Nov. 4, 1977. Engineering Foundation, New York. 750.

Rybczynski, W. (1911). On the translatory motion of a fluid sphere in a viscous medium (in German). *Bull Int. Acad. Sci. Math. Natur., Ser.* A, 40-46.

Ryskin G., and Leal, L. G. (1983). Orthogonal mapping. *J. Comp. Phys.*, 50, 71-100.

Ryskin, G., and Leal, L. G. (1984a). Numerical solution of free-boundary problems in fluid mechanics. Part 1. The finite-difference technique. *J. Fluid Mech.*, 148, 1-17.

Ryskin, G., and Leal, L. G. (1984b). Numerical solution of free-boundary problems in fluid mechanics. Part 2. Buoyancy-driven motion of a gas bubble through a quiescent liquid. *J. Fluid Mech.*, 148, 19-35.

Sadhal, S. S., and Johnson, R. E. (1983). Stokes flow past bubbles and drops partially coated with thin films - exact solution. *J. Fluid Mech.*, 126, 237-250.

Sam, A. (1995). Single bubble behaviour study in a flotation column. Ph. D. thesis, McGill University.

Sam, A., Gomez, C. O., and Finch, J. A. (1996). Axial velocity profiles of single bubbles in water/frother solutions. *Int. J. Miner. Process.*, 47, 177-196.

Savic, P. (1953). Circulation and distortion of liquid drops falling through a viscous medium. *Nat. Res. Counc. Can. Div. Mech. Eng. Report* MT-22.

Saville, D. A. (1973). The effect of interfacial tension gradients and droplet behaviour. *Chem. Eng. J.*, 5, 251-259.

Sawi, M. E. (1974). Distorted gas bubbles at large Reynolds number. *J. Fluid Mech.*, 62, 163-183.

Schechter, R. S., and Fairley, R. W. (1963). Interfacial tension gradients and droplet behaviour. *Can. J. Chem. Eng.*, 41, 103-107.

Schiller, V. L., and Naumann, A. (1933). Über die grundlegenden Berechnungen bei der Schwerkraftaufbereitung, *Zettschrifi Des Vereines Deutscher Ingenieure (Z. Ver. dt Ing.)*, 77(12), 318-320.

Schlichting, H. (1979). *Boundary layer Theory*, 7th ed. New York, McGraw-Hill.

Skelland, A. H. (1974). *Diffusional mass transfer*. New York, Wiley Interscience.

Smith, J. S., Kalliate, T. V., and Louis, J. T. (1996). Bubble column reactors for wastewater treatment. 1. Theory and modelling of continuous countercurrent solvent sublation. *Industrial Engineering Chemical Research*, 35, 1688-1699.

Streletzky, K., and Phillies, G. D. J. (1995). Temperature dependence of Triton X-100 Micelle size and hydration. *Langmuir*, 11, 42-47.

Takagi, S., and Yamamoto, A. (1999). Numerical analysis of a rising bubble in a contaminated liquid. *Proceedings of FEDSM'99, 3rd ASME/JSME joint fluids engineering conference*, 1-6.

Tharapiwattananon, N., Scamehorn, J. F., Osuwan, S., Harwell, J., and Haller, K. J. (1996). Surfactant recovery from water using foam fraction. *Separation Science and Technology*, 31(9), 1233-1258.

Thind, B. B., and Wallace, D. J. (1984). Modified flotation technique for quantitative determination of mite populations in feedstuffs. *Journal of the Association of Official Analytical Chemists*, 67, 866-868.

Tsujii, K. (1997). *Surface Activity, principles, phenomena, and applications*. Academic Press.

Van, H. J., Bleys, G., and Joos, P. (1986). Adsorption kinetics at the oil/water interface. *J. Colloid Interface Sci.*, 114(2), 432-441.

Warszynski, P., Jachimska, B., and Malysa, K. (1996). Experimental evidence of the existence of non-equilibrium coverages over the surface of the floating bubble. *Colloids and Surfaces A: Physicochem. Eng. Aspects* 108, 321-325.

Weinheimer, R. M., Evans, D. F., and Gussler, E. L. (1981). Diffusion in surfactant solution. *Colloid Interface Sci.*, 80, 357

Wesselingh, J. A. (1987). The velocity of particles, drops and bubbles. *Chem. Eng. Process*, 21, 9-14.

Wilke, C. R., and Chang, P. (1955). Correlation of diffusion coefficients in dilute solutions. *AIChE J.*, 1, 264-270.

Winnikow, S. (1967). Letter to editors. *Chem. Eng. Sci.*, 22, 477.

Yamamoto, T., and Ishii, T. (1987). Effect of surface active materials on the drag coefficient and shape of single large gas bubbles. *Chem. Eng. Sci.*, 42(6), 1297-1303.

Zhang, Y., Gomez, C., and Finch, J. A. (1996). Terminal velocity of a 1.5 mm diameter bubble in water alone and surfactant solutions. *Column'96. Proceedings of the International Symposium on Column Flotation, (Eds. Gomez, C., and Finch, J. A.), CIM,* 63-69.

Zhang, Y., and Finch, J. A. (1999). Single bubble terminal velocity - experiment and modelling. *Advances in Flotation Technology,* Edited by Parekh, B. K., and Miller, J. D., 83-94.

Zhou, Z. A., Egiebor, N. O., and Plitt, L. R. (1991). Effects of Frothers on bubble rise velocity in a flotation column - single bubble system. *Column 91,* 1, 249-261.

Zhou, Z. A., Egiebor, N. O., and Plitt, L. R. (1992). Frother effects on single bubble motion in a water column. *Canadian Metallurgical Quarterly*, 31(1), 11-16.

# APPENDIX OF DATA

Fig. 4.3 data

| **Residence time** | | | | | |
|---|---|---|---|---|---|
| **0 h.** | | **2.5 h** | | **5 h.** | |
| **Time, s** | **Velocity, m/s** | **Time, s** | **Velocity, m/s** | **Time, s** | **Velocity, m/s** |
| 0.05 | 0.33 | 0.02 | 0.24 | 0.02 | 0.14 |
| 0.25 | 0.36 | 0.28 | 0.36 | 0.08 | 0.33 |
| 0.30 | 0.35 | 0.32 | 0.35 | 0.32 | 0.36 |
| 0.35 | 0.36 | 0.50 | 0.36 | 0.35 | 0.35 |
| 0.53 | 0.36 | 1.02 | 0.35 | 0.53 | 0.35 |
| 1.03 | 0.35 | 1.87 | 0.34 | 1.03 | 0.35 |
| 1.87 | 0.35 | 2.92 | 0.33 | 1.87 | 0.33 |
| 3.08 | 0.35 | 4.20 | 0.33 | 2.93 | 0.32 |
| 4.78 | 0.35 | 5.97 | 0.31 | 4.03 | 0.30 |
| 6.68 | 0.35 | 8.03 | 0.29 | 5.70 | 0.27 |
| 8.67 | 0.34 | 9.80 | 0.28 | 8.13 | 0.24 |
| | | 11.38 | 0.26 | 10.13 | 0.23 |
| | | | | 11.57 | 0.22 |
| | | | | 13.32 | 0.20 |

Fig. 4.5 data

| **Bubble 1** | | **Bubble 2** | | **Bubble 3** | |
|---|---|---|---|---|---|
| **Time, s** | **Velocity, m/s** | **Time, s** | **Velocity, m/s** | **Time, s** | **Velocity, m/s** |
| 0.02 | 0.15 | 0.02 | 0.27 | 0.02 | 0.17 |
| 0.25 | 0.38 | 0.12 | 0.38 | 0.12 | 0.38 |
| 0.28 | 0.35 | 0.25 | 0.36 | 0.25 | 0.38 |
| 0.42 | 0.27 | 0.48 | 0.30 | 0.35 | 0.33 |
| 0.52 | 0.29 | 0.58 | 0.27 | 0.47 | 0.30 |
| 0.75 | 0.26 | 1.15 | 0.23 | 0.70 | 0.27 |
| 0.88 | 0.24 | 1.72 | 0.20 | 0.97 | 0.24 |
| 1.25 | 0.23 | 2.05 | 0.18 | 1.30 | 0.21 |
| 1.35 | 0.20 | 3.43 | 0.16 | 1.63 | 0.20 |
| 1.52 | 0.21 | 7.40 | 0.16 | 2.23 | 0.17 |
| 2.35 | 0.18 | 12.58 | 0.16 | 2.57 | 0.19 |
| 3.92 | 0.17 | 17.58 | 0.16 | 3.23 | 0.17 |
| 7.52 | 0.16 | 22.08 | 0.16 | 4.85 | 0.17 |
| 8.35 | 0.16 | 22.75 | 0.16 | 6.35 | 0.16 |
| 12.35 | 0.16 | 0.75 | 0.27 | 8.43 | 0.15 |
| 13.35 | 0.16 | | | 12.43 | 0.16 |
| 17.35 | 0.16 | | | 15.43 | 0.16 |
| 21.68 | 0.16 | | | 19.10 | 0.16 |
| 22.05 | 0.16 | | | 22.02 | 0.16 |

Fig. 4.6 data

| **Tap water** | | **$1,3\times10^{-7}$ mol/m$^3$** | | **$13\times10^{-7}$ mol/m$^3$** | | **$130\times10^{-7}$ mol/m$^3$** | | **$260\times10^{-7}$ mol/m$^3$** | |
|---|---|---|---|---|---|---|---|---|---|
| **t, s** | **u, m/s** | **t, s** | **u, m/s** | **t, s** | **u, m/s** | **t, s** | **u, m/s** | **t, s** | **u, m/s** |
| 0.02 | 0.20 | 0.02 | 0.26 | 0.02 | 0.14 | 0.02 | 0.17 | 0.02 | 0.11 |
| 0.05 | 0.30 | 0.05 | 0.33 | 0.05 | 0.33 | 0.05 | 0.33 | 0.05 | 0.30 |
| 0.08 | 0.33 | 0.08 | 0.36 | 0.08 | 0.35 | 0.08 | 0.35 | 0.08 | 0.33 |
| 0.12 | 0.36 | 0.35 | 0.36 | 0.15 | 0.36 | 0.12 | 0.36 | 0.12 | 0.36 |
| 0.30 | 0.35 | 0.53 | 0.35 | 0.53 | 0.36 | 0.57 | 0.35 | 0.32 | 0.35 |
| 0.53 | 0.35 | 1.03 | 0.35 | 0.92 | 0.35 | 1.10 | 0.35 | 0.53 | 0.35 |
| 1.03 | 0.34 | 1.70 | 0.34 | 1.43 | 0.35 | 1.95 | 0.34 | 1.03 | 0.35 |
| 1.87 | 0.34 | 2.53 | 0.34 | 2.25 | 0.35 | 2.97 | 0.34 | 1.98 | 0.34 |
| 3.08 | 0.34 | 3.62 | 0.34 | 3.33 | 0.35 | 4.17 | 0.34 | 3.17 | 0.33 |
| 4.32 | 0.34 | 5.02 | 0.34 | 4.85 | 0.35 | 5.50 | 0.33 | 4.37 | 0.33 |
| 5.88 | 0.34 | 6.38 | 0.34 | 6.35 | 0.35 | 6.97 | 0.32 | 5.77 | 0.30 |
| 7.50 | 0.34 | 7.55 | 0.34 | 7.57 | 0.35 | 8.67 | 0.31 | 7.13 | 0.27 |
| 8.70 | 0.33 | 8.72 | 0.34 | 8.87 | 0.34 | 10.58 | 0.28 | 8.67 | 0.24 |
| 9.90 | 0.33 | 9.87 | 0.34 | 10.18 | 0.33 | | | 10.70 | 0.22 |
| 10.90 | 0.32 | 10.75 | 0.33 | | | | | 12.77 | 0.20 |

Fig. 4.7 data

| Tap water | | | | | |
|---|---|---|---|---|---|
| **Day 1** | | **Day 2** | | **Day 3** | |
| **Time, s** | **Velocity, m/s** | **Time, s** | **Velocity, m/s** | **Time, s** | **Velocity, m/s** |
| 0.02 | 0.05 | 0.02 | 0.14 | 0.02 | 0.02 |
| 0.05 | 0.26 | 0.05 | 0.33 | 0.05 | 0.23 |
| 0.08 | 0.35 | 0.08 | 0.35 | 0.08 | 0.36 |
| 0.13 | 0.36 | 0.12 | 0.37 | 0.17 | 0.36 |
| 0.23 | 0.36 | 0.20 | 0.36 | 0.30 | 0.37 |
| 0.37 | 0.36 | 0.33 | 0.36 | 0.43 | 0.36 |
| 0.52 | 0.36 | 0.57 | 0.36 | 0.58 | 0.35 |
| 0.68 | 0.36 | 0.90 | 0.35 | 1.18 | 0.36 |
| 0.93 | 0.36 | 1.40 | 0.35 | 2.42 | 0.35 |
| 1.27 | 0.36 | 2.07 | 0.35 | 3.73 | 0.33 |
| 1.77 | 0.35 | 2.97 | 0.35 | 5.12 | 0.32 |
| 2.43 | 0.35 | 4.17 | 0.35 | 6.63 | 0.31 |
| 3.33 | 0.35 | 5.47 | 0.35 | 8.35 | 0.30 |
| 4.55 | 0.35 | 6.70 | 0.34 | 9.87 | 0.28 |
| 5.78 | 0.35 | 7.83 | 0.34 | | |
| 6.93 | 0.34 | 9.17 | 0.33 | | |
| 8.20 | 0.34 | 10.52 | 0.32 | | |
| 9.33 | 0.33 | | | | |
| 10.32 | 0.32 | | | | |
| **Triton solution** | | | | | |
| **Day 1** | | **Day 2** | | **Day 3** | |
| **Time, s** | **Velocity, m/s** | **Time, s** | **Velocity, m/s** | **Time, s** | **Velocity, m/s** |
| 0.02 | 0.12 | 0.02 | 0.26 | 0.02 | 0.08 |
| 0.05 | 0.32 | 0.05 | 0.35 | 0.05 | 0.30 |
| 0.08 | 0.36 | 0.08 | 0.35 | 0.08 | 0.35 |
| 0.12 | 0.33 | 0.12 | 0.35 | 0.12 | 0.35 |
| 0.15 | 0.36 | 0.15 | 0.36 | 0.15 | 0.35 |
| 0.18 | 0.36 | 0.18 | 0.35 | 0.18 | 0.36 |
| 0.22 | 0.35 | 0.22 | 0.36 | 0.22 | 0.35 |
| 0.25 | 0.35 | 0.25 | 0.35 | 0.25 | 0.36 |
| 0.32 | 0.35 | 0.28 | 0.36 | 0.32 | 0.35 |
| 0.38 | 0.36 | 0.32 | 0.36 | 0.35 | 0.35 |
| 0.45 | 0.35 | 0.35 | 0.36 | 0.38 | 0.35 |
| 0.58 | 0.31 | 0.45 | 0.34 | 0.60 | 0.32 |
| 1.15 | 0.21 | 0.62 | 0.33 | 0.93 | 0.27 |
| 2.93 | 0.15 | 0.78 | 0.23 | 1.43 | 0.19 |
| 5.47 | 0.14 | 1.20 | 0.23 | 2.10 | 0.16 |

| | | | | | |
|---|---|---|---|---|---|
| 8.33 | 0.15 | 1.70 | 0.17 | 2.78 | 0.15 |
| 11.50 | 0.15 | 2.22 | 0.16 | 4.17 | 0.15 |
| 14.50 | 0.15 | 2.92 | 0.16 | 6.50 | 0.14 |
| 17.70 | 0.15 | 3.95 | 0.15 | 9.10 | 0.15 |
| | | 5.47 | 0.15 | 11.97 | 0.15 |
| | | 7.67 | 0.15 | 14.93 | 0.15 |
| | | 10.67 | 0.15 | 17.90 | 0.15 |
| | | 13.70 | 0.15 | 20.80 | 0.15 |
| | | 16.70 | 0.15 | 23.13 | 0.15 |
| | | 19.60 | 0.15 | | |

Fig. 4.8 data

| d-water | | d-water | | h-water | | h-water | |
|---|---|---|---|---|---|---|---|
| t, s | u, m/s | t, s | u, m/s | t, s | u, m/s | t, s | u, m/s |
| 1.15 | 0.21 | 1.03 | 0.14 | 1.10 | 0.15 | 1.15 | 0.18 |
| 2.1 | 0.36 | 1.78 | 0.32 | 1.88 | 0.32 | 2.03 | 0.35 |
| 3.25 | 0.33 | 2.90 | 0.36 | 3.00 | 0.36 | 6.25 | 0.37 |
| 4.425 | 0.38 | 6.53 | 0.38 | 4.20 | 0.36 | 10.50 | 0.36 |
| 9.375 | 0.38 | 10.23 | 0.38 | 5.40 | 0.36 | 11.68 | 0.35 |
| 10.6 | 0.36 | 11.43 | 0.35 | 6.60 | 0.36 | 13.45 | 0.36 |
| 11.8 | 0.36 | 18.93 | 0.34 | 9.08 | 0.38 | 17.48 | 0.34 |
| 13 | 0.36 | 34.95 | 0.31 | 11.50 | 0.36 | 23.03 | 0.33 |
| 17.725 | 0.35 | 55.15 | 0.30 | 17.85 | 0.35 | 28.38 | 0.32 |
| 18.875 | 0.35 | 79.20 | 0.28 | 28.88 | 0.32 | 36.75 | 0.31 |
| 30.025 | 0.32 | 101.28 | 0.28 | 44.33 | 0.31 | 52.48 | 0.30 |
| | | | | 64.23 | 0.29 | 72.08 | 0.29 |
| | | | | 84.33 | 0.28 | 89.75 | 0.28 |
| | | | | 101.68 | 0.28 | 104.20 | 0.27 |

| d-solution | | d-solution | | h-solution | | h-solution | |
|---|---|---|---|---|---|---|---|
| t, s | u, m/s | t, s | u, m/s | t, s | u, m/s | t, s | u, m/s |
| 1.23 | 0.26 | 1.05 | 0.21 | 1.10 | 0.18 | 0.90 | 0.06 |
| 2.23 | 0.35 | 1.94 | 0.32 | 1.94 | 0.32 | 1.50 | 0.30 |
| 3.37 | 0.34 | 3.07 | 0.35 | 3.04 | 0.34 | 3.18 | 0.35 |
| 4.54 | 0.37 | 4.28 | 0.38 | 4.23 | 0.38 | 7.95 | 0.38 |
| 6.38 | 0.37 | 7.95 | 0.37 | 10.35 | 0.36 | 12.40 | 0.32 |
| 11.05 | 0.35 | 13.55 | 0.31 | 16.58 | 0.29 | 18.48 | 0.29 |
| 17.35 | 0.29 | 41.55 | 0.26 | 32.53 | 0.28 | 26.00 | 0.28 |
| 23.00 | 0.28 | 59.40 | 0.23 | 71.38 | 0.22 | 40.18 | 0.26 |
| 36.03 | 0.27 | 79.15 | 0.21 | 87.38 | 0.20 | 59.35 | 0.23 |
| 55.83 | 0.24 | 97.30 | 0.19 | 108.65 | 0.19 | 76.05 | 0.21 |
| 74.78 | 0.22 | 106.10 | 0.17 | | | 90.10 | 0.20 |
| 95.28 | 0.20 | | | | | 108.90 | 0.19 |

Fig. 5.2 data

| Experimental | | Moore | | Moore & Sawi | | Clift | |
|---|---|---|---|---|---|---|---|
| **de, mm** | **u, m/s** | **de, mm** | **u, m/s** | **de, mm** | **u, m/s** | **de, mm** | **u, m/s** |
| 0.80 | 0.23 | 0.40 | 0.06 | 0.68 | 0.16 | 1.00 | 0.39 |
| 1.40 | 0.36 | 0.60 | 0.13 | 0.83 | 0.22 | 1.20 | 0.37 |
| 1.80 | 0.38 | 0.80 | 0.22 | 1.01 | 0.27 | 1.30 | 0.35 |
| | | 1.00 | 0.34 | 1.17 | 0.31 | 1.40 | 0.34 |
| | | 1.20 | 0.48 | 1.34 | 0.33 | 1.50 | 0.33 |
| | | | | 1.64 | 0.34 | 1.70 | 0.32 |
| | | | | 2.02 | 0.33 | 1.80 | 0.31 |
| | | | | | | 1.90 | 0.30 |
| | | | | | | 2.00 | 0.30 |

Fig. 5.3 data

| Tap water | | $50\times10^{-6}$mol/m$^3$ | | $125\times10^{-6}$mol/m$^3$ | | $750\times10^{-6}$mol/m$^3$ | |
|---|---|---|---|---|---|---|---|
| **t, s** | **u, m/s** | **t, s** | **u, m/s** | **t, s** | **u, m/s** | **t, s** | **u, m/s** |
| 0.02 | 0.20 | 0.02 | 0.12 | 0.02 | 0.05 | 0.02 | 0.12 |
| 0.05 | 0.30 | 0.05 | 0.27 | 0.05 | 0.27 | 0.05 | 0.32 |
| 0.08 | 0.33 | 0.08 | 0.33 | 0.08 | 0.32 | 0.08 | 0.30 |
| 0.12 | 0.36 | 0.12 | 0.36 | 0.12 | 0.36 | 0.12 | 0.35 |
| 0.35 | 0.36 | 0.38 | 0.35 | 0.35 | 0.35 | 0.15 | 0.33 |
| 0.53 | 0.35 | 0.42 | 0.35 | 0.38 | 0.35 | 0.25 | 0.32 |
| 1.03 | 0.34 | 0.60 | 0.35 | 0.70 | 0.34 | 0.35 | 0.30 |
| 1.87 | 0.34 | 1.12 | 0.34 | 1.23 | 0.32 | 0.38 | 0.28 |
| 3.08 | 0.34 | 1.80 | 0.34 | 1.55 | 0.30 | 0.42 | 0.26 |
| 4.32 | 0.34 | 2.30 | 0.33 | 1.73 | 0.27 | 0.47 | 0.23 |
| 5.88 | 0.34 | 2.67 | 0.32 | 1.92 | 0.25 | 0.53 | 0.19 |
| 7.50 | 0.34 | 3.00 | 0.31 | 2.08 | 0.23 | 0.60 | 0.18 |
| 8.70 | 0.33 | 3.17 | 0.30 | 2.25 | 0.22 | 0.67 | 0.17 |
| 9.90 | 0.33 | 3.33 | 0.30 | 2.40 | 0.21 | 0.73 | 0.17 |
| 10.90 | 0.32 | 3.63 | 0.28 | 2.57 | 0.21 | 0.83 | 0.16 |
| | | 3.97 | 0.27 | 2.77 | 0.19 | 0.95 | 0.16 |
| | | 4.27 | 0.26 | 2.97 | 0.19 | 1.08 | 0.15 |
| | | 4.55 | 0.25 | 3.17 | 0.18 | 1.25 | 0.15 |
| | | 4.87 | 0.23 | 3.37 | 0.18 | 1.38 | 0.15 |
| | | 5.20 | 0.22 | 3.72 | 0.17 | 1.93 | 0.15 |
| | | 5.53 | 0.21 | 4.03 | 0.17 | 3.02 | 0.15 |
| | | 5.87 | 0.21 | 4.38 | 0.17 | 4.60 | 0.15 |
| | | 6.17 | 0.20 | 5.10 | 0.16 | 6.75 | 0.16 |
| | | 6.82 | 0.19 | 5.87 | 0.15 | 8.83 | 0.16 |
| | | 7.60 | 0.18 | 7.23 | 0.15 | 11.17 | 0.16 |
| | | 8.07 | 0.18 | 9.60 | 0.15 | 13.67 | 0.16 |
| | | 8.47 | 0.18 | 12.70 | 0.15 | 16.47 | 0.16 |
| | | 8.87 | 0.17 | 15.90 | 0.15 | 19.13 | 0.17 |
| | | 10.10 | 0.17 | 18.33 | 0.15 | 21.63 | 0.17 |
| | | 12.23 | 0.16 | 20.90 | 0.15 | | |
| | | 14.47 | 0.16 | | | | |
| | | 16.97 | 0.15 | | | | |

**Fig. 6.1 data**

| x | y | x | y | x | y |
|---|---|---|---|---|---|
| 0.966539 | 0 | 0.782001 | 0.592906 | -0.12542 | 1.011981 |
| 0.966351 | 0.019946 | 0.764462 | 0.617338 | -0.17269 | 1.004901 |
| 0.965786 | 0.039923 | 0.745798 | 0.641758 | -0.22008 | 0.99518 |
| 0.964836 | 0.059935 | 0.725972 | 0.666116 | -0.26746 | 0.982746 |
| 0.963504 | 0.080021 | 0.704947 | 0.690355 | -0.31465 | 0.967538 |
| 0.961772 | 0.100194 | 0.682689 | 0.714412 | -0.3615 | 0.949508 |
| 0.959642 | 0.120477 | 0.659167 | 0.738222 | -0.40782 | 0.92862 |
| 0.957089 | 0.140894 | 0.634352 | 0.761709 | -0.45345 | 0.904853 |
| 0.954111 | 0.161458 | 0.60822 | 0.784797 | -0.49821 | 0.878202 |
| 0.950682 | 0.182193 | 0.580752 | 0.807401 | -0.5419 | 0.848679 |
| 0.946791 | 0.203111 | 0.551933 | 0.829432 | -0.58436 | 0.816309 |
| 0.942411 | 0.224231 | 0.521752 | 0.850796 | -0.62538 | 0.781139 |
| 0.937524 | 0.245564 | 0.490206 | 0.871395 | -0.6648 | 0.743231 |
| 0.932102 | 0.267123 | 0.457298 | 0.891126 | -0.70243 | 0.702665 |
| 0.92612 | 0.288916 | 0.423036 | 0.90988 | -0.73809 | 0.659539 |
| 0.919548 | 0.310952 | 0.38744 | 0.927548 | -0.77161 | 0.613968 |
| 0.912356 | 0.333235 | 0.350534 | 0.944014 | -0.80283 | 0.566085 |
| 0.904512 | 0.355768 | 0.312352 | 0.959163 | -0.83159 | 0.516041 |
| 0.895981 | 0.378548 | 0.272937 | 0.972876 | -0.85775 | 0.463999 |
| 0.886727 | 0.401573 | 0.232342 | 0.985031 | -0.88117 | 0.410142 |
| 0.876714 | 0.424835 | 0.19063 | 0.995509 | -0.90172 | 0.354663 |
| 0.865902 | 0.448323 | 0.14787 | 1.004188 | -0.91931 | 0.297768 |
| 0.854252 | 0.472024 | 0.104146 | 1.010949 | -0.93383 | 0.239676 |
| 0.841724 | 0.495917 | 0.059548 | 1.015674 | -0.9452 | 0.180615 |
| 0.828276 | 0.519981 | 0.014177 | 1.018248 | -0.95337 | 0.120819 |
| 0.813868 | 0.544189 | -0.03186 | 1.018559 | -0.9583 | 0.060528 |
| 0.798456 | 0.56851 | -0.07843 | 1.016503 | -0.95995 | 0 |

Fig. 6.2 data

| Angle, ° | $C_D$ | Angle, ° | $C_D$ | Angle, ° | $C_D$ |
|---|---|---|---|---|---|
| 0 | 0.209324 | 37.47454 | 0.229663 | 98.97386 | 0.884905 |
| 1.500685 | 0.209913 | 39.82885 | 0.234958 | 102.8234 | 0.94235 |
| 3.00548 | 0.210013 | 42.25489 | 0.241872 | 106.7364 | 0.994992 |
| 4.518483 | 0.210077 | 44.75424 | 0.249085 | 110.7105 | 1.038158 |
| 6.043769 | 0.2101 | 47.32826 | 0.257727 | 114.7429 | 1.073781 |
| 7.585381 | 0.210122 | 49.97814 | 0.268946 | 118.8308 | 1.103944 |
| 9.147315 | 0.210168 | 52.70481 | 0.283123 | 122.9713 | 1.130592 |
| 10.73351 | 0.210254 | 55.50905 | 0.300193 | 127.1612 | 1.154603 |
| 12.34785 | 0.210394 | 58.39137 | 0.321321 | 131.3972 | 1.166622 |
| 13.99413 | 0.210626 | 61.35211 | 0.346104 | 135.6761 | 1.183672 |
| 15.67606 | 0.210941 | 64.39137 | 0.378595 | 139.9941 | 1.192643 |
| 17.39724 | 0.211394 | 67.50905 | 0.416152 | 144.3479 | 1.197961 |
| 19.16119 | 0.211884 | 70.70481 | 0.455519 | 148.733 | 1.201652 |
| 20.9713 | 0.212461 | 73.97814 | 0.501918 | 153.1473 | 1.203353 |
| 22.83082 | 0.213342 | 77.32826 | 0.552015 | 157.5854 | 1.204224 |
| 24.74288 | 0.214841 | 80.75424 | 0.602758 | 162.0438 | 1.204585 |
| 26.71047 | 0.216233 | 84.25489 | 0.661512 | 166.5185 | 1.204696 |
| 28.73641 | 0.217738 | 87.82885 | 0.718622 | 171.0055 | 1.204743 |
| 30.82337 | 0.219591 | 91.47454 | 0.778083 | 175.5007 | 1.201604 |
| 32.97386 | 0.222208 | 95.1902 | 0.832431 | 180 | 1.20178 |
| 35.1902 | 0.225486 |  |  |  |  |

Fig. 6.3 data

| **Angle, °** | **$\Gamma$, mol/m$^2$** | **Angle, °** | **$\Gamma$, mol/m$^2$** | **Angle, °** | **$\Gamma$, mol/m$^2$** |
|---|---|---|---|---|---|
| 0 | 0 | 37.47454 | 7.83E-08 | 98.97386 | 1.51E-07 |
| 1.500685 | 0 | 39.82885 | 8.53E-08 | 102.8234 | 1.54E-07 |
| 3.00548 | 1.29E-09 | 42.25489 | 9.22E-08 | 106.7364 | 1.57E-07 |
| 4.518483 | 3.16E-09 | 44.75424 | 9.96E-08 | 110.7105 | 1.63E-07 |
| 6.043769 | 5.18E-09 | 47.32826 | 1.07E-07 | 114.7429 | 1.7E-07 |
| 7.585381 | 7.32E-09 | 49.97814 | 1.14E-07 | 118.8308 | 1.77E-07 |
| 9.147315 | 9.6E-09 | 52.70481 | 1.2E-07 | 122.9713 | 1.85E-07 |
| 10.73351 | 1.2E-08 | 55.50905 | 1.25E-07 | 127.1612 | 1.91E-07 |
| 12.34785 | 1.47E-08 | 58.39137 | 1.29E-07 | 131.3972 | 2.02E-07 |
| 13.99413 | 1.76E-08 | 61.35211 | 1.33E-07 | 135.6761 | 2.08E-07 |
| 15.67606 | 2.07E-08 | 64.39137 | 1.35E-07 | 139.9941 | 2.16E-07 |
| 17.39724 | 2.41E-08 | 67.50905 | 1.35E-07 | 144.3479 | 2.25E-07 |
| 19.16119 | 2.78E-08 | 70.70481 | 1.37E-07 | 148.733 | 2.32E-07 |
| 20.9713 | 3.19E-08 | 73.97814 | 1.38E-07 | 153.1473 | 2.4E-07 |
| 22.83082 | 3.63E-08 | 77.32826 | 1.38E-07 | 157.5854 | 2.46E-07 |
| 24.74288 | 4.1E-08 | 80.75424 | 1.4E-07 | 162.0438 | 2.52E-07 |
| 26.71047 | 4.62E-08 | 84.25489 | 1.4E-07 | 166.5185 | 2.56E-07 |
| 28.73641 | 5.19E-08 | 87.82885 | 1.42E-07 | 171.0055 | 2.6E-07 |
| 30.82337 | 5.81E-08 | 91.47454 | 1.44E-07 | 175.5007 | 2.64E-07 |
| 32.97386 | 6.45E-08 | 95.1902 | 1.47E-07 | 180 | 2.66E-07 |
| 35.1902 | 7.13E-08 | | | | |

Fig. 7.1 data

| Stagnant cap angle, ° | Separation angle, ° |
|---|---|
| 35.19 | 3.95 |
| 37.47 | 9.63 |
| 39.83 | 13.21 |
| 47.33 | 21.76 |
| 55.51 | 29.15 |
| 61.35 | 33.70 |
| 67.51 | 37.88 |
| 73.98 | 41.77 |
| 84.25 | 46.60 |
| 95.19 | 49.92 |
| 102.82 | 50.87 |
| 110.71 | 51.00 |
| 118.83 | 50.74 |
| 127.16 | 50.11 |
| 135.68 | 49.53 |
| 144.35 | 49.14 |
| 153.15 | 48.95 |
| 162.04 | 48.89 |
| 175.50 | 48.96 |

Fig. 7.2 – 7.9 experimental data used for model validation

| $2.5\times10^{-5}$ mol/m$^3$ | | $12.5\times10^{-5}$ mol/m$^3$ | | $74.9\times10^{-5}$ mol/m$^3$ | |
|---|---|---|---|---|---|
| **t, s** | **u, m/s** | **t, s** | **u, m/s** | **t, s** | **u, m/s** |
| 0.02 | 0.05 | 0.02 | 0.18 | 0.02 | 0.05 |
| 0.15 | 0.23 | 0.07 | 0.22 | 0.07 | 0.16 |
| 0.55 | 0.22 | 0.20 | 0.21 | 0.15 | 0.14 |
| 1.13 | 0.21 | 0.40 | 0.20 | 0.25 | 0.12 |
| 2.00 | 0.19 | 0.62 | 0.18 | 0.37 | 0.11 |
| 2.97 | 0.17 | 1.02 | 0.16 | 0.53 | 0.11 |
| 3.97 | 0.16 | 1.50 | 0.13 | 1.00 | 0.10 |
| 4.98 | 0.15 | 2.57 | 0.12 | 1.93 | 0.10 |
| 6.00 | 0.14 | 4.27 | 0.11 | 3.25 | 0.10 |
| 7.38 | 0.13 | 6.13 | 0.10 | 5.13 | 0.10 |
| 9.23 | 0.13 | 8.08 | 0.10 | 8.50 | 0.10 |
| 11.90 | 0.12 | 10.28 | 0.10 | 12.93 | 0.10 |
| 14.30 | 0.12 | 12.87 | 0.10 | 17.70 | 0.10 |
| 16.13 | 0.12 | 16.53 | 0.10 | 24.63 | 0.11 |
| 20.40 | 0.12 | 22.70 | 0.10 | 32.30 | 0.11 |
| 25.63 | 0.12 | 30.47 | 0.11 | 35.93 | 0.11 |
| 28.00 | 0.12 | 34.65 | 0.11 | | |

Fig. 7.2 model data

| **Stagnant cap angle, °** | **[c], mol/ m$^3$** | | | **u, m/s** |
|---|---|---|---|---|
| | **$2.5\times10^{-3}$** | **$12.5\times10^{-3}$** | **$74.9\times10^{-3}$** | |
| | **t, s** | **t, s** | **t, s** | |
| 0.00 | 0.00E+00 | 0.00E+00 | 0.00E+00 | 0.2234 |
| 1.50 | 0.00E+00 | 0.00E+00 | 0.00E+00 | 0.2230 |
| 3.01 | 1.32E-04 | 2.63E-05 | 4.39E-06 | 0.2230 |
| 4.52 | 7.27E-04 | 1.45E-04 | 2.42E-05 | 0.2230 |
| 6.04 | 2.13E-03 | 4.27E-04 | 7.11E-05 | 0.2230 |
| 7.59 | 4.75E-03 | 9.51E-04 | 1.58E-04 | 0.2229 |
| 9.15 | 9.07E-03 | 1.81E-03 | 3.02E-04 | 0.2229 |
| 10.73 | 1.57E-02 | 3.14E-03 | 5.23E-04 | 0.2229 |
| 12.35 | 2.54E-02 | 5.07E-03 | 8.46E-04 | 0.2228 |
| 13.99 | 3.90E-02 | 7.80E-03 | 1.30E-03 | 0.2227 |
| 15.68 | 5.77E-02 | 1.15E-02 | 1.92E-03 | 0.2225 |
| 17.40 | 8.29E-02 | 1.66E-02 | 2.76E-03 | 0.2223 |
| 19.16 | 1.16E-01 | 2.33E-02 | 3.88E-03 | 0.2220 |
| 20.97 | 1.60E-01 | 3.21E-02 | 5.34E-03 | 0.2217 |
| 22.83 | 2.17E-01 | 4.34E-02 | 7.23E-03 | 0.2213 |
| 24.74 | 2.89E-01 | 5.78E-02 | 9.63E-03 | 0.2205 |
| 26.71 | 3.81E-01 | 7.61E-02 | 1.27E-02 | 0.2198 |
| 28.74 | 4.97E-01 | 9.94E-02 | 1.66E-02 | 0.2190 |
| 30.82 | 6.43E-01 | 1.29E-01 | 2.14E-02 | 0.2181 |
| 32.97 | 8.22E-01 | 1.64E-01 | 2.74E-02 | 0.2168 |
| 35.19 | 1.04E+00 | 2.08E-01 | 3.47E-02 | 0.2152 |
| 37.47 | 1.31E+00 | 2.61E-01 | 4.35E-02 | 0.2132 |
| 39.83 | 1.62E+00 | 3.24E-01 | 5.40E-02 | 0.2108 |
| 42.25 | 1.99E+00 | 3.98E-01 | 6.63E-02 | 0.2078 |
| 44.75 | 2.44E+00 | 4.87E-01 | 8.12E-02 | 0.2048 |
| 47.33 | 2.96E+00 | 5.92E-01 | 9.86E-02 | 0.2013 |
| 49.98 | 3.55E+00 | 7.10E-01 | 1.18E-01 | 0.1971 |
| 52.70 | 4.21E+00 | 8.42E-01 | 1.40E-01 | 0.1921 |
| 55.51 | 4.95E+00 | 9.89E-01 | 1.65E-01 | 0.1865 |
| 58.39 | 5.75E+00 | 1.15E+00 | 1.92E-01 | 0.1803 |
| 61.35 | 6.64E+00 | 1.33E+00 | 2.21E-01 | 0.1737 |
| 64.39 | 7.51E+00 | 1.50E+00 | 2.50E-01 | 0.1661 |
| 67.51 | 8.44E+00 | 1.69E+00 | 2.81E-01 | 0.1584 |
| 70.70 | 9.58E+00 | 1.92E+00 | 3.19E-01 | 0.1514 |
| 73.98 | 1.07E+01 | 2.15E+00 | 3.58E-01 | 0.1442 |
| 77.33 | 1.21E+01 | 2.42E+00 | 4.03E-01 | 0.1375 |
| 80.75 | 1.37E+01 | 2.75E+00 | 4.58E-01 | 0.1316 |
| 84.25 | 1.54E+01 | 3.07E+00 | 5.12E-01 | 0.1256 |

| | | | | |
|---|---|---|---|---|
| 87.83 | 1.75E+01 | 3.50E+00 | 5.83E-01 | 0.1206 |
| 91.47 | 1.99E+01 | 3.97E+00 | 6.62E-01 | 0.1159 |
| 95.19 | 2.31E+01 | 4.61E+00 | 7.69E-01 | 0.1120 |
| 98.97 | 2.69E+01 | 5.39E+00 | 8.98E-01 | 0.1086 |
| 102.82 | 3.08E+01 | 6.15E+00 | 1.03E+00 | 0.1053 |
| 106.74 | 3.55E+01 | 7.10E+00 | 1.18E+00 | 0.1024 |
| 110.71 | 4.20E+01 | 8.40E+00 | 1.40E+00 | 0.1003 |
| 114.74 | 5.03E+01 | 1.01E+01 | 1.68E+00 | 0.0986 |
| 118.83 | 6.06E+01 | 1.21E+01 | 2.02E+00 | 0.0973 |
| 122.97 | 7.25E+01 | 1.45E+01 | 2.42E+00 | 0.0961 |
| 127.16 | 8.62E+01 | 1.72E+01 | 2.87E+00 | 0.0951 |
| 131.40 | 1.06E+02 | 2.12E+01 | 3.54E+00 | 0.0946 |
| 135.68 | 1.25E+02 | 2.50E+01 | 4.17E+00 | 0.0939 |
| 139.99 | 1.52E+02 | 3.03E+01 | 5.05E+00 | 0.0936 |
| 144.35 | 1.85E+02 | 3.70E+01 | 6.17E+00 | 0.0934 |
| 148.73 | 2.26E+02 | 4.51E+01 | 7.52E+00 | 0.0932 |
| 153.15 | 2.78E+02 | 5.55E+01 | 9.25E+00 | 0.0932 |
| 157.59 | 3.44E+02 | 6.87E+01 | 1.15E+01 | 0.0931 |
| 162.04 | 4.32E+02 | 8.63E+01 | 1.44E+01 | 0.0931 |
| 166.52 | 5.59E+02 | 1.12E+02 | 1.86E+01 | 0.0931 |
| 171.01 | 7.78E+02 | 1.56E+02 | 2.59E+01 | 0.0931 |
| 175.50 | 1.68E+03 | 3.36E+02 | 5.60E+01 | 0.0932 |
| 180.00 | | | | 0.0932 |

Fig. 7.3 model data

| **Stagnant cap angle, °** | **[c], mol/ m$^3$** | | | **u, m/s** |
|---|---|---|---|---|
| | **2.5×10$^{-3}$** | **12.5×10$^{-3}$** | **74.9×10$^{-3}$** | |
| | **t, s** | **t, s** | **t, s** | |
| 0.00 | 0.00E+00 | 0.00E+00 | 0.00E+00 | 0.2234 |
| 1.50 | 0.00E+00 | 0.00E+00 | 0.00E+00 | 0.2230 |
| 3.01 | 1.32E-04 | 2.63E-05 | 4.39E-06 | 0.2230 |
| 4.52 | 7.27E-04 | 1.45E-04 | 2.42E-05 | 0.2230 |
| 6.04 | 2.13E-03 | 4.27E-04 | 7.11E-05 | 0.2230 |
| 7.59 | 4.75E-03 | 9.50E-04 | 1.58E-04 | 0.2229 |
| 9.15 | 9.07E-03 | 1.81E-03 | 3.02E-04 | 0.2229 |
| 10.73 | 1.57E-02 | 3.14E-03 | 5.23E-04 | 0.2229 |
| 12.35 | 2.53E-02 | 5.07E-03 | 8.45E-04 | 0.2228 |
| 13.99 | 3.90E-02 | 7.79E-03 | 1.30E-03 | 0.2227 |
| 15.68 | 5.77E-02 | 1.15E-02 | 1.92E-03 | 0.2225 |
| 17.40 | 8.28E-02 | 1.66E-02 | 2.76E-03 | 0.2223 |
| 19.16 | 1.16E-01 | 2.32E-02 | 3.87E-03 | 0.2220 |
| 20.97 | 1.60E-01 | 3.20E-02 | 5.33E-03 | 0.2217 |
| 22.83 | 2.16E-01 | 4.33E-02 | 7.21E-03 | 0.2213 |
| 24.74 | 2.88E-01 | 5.76E-02 | 9.59E-03 | 0.2205 |
| 26.71 | 3.80E-01 | 7.58E-02 | 1.26E-02 | 0.2198 |
| 28.74 | 4.96E-01 | 9.90E-02 | 1.65E-02 | 0.2190 |
| 30.82 | 6.41E-01 | 1.28E-01 | 2.13E-02 | 0.2181 |
| 32.97 | 8.19E-01 | 1.63E-01 | 2.72E-02 | 0.2168 |
| 35.19 | 1.04E+00 | 2.07E-01 | 3.44E-02 | 0.2152 |
| 37.47 | 1.30E+00 | 2.59E-01 | 4.32E-02 | 0.2132 |
| 39.83 | 1.62E+00 | 3.21E-01 | 5.35E-02 | 0.2108 |
| 42.25 | 1.98E+00 | 3.94E-01 | 6.56E-02 | 0.2078 |
| 44.75 | 2.43E+00 | 4.82E-01 | 8.02E-02 | 0.2048 |
| 47.33 | 2.95E+00 | 5.85E-01 | 9.72E-02 | 0.2013 |
| 49.98 | 3.54E+00 | 7.01E-01 | 1.16E-01 | 0.1971 |
| 52.70 | 4.21E+00 | 8.29E-01 | 1.38E-01 | 0.1921 |
| 55.51 | 4.95E+00 | 9.73E-01 | 1.62E-01 | 0.1865 |
| 58.39 | 5.76E+00 | 1.13E+00 | 1.87E-01 | 0.1803 |
| 61.35 | 6.66E+00 | 1.30E+00 | 2.16E-01 | 0.1737 |
| 64.39 | 7.54E+00 | 1.47E+00 | 2.43E-01 | 0.1661 |
| 67.51 | 8.49E+00 | 1.65E+00 | 2.73E-01 | 0.1584 |
| 70.70 | 9.66E+00 | 1.86E+00 | 3.08E-01 | 0.1514 |
| 73.98 | 1.09E+01 | 2.08E+00 | 3.44E-01 | 0.1442 |
| 77.33 | 1.22E+01 | 2.33E+00 | 3.85E-01 | 0.1375 |
| 80.75 | 1.40E+01 | 2.64E+00 | 4.35E-01 | 0.1316 |
| 84.25 | 1.57E+01 | 2.94E+00 | 4.84E-01 | 0.1256 |

| | | | | |
|---|---|---|---|---|
| 87.83 | 1.79E+01 | 3.32E+00 | 5.45E-01 | 0.1206 |
| 91.47 | 2.04E+01 | 3.74E+00 | 6.13E-01 | 0.1159 |
| 95.19 | 2.39E+01 | 4.30E+00 | 7.03E-01 | 0.1120 |
| 98.97 | 2.83E+01 | 4.97E+00 | 8.08E-01 | 0.1086 |
| 102.82 | 3.27E+01 | 5.61E+00 | 9.10E-01 | 0.1053 |
| 106.74 | 3.84E+01 | 6.39E+00 | 1.03E+00 | 0.1024 |
| 110.71 | 4.66E+01 | 7.42E+00 | 1.19E+00 | 0.1003 |
| 114.74 | 5.82E+01 | 8.71E+00 | 1.39E+00 | 0.0986 |
| 118.83 | 7.46E+01 | 1.02E+01 | 1.62E+00 | 0.0973 |
| 122.97 | 9.83E+01 | 1.19E+01 | 1.87E+00 | 0.0961 |
| 127.16 | 1.37E+02 | 1.38E+01 | 2.13E+00 | 0.0951 |
| 131.40 | 3.11E+02 | 1.64E+01 | 2.49E+00 | 0.0946 |
| 135.68 | 1.99E+02 | 1.87E+01 | 2.80E+00 | 0.0939 |
| 139.99 | 1.54E+02 | 2.16E+01 | 3.19E+00 | 0.0936 |
| 144.35 | 1.26E+02 | 2.49E+01 | 3.60E+00 | 0.0934 |
| 148.73 | 1.07E+02 | 2.85E+01 | 4.03E+00 | 0.0932 |
| 153.15 | | 3.23E+01 | 4.45E+00 | 0.0932 |
| 157.59 | | 3.61E+01 | 4.86E+00 | 0.0931 |
| 162.04 | | 3.99E+01 | 5.24E+00 | 0.0931 |
| 166.52 | | 4.32E+01 | 5.56E+00 | 0.0931 |
| 171.01 | | 4.60E+01 | 5.81E+00 | 0.0931 |
| 175.50 | | 4.92E+01 | 6.08E+00 | 0.0932 |
| 180.00 | | 5.04E+01 | 6.18E+00 | 0.0932 |

Fig. 7.4 model data

| **Stagnant cap angle, °** | **[c], mol/ m$^3$** | | | **u, m/s** |
|---|---|---|---|---|
| | **2.5×10$^{-5}$** | **12.5×10$^{-5}$** | **74.9×10$^{-5}$** | |
| | **t, s** | **t, s** | **t, s** | |
| 0.00 | 0.00E+00 | 0.00E+00 | 0.00E+00 | 0.2234 |
| 1.50 | 0.00E+00 | 0.00E+00 | 0.00E+00 | 0.2230 |
| 3.01 | 2.45E-04 | 4.89E-05 | 8.16E-06 | 0.2230 |
| 4.52 | 1.35E-03 | 2.70E-04 | 4.50E-05 | 0.2230 |
| 6.04 | 3.96E-03 | 7.92E-04 | 1.32E-04 | 0.2230 |
| 7.59 | 8.82E-03 | 1.76E-03 | 2.94E-04 | 0.2229 |
| 9.15 | 1.68E-02 | 3.36E-03 | 5.60E-04 | 0.2229 |
| 10.73 | 2.90E-02 | 5.80E-03 | 9.67E-04 | 0.2229 |
| 12.35 | 4.68E-02 | 9.36E-03 | 1.56E-03 | 0.2228 |
| 13.99 | 7.19E-02 | 1.44E-02 | 2.39E-03 | 0.2227 |
| 15.68 | 1.06E-01 | 2.12E-02 | 3.53E-03 | 0.2225 |
| 17.40 | 0.152148 | 0.030356 | 0.005057 | 0.2223 |
| 19.16 | 0.213015 | 0.042461 | 0.007072 | 0.2220 |
| 20.97 | 0.292525 | 0.058241 | 0.009698 | 0.2217 |
| 22.83 | 0.394755 | 0.078474 | 0.013063 | 0.2213 |
| 24.74 | 0.523684 | 0.103904 | 0.017289 | 0.2205 |
| 26.71 | 0.688068 | 0.136187 | 0.022649 | 0.2198 |
| 28.74 | 0.895556 | 0.176711 | 0.02937 | 0.2190 |
| 30.82 | 1.154441 | 0.226926 | 0.037687 | 0.2181 |
| 32.97 | 1.471467 | 0.287902 | 0.047769 | 0.2168 |
| 35.19 | 1.858272 | 0.361537 | 0.05992 | 0.2152 |
| 37.47 | 2.324958 | 0.449279 | 0.074363 | 0.2132 |
| 39.83 | 2.87854 | 0.551828 | 0.091196 | 0.2108 |
| 42.25 | 3.524054 | 0.669354 | 0.110424 | 0.2078 |
| 44.75 | 4.308719 | 0.80923 | 0.133221 | 0.2048 |
| 47.33 | 5.230435 | 0.9695 | 0.159225 | 0.2013 |
| 49.98 | 6.272932 | 1.145718 | 0.187677 | 0.1971 |
| 52.70 | 7.436649 | 1.336285 | 0.218283 | 0.1921 |
| 55.51 | 8.74414 | 1.542858 | 0.251268 | 0.1865 |
| 58.39 | 10.16552 | 1.758789 | 0.28554 | 0.1803 |
| 61.35 | 11.74933 | 1.98905 | 0.321851 | 0.1737 |
| 64.39 | 13.27686 | 2.201825 | 0.355205 | 0.1661 |
| 67.51 | 14.91292 | 2.419438 | 0.389108 | 0.1584 |
| 70.70 | 16.91155 | 2.670658 | 0.42797 | 0.1514 |
| 73.98 | 18.93762 | 2.91101 | 0.464898 | 0.1442 |
| 77.33 | 21.27394 | 3.170192 | 0.504428 | 0.1375 |
| 80.75 | 24.26179 | 3.474401 | 0.550425 | 0.1316 |
| 84.25 | 27.21501 | 3.750356 | 0.591822 | 0.1256 |

| | | | | |
|---|---|---|---|---|
| 87.83 | 31.24526 | 4.085518 | 0.641622 | 0.1206 |
| 91.47 | 36.09352 | 4.435915 | 0.693164 | 0.1159 |
| 95.19 | 43.62735 | 4.875961 | 0.757078 | 0.1120 |
| 98.97 | 55.20301 | 5.369122 | 0.827694 | 0.1086 |
| 102.82 | 71.33221 | 5.819134 | 0.891294 | 0.1053 |
| 106.74 | 118.4091 | 6.331143 | 0.962584 | 0.1024 |
| 110.71 | | 6.972859 | 1.050274 | 0.1003 |
| 114.74 | | 7.730288 | 1.151498 | 0.0986 |
| 118.83 | | 8.575268 | 1.261638 | 0.0973 |
| 122.97 | | 9.470378 | 1.375248 | 0.0961 |
| 127.16 | | 10.38394 | 1.488067 | 0.0951 |
| 131.40 | | 11.57752 | 1.630268 | 0.0946 |
| 135.68 | | 12.56639 | 1.744584 | 0.0939 |
| 139.99 | | 13.74814 | 1.876341 | 0.0936 |
| 144.35 | | 14.99858 | 2.010477 | 0.0934 |
| 148.73 | | 16.23303 | 2.1379 | 0.0932 |
| 153.15 | | 17.45849 | 2.259614 | 0.0932 |
| 157.59 | | 18.60148 | 2.36909 | 0.0931 |
| 162.04 | | 19.62226 | 2.463714 | 0.0931 |
| 166.52 | | 20.48531 | 2.541514 | 0.0931 |
| 171.01 | | 21.16527 | 2.601465 | 0.0931 |
| 175.50 | | 21.88851 | 2.66374 | 0.0932 |
| 180.00 | | 22.16789 | 2.687575 | 0.0932 |

Fig. 7.5 model data

| **Stagnant cap angle, °** | **[c], mol/ m$^3$** | | | **u, m/s** |
|---|---|---|---|---|
| | **$2.5\times10^{-3}$** | **$12.5\times10^{-3}$** | **$74.9\times10^{-3}$** | |
| | **t, s** | **t, s** | **t, s** | |
| 0.00 | 0.00E+00 | 0.00E+00 | 0.00E+00 | 0.2234 |
| 1.50 | 0.00E+00 | 0.00E+00 | 0.00E+00 | 0.2230 |
| 3.01 | 1.22E-04 | 2.45E-05 | 4.08E-06 | 0.2230 |
| 4.52 | 6.76E-04 | 1.35E-04 | 2.25E-05 | 0.2230 |
| 6.04 | 1.98E-03 | 3.96E-04 | 6.60E-05 | 0.2230 |
| 7.59 | 4.41E-03 | 8.82E-04 | 1.47E-04 | 0.2229 |
| 9.15 | 8.40E-03 | 1.68E-03 | 2.80E-04 | 0.2229 |
| 10.73 | 1.45E-02 | 2.90E-03 | 4.84E-04 | 0.2229 |
| 12.35 | 2.34E-02 | 4.68E-03 | 7.80E-04 | 0.2228 |
| 13.99 | 3.59E-02 | 7.18E-03 | 1.20E-03 | 0.2227 |
| 15.68 | 5.31E-02 | 1.06E-02 | 1.77E-03 | 0.2225 |
| 17.40 | 7.61E-02 | 1.52E-02 | 2.53E-03 | 0.2223 |
| 19.16 | 1.07E-01 | 2.12E-02 | 3.54E-03 | 0.2220 |
| 20.97 | 1.46E-01 | 2.91E-02 | 4.85E-03 | 0.2217 |
| 22.83 | 1.97E-01 | 3.92E-02 | 6.53E-03 | 0.2213 |
| 24.74 | 2.62E-01 | 5.20E-02 | 8.64E-03 | 0.2205 |
| 26.71 | 3.44E-01 | 6.81E-02 | 1.13E-02 | 0.2198 |
| 28.74 | 4.48E-01 | 8.84E-02 | 1.47E-02 | 0.2190 |
| 30.82 | 5.77E-01 | 1.13E-01 | 1.88E-02 | 0.2181 |
| 32.97 | 7.36E-01 | 1.44E-01 | 2.39E-02 | 0.2168 |
| 35.19 | 9.29E-01 | 1.81E-01 | 3.00E-02 | 0.2152 |
| 37.47 | 1.16E+00 | 2.25E-01 | 3.72E-02 | 0.2132 |
| 39.83 | 1.44E+00 | 2.76E-01 | 4.56E-02 | 0.2108 |
| 42.25 | 1.76E+00 | 3.35E-01 | 5.52E-02 | 0.2078 |
| 44.75 | 2.15E+00 | 4.05E-01 | 6.66E-02 | 0.2048 |
| 47.33 | 2.62E+00 | 4.85E-01 | 7.96E-02 | 0.2013 |
| 49.98 | 3.14E+00 | 5.73E-01 | 9.38E-02 | 0.1971 |
| 52.70 | 3.72E+00 | 6.68E-01 | 1.09E-01 | 0.1921 |
| 55.51 | 4.37E+00 | 7.71E-01 | 1.26E-01 | 0.1865 |
| 58.39 | 5.08E+00 | 8.79E-01 | 1.43E-01 | 0.1803 |
| 61.35 | 5.87E+00 | 9.95E-01 | 1.61E-01 | 0.1737 |
| 64.39 | 6.64E+00 | 1.10E+00 | 1.78E-01 | 0.1661 |
| 67.51 | 7.46E+00 | 1.21E+00 | 1.95E-01 | 0.1584 |
| 70.70 | 8.46E+00 | 1.34E+00 | 2.14E-01 | 0.1514 |
| 73.98 | 9.47E+00 | 1.46E+00 | 2.32E-01 | 0.1442 |
| 77.33 | 1.06E+01 | 1.59E+00 | 2.52E-01 | 0.1375 |
| 80.75 | 1.21E+01 | 1.74E+00 | 2.75E-01 | 0.1316 |
| 84.25 | 1.36E+01 | 1.88E+00 | 2.96E-01 | 0.1256 |

| | | | | |
|---|---|---|---|---|
| 87.83 | 1.56E+01 | 2.04E+00 | 3.21E-01 | 0.1206 |
| 91.47 | 1.80E+01 | 2.22E+00 | 3.47E-01 | 0.1159 |
| 95.19 | 2.18E+01 | 2.44E+00 | 3.79E-01 | 0.1120 |
| 98.97 | 2.76E+01 | 2.68E+00 | 4.14E-01 | 0.1086 |
| 102.82 | 3.57E+01 | 2.91E+00 | 4.46E-01 | 0.1053 |
| 106.74 | 5.92E+01 | 3.17E+00 | 4.81E-01 | 0.1024 |
| 110.71 | | 3.49E+00 | 5.25E-01 | 0.1003 |
| 114.74 | | 3.87E+00 | 5.76E-01 | 0.0986 |
| 118.83 | | 4.29E+00 | 6.31E-01 | 0.0973 |
| 122.97 | | 4.74E+00 | 6.88E-01 | 0.0961 |
| 127.16 | | 5.19E+00 | 7.44E-01 | 0.0951 |
| 131.40 | | 5.79E+00 | 8.15E-01 | 0.0946 |
| 135.68 | | 6.28E+00 | 8.72E-01 | 0.0939 |
| 139.99 | | 6.87E+00 | 9.38E-01 | 0.0936 |
| 144.35 | | 7.50E+00 | 1.01E+00 | 0.0934 |
| 148.73 | | 8.12E+00 | 1.07E+00 | 0.0932 |
| 153.15 | | 8.73E+00 | 1.13E+00 | 0.0932 |
| 157.59 | | 9.30E+00 | 1.18E+00 | 0.0931 |
| 162.04 | | 9.81E+00 | 1.23E+00 | 0.0931 |
| 166.52 | | 1.02E+01 | 1.27E+00 | 0.0931 |
| 171.01 | | 1.06E+01 | 1.30E+00 | 0.0931 |
| 175.50 | | 1.09E+01 | 1.33E+00 | 0.0932 |
| 180.00 | | 1.11E+01 | 1.34E+00 | 0.0932 |

Fig. 7.6 model data

| **Stagnant cap angle, °** | **[c], mol/ m$^3$** | | | **u, m/s** |
|---|---|---|---|---|
| | **$2.5\times10^{-5}$** | **$12.5\times10^{-5}$** | **$74.9\times10^{-5}$** | |
| | **t, s** | **t, s** | **t, s** | |
| 0.00 | 0.00E+00 | 0.00E+00 | 0.00E+00 | 0.2234 |
| 1.50 | 0.00E+00 | 0.00E+00 | 0.00E+00 | 0.2230 |
| 3.01 | 6.12E-05 | 1.22E-05 | 2.04E-06 | 0.2230 |
| 4.52 | 3.38E-04 | 6.76E-05 | 1.13E-05 | 0.2230 |
| 6.04 | 9.91E-04 | 1.98E-04 | 3.30E-05 | 0.2230 |
| 7.59 | 2.20E-03 | 4.41E-04 | 7.35E-05 | 0.2229 |
| 9.15 | 4.20E-03 | 8.40E-04 | 1.40E-04 | 0.2229 |
| 10.73 | 7.26E-03 | 1.45E-03 | 2.42E-04 | 0.2229 |
| 12.35 | 1.17E-02 | 2.34E-03 | 3.90E-04 | 0.2228 |
| 13.99 | 1.80E-02 | 3.59E-03 | 5.98E-04 | 0.2227 |
| 15.68 | 2.65E-02 | 5.30E-03 | 8.83E-04 | 0.2225 |
| 17.40 | 3.80E-02 | 7.59E-03 | 1.26E-03 | 0.2223 |
| 19.16 | 5.33E-02 | 1.06E-02 | 1.77E-03 | 0.2220 |
| 20.97 | 7.31E-02 | 1.46E-02 | 2.42E-03 | 0.2217 |
| 22.83 | 9.87E-02 | 1.96E-02 | 3.27E-03 | 0.2213 |
| 24.74 | 1.31E-01 | 2.60E-02 | 4.32E-03 | 0.2205 |
| 26.71 | 1.72E-01 | 3.40E-02 | 5.66E-03 | 0.2198 |
| 28.74 | 2.24E-01 | 4.42E-02 | 7.34E-03 | 0.2190 |
| 30.82 | 2.89E-01 | 5.67E-02 | 9.42E-03 | 0.2181 |
| 32.97 | 3.68E-01 | 7.20E-02 | 1.19E-02 | 0.2168 |
| 35.19 | 4.65E-01 | 9.04E-02 | 1.50E-02 | 0.2152 |
| 37.47 | 5.81E-01 | 1.12E-01 | 1.86E-02 | 0.2132 |
| 39.83 | 7.20E-01 | 1.38E-01 | 2.28E-02 | 0.2108 |
| 42.25 | 8.81E-01 | 1.67E-01 | 2.76E-02 | 0.2078 |
| 44.75 | 1.08E+00 | 2.02E-01 | 3.33E-02 | 0.2048 |
| 47.33 | 1.31E+00 | 2.42E-01 | 3.98E-02 | 0.2013 |
| 49.98 | 1.57E+00 | 2.86E-01 | 4.69E-02 | 0.1971 |
| 52.70 | 1.86E+00 | 3.34E-01 | 5.46E-02 | 0.1921 |
| 55.51 | 2.19E+00 | 3.86E-01 | 6.28E-02 | 0.1865 |
| 58.39 | 2.54E+00 | 4.40E-01 | 7.14E-02 | 0.1803 |
| 61.35 | 2.94E+00 | 4.97E-01 | 8.05E-02 | 0.1737 |
| 64.39 | 3.32E+00 | 5.50E-01 | 8.88E-02 | 0.1661 |
| 67.51 | 3.73E+00 | 6.05E-01 | 9.73E-02 | 0.1584 |
| 70.70 | 4.23E+00 | 6.68E-01 | 1.07E-01 | 0.1514 |
| 73.98 | 4.73E+00 | 7.28E-01 | 1.16E-01 | 0.1442 |
| 77.33 | 5.32E+00 | 7.93E-01 | 1.26E-01 | 0.1375 |
| 80.75 | 6.07E+00 | 8.69E-01 | 1.38E-01 | 0.1316 |
| 84.25 | 6.80E+00 | 9.38E-01 | 1.48E-01 | 0.1256 |

| | | | | |
|---|---|---|---|---|
| 87.83 | 7.81E+00 | 1.02E+00 | 1.60E-01 | 0.1206 |
| 91.47 | 9.02E+00 | 1.11E+00 | 1.73E-01 | 0.1159 |
| 95.19 | 1.09E+01 | 1.22E+00 | 1.89E-01 | 0.1120 |
| 98.97 | 1.38E+01 | 1.34E+00 | 2.07E-01 | 0.1086 |
| 102.82 | 1.78E+01 | 1.45E+00 | 2.23E-01 | 0.1053 |
| 106.74 | 2.96E+01 | 1.58E+00 | 2.41E-01 | 0.1024 |
| 110.71 | | 1.74E+00 | 2.63E-01 | 0.1003 |
| 114.74 | | 1.93E+00 | 2.88E-01 | 0.0986 |
| 118.83 | | 2.14E+00 | 3.15E-01 | 0.0973 |
| 122.97 | | 2.37E+00 | 3.44E-01 | 0.0961 |
| 127.16 | | 2.60E+00 | 3.72E-01 | 0.0951 |
| 131.40 | | 2.89E+00 | 4.08E-01 | 0.0946 |
| 135.68 | | 3.14E+00 | 4.36E-01 | 0.0939 |
| 139.99 | | 3.44E+00 | 4.69E-01 | 0.0936 |
| 144.35 | | 3.75E+00 | 5.03E-01 | 0.0934 |
| 148.73 | | 4.06E+00 | 5.34E-01 | 0.0932 |
| 153.15 | | 4.36E+00 | 5.65E-01 | 0.0932 |
| 157.59 | | 4.65E+00 | 5.92E-01 | 0.0931 |
| 162.04 | | 4.91E+00 | 6.16E-01 | 0.0931 |
| 166.52 | | 5.12E+00 | 6.35E-01 | 0.0931 |
| 171.01 | | 5.29E+00 | 6.50E-01 | 0.0931 |
| 175.50 | | 5.47E+00 | 6.66E-01 | 0.0932 |
| 180.00 | | 5.54E+00 | 6.72E-01 | 0.0932 |

Fig. 7.7 model data

| **Stagnant cap angle, °** | **[c], mol/ m$^3$** | | | **u, m/s** |
|---|---|---|---|---|
| | **$2.5\times10^{-3}$** | **$12.5\times10^{-3}$** | **$74.9\times10^{-3}$** | |
| | **t, s** | **t, s** | **t, s** | |
| 0.00 | 0.00E+00 | 0.00E+00 | 0.00E+00 | 0.2234 |
| 1.50 | 7.39E-02 | 1.48E-02 | 2.46E-03 | 0.2230 |
| 3.01 | 2.96E-01 | 5.93E-02 | 9.88E-03 | 0.2230 |
| 4.52 | 6.70E-01 | 1.34E-01 | 2.23E-02 | 0.2230 |
| 6.04 | 1.20E+00 | 2.40E-01 | 4.00E-02 | 0.2230 |
| 7.59 | 1.89E+00 | 3.78E-01 | 6.30E-02 | 0.2229 |
| 9.15 | 2.75E+00 | 5.50E-01 | 9.16E-02 | 0.2229 |
| 10.73 | 3.79E+00 | 7.57E-01 | 1.26E-01 | 0.2229 |
| 12.35 | 5.02E+00 | 1.00E+00 | 1.67E-01 | 0.2228 |
| 13.99 | 6.45E+00 | 1.29E+00 | 2.15E-01 | 0.2227 |
| 15.68 | 8.10E+00 | 1.62E+00 | 2.70E-01 | 0.2225 |
| 17.40 | 9.99E+00 | 2.00E+00 | 3.33E-01 | 0.2223 |
| 19.16 | 1.21E+01 | 2.43E+00 | 4.04E-01 | 0.2220 |
| 20.97 | 1.46E+01 | 2.91E+00 | 4.85E-01 | 0.2217 |
| 22.83 | 1.73E+01 | 3.46E+00 | 5.76E-01 | 0.2213 |
| 24.74 | 2.03E+01 | 4.07E+00 | 6.78E-01 | 0.2205 |
| 26.71 | 2.38E+01 | 4.75E+00 | 7.92E-01 | 0.2198 |
| 28.74 | 2.76E+01 | 5.51E+00 | 9.19E-01 | 0.2190 |
| 30.82 | 3.18E+01 | 6.36E+00 | 1.06E+00 | 0.2181 |
| 32.97 | 3.65E+01 | 7.31E+00 | 1.22E+00 | 0.2168 |
| 35.19 | 4.18E+01 | 8.35E+00 | 1.39E+00 | 0.2152 |
| 37.47 | 4.76E+01 | 9.52E+00 | 1.59E+00 | 0.2132 |
| 39.83 | 5.40E+01 | 1.08E+01 | 1.80E+00 | 0.2108 |
| 42.25 | 6.12E+01 | 1.22E+01 | 2.04E+00 | 0.2078 |
| 44.75 | 6.91E+01 | 1.38E+01 | 2.30E+00 | 0.2048 |
| 47.33 | 7.79E+01 | 1.56E+01 | 2.60E+00 | 0.2013 |
| 49.98 | 8.77E+01 | 1.75E+01 | 2.92E+00 | 0.1971 |
| 52.70 | 9.85E+01 | 1.97E+01 | 3.28E+00 | 0.1921 |
| 55.51 | 1.11E+02 | 2.21E+01 | 3.69E+00 | 0.1865 |
| 58.39 | 1.24E+02 | 2.48E+01 | 4.13E+00 | 0.1803 |
| 61.35 | 1.39E+02 | 2.78E+01 | 4.63E+00 | 0.1737 |
| 64.39 | 1.56E+02 | 3.12E+01 | 5.19E+00 | 0.1661 |
| 67.51 | 1.75E+02 | 3.49E+01 | 5.82E+00 | 0.1584 |
| 70.70 | 1.96E+02 | 3.91E+01 | 6.52E+00 | 0.1514 |
| 73.98 | 2.19E+02 | 4.39E+01 | 7.31E+00 | 0.1442 |
| 77.33 | 2.46E+02 | 4.91E+01 | 8.19E+00 | 0.1375 |
| 80.75 | 2.75E+02 | 5.50E+01 | 9.17E+00 | 0.1316 |
| 84.25 | 3.08E+02 | 6.17E+01 | 1.03E+01 | 0.1256 |

| | | | | |
|---|---|---|---|---|
| 87.83 | 3.45E+02 | 6.90E+01 | 1.15E+01 | 0.1206 |
| 91.47 | 3.86E+02 | 7.73E+01 | 1.29E+01 | 0.1159 |
| 95.19 | 4.32E+02 | 8.64E+01 | 1.44E+01 | 0.1120 |
| 98.97 | 4.83E+02 | 9.66E+01 | 1.61E+01 | 0.1086 |
| 102.82 | 5.39E+02 | 1.08E+02 | 1.80E+01 | 0.1053 |
| 106.74 | 6.02E+02 | 1.20E+02 | 2.01E+01 | 0.1024 |
| 110.71 | 6.72E+02 | 1.34E+02 | 2.24E+01 | 0.1003 |
| 114.74 | 7.50E+02 | 1.50E+02 | 2.50E+01 | 0.0986 |
| 118.83 | 8.36E+02 | 1.67E+02 | 2.79E+01 | 0.0973 |
| 122.97 | 9.32E+02 | 1.86E+02 | 3.11E+01 | 0.0961 |
| 127.16 | 1.04E+03 | 2.08E+02 | 3.46E+01 | 0.0951 |
| 131.40 | 1.16E+03 | 2.32E+02 | 3.86E+01 | 0.0946 |
| 135.68 | 1.30E+03 | 2.59E+02 | 4.32E+01 | 0.0939 |
| 139.99 | 1.45E+03 | 2.90E+02 | 4.83E+01 | 0.0936 |
| 144.35 | 1.63E+03 | 3.26E+02 | 5.43E+01 | 0.0934 |
| 148.73 | 1.84E+03 | 3.68E+02 | 6.13E+01 | 0.0932 |
| 153.15 | 2.09E+03 | 4.17E+02 | 6.96E+01 | 0.0932 |
| 157.59 | 2.39E+03 | 4.79E+02 | 7.98E+01 | 0.0931 |
| 162.04 | 2.79E+03 | 5.58E+02 | 9.30E+01 | 0.0931 |
| 166.52 | 3.34E+03 | 6.69E+02 | 1.11E+02 | 0.0931 |
| 171.01 | 4.24E+03 | 8.47E+02 | 1.41E+02 | 0.0931 |
| 175.50 | 6.39E+03 | 1.28E+03 | 2.13E+02 | 0.0932 |
| 180.00 | | | | 0.0932 |

Fig. 7.8 model data

| **Stagnant cap angle, °** | **[c], mol/ m$^3$** | | | **u, m/s** |
|---|---|---|---|---|
| | **$2.5\times10^{-6}$** | **$12.5\times10^{-6}$** | **$74.9\times10^{-6}$** | |
| | **t, s** | **t, s** | **t, s** | |
| 0.00 | 0.00E+00 | 0.00E+00 | 0.00E+00 | 0.2234 |
| 1.50 | 2.68E-03 | 2.34E-03 | 1.31E-03 | 0.2230 |
| 3.01 | 1.08E-02 | 9.40E-03 | 5.24E-03 | 0.2230 |
| 4.52 | 2.43E-02 | 2.13E-02 | 1.19E-02 | 0.2230 |
| 6.04 | 4.36E-02 | 3.80E-02 | 2.12E-02 | 0.2230 |
| 7.59 | 6.86E-02 | 5.99E-02 | 3.34E-02 | 0.2229 |
| 9.15 | 9.99E-02 | 8.72E-02 | 4.87E-02 | 0.2229 |
| 10.73 | 1.38E-01 | 1.20E-01 | 6.70E-02 | 0.2229 |
| 12.35 | 1.82E-01 | 1.59E-01 | 8.88E-02 | 0.2228 |
| 13.99 | 2.34E-01 | 2.05E-01 | 1.14E-01 | 0.2227 |
| 15.68 | 2.94E-01 | 2.57E-01 | 1.43E-01 | 0.2225 |
| 17.40 | 3.63E-01 | 3.17E-01 | 1.77E-01 | 0.2223 |
| 19.16 | 4.41E-01 | 3.85E-01 | 2.15E-01 | 0.2220 |
| 20.97 | 5.29E-01 | 4.62E-01 | 2.58E-01 | 0.2217 |
| 22.83 | 6.28E-01 | 5.48E-01 | 3.06E-01 | 0.2213 |
| 24.74 | 7.39E-01 | 6.45E-01 | 3.60E-01 | 0.2205 |
| 26.71 | 8.63E-01 | 7.54E-01 | 4.20E-01 | 0.2198 |
| 28.74 | 1.00E+00 | 8.74E-01 | 4.88E-01 | 0.2190 |
| 30.82 | 1.16E+00 | 1.01E+00 | 5.63E-01 | 0.2181 |
| 32.97 | 1.33E+00 | 1.16E+00 | 6.46E-01 | 0.2168 |
| 35.19 | 1.52E+00 | 1.33E+00 | 7.39E-01 | 0.2152 |
| 37.47 | 1.73E+00 | 1.51E+00 | 8.42E-01 | 0.2132 |
| 39.83 | 1.96E+00 | 1.71E+00 | 9.56E-01 | 0.2108 |
| 42.25 | 2.22E+00 | 1.94E+00 | 1.08E+00 | 0.2078 |
| 44.75 | 2.51E+00 | 2.19E+00 | 1.22E+00 | 0.2048 |
| 47.33 | 2.83E+00 | 2.47E+00 | 1.38E+00 | 0.2013 |
| 49.98 | 3.19E+00 | 2.78E+00 | 1.55E+00 | 0.1971 |
| 52.70 | 3.58E+00 | 3.13E+00 | 1.74E+00 | 0.1921 |
| 55.51 | 4.02E+00 | 3.51E+00 | 1.96E+00 | 0.1865 |
| 58.39 | 4.51E+00 | 3.94E+00 | 2.20E+00 | 0.1803 |
| 61.35 | 5.05E+00 | 4.41E+00 | 2.46E+00 | 0.1737 |
| 64.39 | 5.66E+00 | 4.94E+00 | 2.76E+00 | 0.1661 |
| 67.51 | 6.34E+00 | 5.54E+00 | 3.09E+00 | 0.1584 |
| 70.70 | 7.11E+00 | 6.21E+00 | 3.46E+00 | 0.1514 |
| 73.98 | 7.97E+00 | 6.96E+00 | 3.88E+00 | 0.1442 |
| 77.33 | 8.93E+00 | 7.80E+00 | 4.35E+00 | 0.1375 |
| 80.75 | 1.00E+01 | 8.73E+00 | 4.87E+00 | 0.1316 |
| 84.25 | 1.12E+01 | 9.78E+00 | 5.46E+00 | 0.1256 |

| | | | | |
|---|---|---|---|---|
| 87.83 | 1.25E+01 | 1.09E+01 | 6.11E+00 | 0.1206 |
| 91.47 | 1.40E+01 | 1.23E+01 | 6.84E+00 | 0.1159 |
| 95.19 | 1.57E+01 | 1.37E+01 | 7.65E+00 | 0.1120 |
| 98.97 | 1.75E+01 | 1.53E+01 | 8.55E+00 | 0.1086 |
| 102.82 | 1.96E+01 | 1.71E+01 | 9.55E+00 | 0.1053 |
| 106.74 | 2.19E+01 | 1.91E+01 | 1.07E+01 | 0.1024 |
| 110.71 | 2.44E+01 | 2.13E+01 | 1.19E+01 | 0.1003 |
| 114.74 | 2.72E+01 | 2.38E+01 | 1.33E+01 | 0.0986 |
| 118.83 | 3.04E+01 | 2.65E+01 | 1.48E+01 | 0.0973 |
| 122.97 | 3.38E+01 | 2.96E+01 | 1.65E+01 | 0.0961 |
| 127.16 | 3.77E+01 | 3.30E+01 | 1.84E+01 | 0.0951 |
| 131.40 | 4.21E+01 | 3.68E+01 | 2.05E+01 | 0.0946 |
| 135.68 | 4.71E+01 | 4.11E+01 | 2.29E+01 | 0.0939 |
| 139.99 | 5.27E+01 | 4.60E+01 | 2.57E+01 | 0.0936 |
| 144.35 | 5.92E+01 | 5.17E+01 | 2.88E+01 | 0.0934 |
| 148.73 | 6.68E+01 | 5.83E+01 | 3.25E+01 | 0.0932 |
| 153.15 | 7.58E+01 | 6.62E+01 | 3.69E+01 | 0.0932 |
| 157.59 | 8.70E+01 | 7.60E+01 | 4.24E+01 | 0.0931 |
| 162.04 | 1.01E+02 | 8.85E+01 | 4.94E+01 | 0.0931 |
| 166.52 | 1.21E+02 | 1.06E+02 | 5.92E+01 | 0.0931 |
| 171.01 | 1.54E+02 | 1.34E+02 | 7.50E+01 | 0.0931 |
| 175.50 | 2.32E+02 | 2.03E+02 | 1.13E+02 | 0.0932 |
| 180.00 | | | | 0.0932 |

Fig. 7.9 model data

| **Stagnant cap angle, °** | **[c], mol/ m$^3$** | | | **u, m/s** |
|---|---|---|---|---|
| | **2.5×10$^{-5}$** | **12.5×10$^{-5}$** | **74.9×10$^{-5}$** | |
| | **t, s** | **t, s** | **t, s** | |
| 0.00 | 0.00E+00 | 0.00E+00 | 0.00E+00 | 0.2234 |
| 1.50 | 5.01E-03 | 4.36E-03 | 2.42E-03 | 0.2230 |
| 3.01 | 2.01E-02 | 1.75E-02 | 9.73E-03 | 0.2230 |
| 4.52 | 4.54E-02 | 3.96E-02 | 2.20E-02 | 0.2230 |
| 6.04 | 8.13E-02 | 7.08E-02 | 3.94E-02 | 0.2230 |
| 7.59 | 1.28E-01 | 1.12E-01 | 6.20E-02 | 0.2229 |
| 9.15 | 1.86E-01 | 1.62E-01 | 9.02E-02 | 0.2229 |
| 10.73 | 2.57E-01 | 2.24E-01 | 1.24E-01 | 0.2229 |
| 12.35 | 3.40E-01 | 2.96E-01 | 1.65E-01 | 0.2228 |
| 13.99 | 4.37E-01 | 3.81E-01 | 2.12E-01 | 0.2227 |
| 15.68 | 5.49E-01 | 4.78E-01 | 2.66E-01 | 0.2225 |
| 17.40 | 6.76E-01 | 5.90E-01 | 3.28E-01 | 0.2223 |
| 19.16 | 8.21E-01 | 7.16E-01 | 3.98E-01 | 0.2220 |
| 20.97 | 9.85E-01 | 8.59E-01 | 4.77E-01 | 0.2217 |
| 22.83 | 1.17E+00 | 1.02E+00 | 5.66E-01 | 0.2213 |
| 24.74 | 1.37E+00 | 1.20E+00 | 6.66E-01 | 0.2205 |
| 26.71 | 1.60E+00 | 1.40E+00 | 7.77E-01 | 0.2198 |
| 28.74 | 1.86E+00 | 1.62E+00 | 9.01E-01 | 0.2190 |
| 30.82 | 2.14E+00 | 1.87E+00 | 1.04E+00 | 0.2181 |
| 32.97 | 2.46E+00 | 2.14E+00 | 1.19E+00 | 0.2168 |
| 35.19 | 2.81E+00 | 2.45E+00 | 1.36E+00 | 0.2152 |
| 37.47 | 3.19E+00 | 2.78E+00 | 1.55E+00 | 0.2132 |
| 39.83 | 3.62E+00 | 3.15E+00 | 1.75E+00 | 0.2108 |
| 42.25 | 4.08E+00 | 3.56E+00 | 1.98E+00 | 0.2078 |
| 44.75 | 4.59E+00 | 4.00E+00 | 2.22E+00 | 0.2048 |
| 47.33 | 5.16E+00 | 4.49E+00 | 2.50E+00 | 0.2013 |
| 49.98 | 5.77E+00 | 5.03E+00 | 2.80E+00 | 0.1971 |
| 52.70 | 6.45E+00 | 5.62E+00 | 3.12E+00 | 0.1921 |
| 55.51 | 7.19E+00 | 6.27E+00 | 3.48E+00 | 0.1865 |
| 58.39 | 7.99E+00 | 6.97E+00 | 3.87E+00 | 0.1803 |
| 61.35 | 8.88E+00 | 7.74E+00 | 4.30E+00 | 0.1737 |
| 64.39 | 9.84E+00 | 8.58E+00 | 4.76E+00 | 0.1661 |
| 67.51 | 1.09E+01 | 9.49E+00 | 5.27E+00 | 0.1584 |
| 70.70 | 1.20E+01 | 1.05E+01 | 5.83E+00 | 0.1514 |
| 73.98 | 1.33E+01 | 1.16E+01 | 6.43E+00 | 0.1442 |
| 77.33 | 1.46E+01 | 1.28E+01 | 7.09E+00 | 0.1375 |
| 80.75 | 1.61E+01 | 1.40E+01 | 7.80E+00 | 0.1316 |
| 84.25 | 1.77E+01 | 1.54E+01 | 8.58E+00 | 0.1256 |

| | | | | |
|---|---|---|---|---|
| 87.83 | 1.95E+01 | 1.70E+01 | 9.43E+00 | 0.1206 |
| 91.47 | 2.14E+01 | 1.86E+01 | 1.03E+01 | 0.1159 |
| 95.19 | 2.34E+01 | 2.04E+01 | 1.14E+01 | 0.1120 |
| 98.97 | 2.57E+01 | 2.24E+01 | 1.25E+01 | 0.1086 |
| 102.82 | 2.82E+01 | 2.46E+01 | 1.37E+01 | 0.1053 |
| 106.74 | 3.09E+01 | 2.69E+01 | 1.50E+01 | 0.1024 |
| 110.71 | 3.39E+01 | 2.95E+01 | 1.64E+01 | 0.1003 |
| 114.74 | 3.71E+01 | 3.24E+01 | 1.80E+01 | 0.0986 |
| 118.83 | 4.07E+01 | 3.55E+01 | 1.97E+01 | 0.0973 |
| 122.97 | 4.47E+01 | 3.89E+01 | 2.16E+01 | 0.0961 |
| 127.16 | 4.91E+01 | 4.28E+01 | 2.38E+01 | 0.0951 |
| 131.40 | 5.40E+01 | 4.71E+01 | 2.62E+01 | 0.0946 |
| 135.68 | 5.96E+01 | 5.19E+01 | 2.88E+01 | 0.0939 |
| 139.99 | 6.59E+01 | 5.74E+01 | 3.19E+01 | 0.0936 |
| 144.35 | 7.31E+01 | 6.38E+01 | 3.54E+01 | 0.0934 |
| 148.73 | 8.16E+01 | 7.11E+01 | 3.95E+01 | 0.0932 |
| 153.15 | 9.17E+01 | 8.00E+01 | 4.44E+01 | 0.0932 |
| 157.59 | 1.04E+02 | 9.08E+01 | 5.05E+01 | 0.0931 |
| 162.04 | 1.20E+02 | 1.05E+02 | 5.83E+01 | 0.0931 |
| 166.52 | 1.43E+02 | 1.24E+02 | 6.91E+01 | 0.0931 |
| 171.01 | 1.79E+02 | 1.56E+02 | 8.66E+01 | 0.0931 |
| 175.50 | 2.66E+02 | 2.32E+02 | 1.29E+02 | 0.0932 |
| 180.00 | | | | 0.0932 |

Fig. 8.1 bubble size measurement data

| **Temperature, °C** | **Capillary size, µm** | | |
|---|---|---|---|
| | **14** | **64** | **125** |
| 6 | 0.75±0.03 | 1.39±0.04 | |
| 15 | | | |
| 25 | 0.81±0.05 | | 1.88±0.05 |
| 30 | | 1.41±0.05 | |
| 45 | | | 1.8±0.05 |

Fig. 8.2 data

| 6 °C | | 25 °C | | 40 °C | |
|---|---|---|---|---|---|
| **t, s** | **u, m/s** | **t, s** | **u, m/s** | **t, s** | **u, m/s** |
| 0.02 | 0.05 | 0.02 | 0.26 | 0.02 | 0.05 |
| 0.05 | 0.23 | 0.05 | 0.35 | 0.05 | 0.29 |
| 0.08 | 0.29 | 0.08 | 0.35 | 0.08 | 0.35 |
| 0.12 | 0.30 | 0.15 | 0.36 | 0.12 | 0.37 |
| 0.18 | 0.32 | 0.22 | 0.38 | 0.15 | 0.38 |
| 0.53 | 0.31 | 0.43 | 0.36 | 0.18 | 0.39 |
| 1.03 | 0.31 | 0.82 | 0.36 | 0.62 | 0.38 |
| 1.92 | 0.31 | 2.07 | 0.36 | 0.87 | 0.37 |
| 3.17 | 0.31 | 3.65 | 0.35 | 1.35 | 0.35 |
| 4.58 | 0.30 | 4.98 | 0.35 | 2.33 | 0.33 |
| 6.08 | 0.31 | 6.48 | 0.35 | 3.93 | 0.31 |
| 7.60 | 0.31 | 8.00 | 0.34 | 5.73 | 0.30 |
| 9.13 | 0.31 | 9.53 | 0.33 | 7.40 | 0.29 |
| 10.67 | 0.31 | 10.65 | 0.31 | 9.17 | 0.28 |
| 11.88 | 0.30 | | | 10.93 | 0.28 |
| | | | | 12.08 | 0.26 |

Fig. 8.3 data

| 6 °C | | 25 °C | | 45 °C | |
|---|---|---|---|---|---|
| **t, s** | **u, m/s** | **t, s** | **u, m/s** | **t, s** | **u, m/s** |
| 0.02 | 0.12 | 0.02 | 0.21 | 0.02 | 0.23 |
| 0.05 | 0.18 | 0.07 | 0.23 | 0.05 | 0.27 |
| 0.12 | 0.17 | 0.13 | 0.23 | 0.08 | 0.30 |
| 0.37 | 0.16 | 0.22 | 0.23 | 0.12 | 0.29 |
| 0.92 | 0.16 | 0.55 | 0.23 | 0.15 | 0.30 |
| 2.18 | 0.16 | 1.20 | 0.22 | 0.18 | 0.30 |
| 4.53 | 0.15 | 2.60 | 0.20 | 0.60 | 0.28 |
| 8.43 | 0.14 | 4.73 | 0.19 | 1.50 | 0.27 |
| 13.37 | 0.14 | 6.97 | 0.18 | 2.57 | 0.25 |
| 19.17 | 0.13 | 9.40 | 0.17 | 4.43 | 0.23 |
| 24.30 | 0.13 | 12.37 | 0.17 | 7.67 | 0.21 |
| 26.53 | 0.14 | 15.77 | 0.17 | 10.83 | 0.18 |
| 26.53 | 0.14 | 18.97 | 0.17 | 13.67 | 0.17 |
| | | 20.63 | 0.17 | 16.70 | 0.16 |

Fig. 8.4 data

| Experimental u, cm/s | Moore & Sawi u, cm/s |
|---|---|
| 17.00 | 14.90 |
| 23.20 | 20.70 |
| 30.00 | 26.40 |
| 31.50 | 28.30 |
| 36.00 | 33.60 |
| 37.00 | 32.70 |
| 37.80 | 33.80 |
| 38.00 | 34.60 |
| 38.30 | 35.90 |

Fig. 8.5 data

| 6 °C | | 25 °C | | 45 °C | |
|---|---|---|---|---|---|
| t, s | u, m/s | t, s | u, m/s | t, s | u, m/s |
| 0.02 | 0.15 | 0.07 | 0.22 | 0.02 | 0.15 |
| 0.07 | 0.15 | 0.13 | 0.22 | 0.05 | 0.27 |
| 0.17 | 0.16 | 0.20 | 0.21 | 0.08 | 0.29 |
| 0.32 | 0.15 | 0.30 | 0.20 | 0.12 | 0.29 |
| 0.72 | 0.14 | 0.40 | 0.20 | 0.19 | 0.27 |
| 1.15 | 0.13 | 0.62 | 0.18 | 0.23 | 0.25 |
| 1.70 | 0.12 | 1.28 | 0.14 | 0.30 | 0.24 |
| 3.62 | 0.10 | 4.43 | 0.11 | 0.53 | 0.20 |
| 8.03 | 0.09 | 9.30 | 0.10 | 1.33 | 0.14 |
| 13.60 | 0.08 | 15.17 | 0.10 | 3.27 | 0.12 |
| 20.63 | 0.08 | 22.70 | 0.10 | 7.87 | 0.12 |
| 28.40 | 0.09 | 30.47 | 0.11 | 14.13 | 0.12 |
| 35.20 | 0.09 | 34.65 | 0.11 | 20.23 | 0.13 |
| 0.22 | 0.15 | 0.13 | 0.21 | 26.18 | 0.13 |
| 0.13 | 0.16 | | | 29.40 | 0.13 |

Fig. 8.6 experimental data used for model validation

| $2.5\times10^{-6}$ mol/m$^3$ | | $12.5\times10^{-6}$ mol/m$^3$ | | $74.9\times10^{-6}$ mol/m$^3$ | |
|---|---|---|---|---|---|
| **t, s** | **u, m/s** | **t, s** | **u, m/s** | **t, s** | **u, m/s** |
| 0.02 | 0.15 | 0.02 | 0.15 | 0.02 | 0.08 |
| 0.07 | 0.16 | 0.07 | 0.15 | 0.05 | 0.11 |
| 0.13 | 0.16 | 0.13 | 0.16 | 0.10 | 0.15 |
| 0.20 | 0.17 | 0.22 | 0.15 | 0.18 | 0.12 |
| 0.27 | 0.16 | 0.32 | 0.15 | 0.28 | 0.11 |
| 0.33 | 0.16 | 0.45 | 0.14 | 0.38 | 0.11 |
| 0.45 | 0.16 | 0.72 | 0.14 | 0.50 | 0.10 |
| 0.62 | 0.16 | 1.15 | 0.13 | 0.63 | 0.10 |
| 0.88 | 0.16 | 1.70 | 0.12 | 0.85 | 0.09 |
| 1.28 | 0.15 | 3.62 | 0.10 | 1.18 | 0.09 |
| 2.22 | 0.14 | 8.03 | 0.09 | 1.62 | 0.09 |
| 4.00 | 0.13 | 13.60 | 0.08 | 2.47 | 0.08 |
| 6.63 | 0.12 | 20.63 | 0.08 | 5.10 | 0.08 |
| 10.40 | 0.11 | 28.40 | 0.09 | 9.57 | 0.08 |
| 14.97 | 0.10 | 35.20 | 0.09 | 15.00 | 0.09 |
| 19.73 | 0.10 | 40.10 | 0.09 | 21.37 | 0.09 |
| 24.87 | 0.10 | 41.83 | 0.09 | 27.87 | 0.09 |
| 30.98 | 0.10 | | | 33.10 | 0.09 |
| 34.77 | 0.10 | | | 38.73 | 0.09 |
| | | | | 42.65 | 0.09 |

Fig. 8.6 model data

| Stagnant cap angle, ° | Triton concentration, mol/m$^3$ | | | u, m/s |
|---|---|---|---|---|
| | 2.5×10$^{-5}$ | 12.5×10$^{-5}$ | 74.9×10$^{-5}$ | |
| | t, s | t, s | t, s | |
| 0.00 | 0.00E+00 | 0.00E+00 | 0.00E+00 | 0.1739 |
| 1.50 | 0.00E+00 | 0.00E+00 | 0.00E+00 | 0.1739 |
| 3.01 | 9.85E-05 | 1.97E-05 | 3.28E-06 | 0.1739 |
| 4.52 | 5.43E-04 | 1.09E-04 | 1.81E-05 | 0.1739 |
| 6.04 | 1.58E-03 | 3.17E-04 | 5.28E-05 | 0.1739 |
| 7.59 | 3.50E-03 | 7.00E-04 | 1.17E-04 | 0.1739 |
| 9.15 | 6.63E-03 | 1.33E-03 | 2.21E-04 | 0.1738 |
| 10.73 | 1.14E-02 | 2.27E-03 | 3.79E-04 | 0.1738 |
| 12.35 | 1.14E-02 | 2.27E-03 | 3.79E-04 | 0.1738 |
| 13.99 | 2.77E-02 | 5.55E-03 | 9.25E-04 | 0.1736 |
| 15.68 | 4.07E-02 | 8.15E-03 | 1.36E-03 | 0.1736 |
| 17.40 | 5.80E-02 | 1.16E-02 | 1.93E-03 | 0.1734 |
| 19.16 | 8.08E-02 | 1.62E-02 | 2.69E-03 | 0.1732 |
| 20.97 | 1.11E-01 | 2.21E-02 | 3.68E-03 | 0.1730 |
| 22.83 | 1.48E-01 | 2.96E-02 | 4.93E-03 | 0.1724 |
| 24.74 | 1.95E-01 | 3.90E-02 | 6.51E-03 | 0.1717 |
| 26.71 | 2.56E-01 | 5.11E-02 | 8.52E-03 | 0.1711 |
| 28.74 | 3.33E-01 | 6.66E-02 | 1.11E-02 | 0.1706 |
| 30.82 | 4.25E-01 | 8.49E-02 | 1.41E-02 | 0.1693 |
| 32.97 | 5.41E-01 | 1.08E-01 | 1.80E-02 | 0.1682 |
| 35.19 | 6.79E-01 | 1.36E-01 | 2.26E-02 | 0.1666 |
| 37.47 | 8.57E-01 | 1.71E-01 | 2.85E-02 | 0.1654 |
| 39.83 | 1.06E+00 | 2.11E-01 | 3.51E-02 | 0.1631 |
| 42.25 | 1.30E+00 | 2.59E-01 | 4.31E-02 | 0.1606 |
| 44.75 | 1.57E+00 | 3.13E-01 | 5.21E-02 | 0.1576 |
| 47.33 | 1.91E+00 | 3.80E-01 | 6.33E-02 | 0.1547 |
| 49.98 | 2.30E+00 | 4.58E-01 | 7.62E-02 | 0.1514 |
| 52.70 | 2.74E+00 | 5.44E-01 | 9.05E-02 | 0.1476 |
| 55.51 | 3.23E+00 | 6.39E-01 | 1.06E-01 | 0.1433 |
| 58.39 | 3.80E+00 | 7.52E-01 | 1.25E-01 | 0.1391 |
| 61.35 | 4.42E+00 | 8.71E-01 | 1.45E-01 | 0.1345 |
| 64.39 | 5.08E+00 | 1.00E+00 | 1.66E-01 | 0.1297 |
| 67.51 | 5.94E+00 | 1.17E+00 | 1.94E-01 | 0.1255 |
| 70.70 | 6.76E+00 | 1.32E+00 | 2.20E-01 | 0.1207 |
| 73.98 | 7.80E+00 | 1.52E+00 | 2.52E-01 | 0.1165 |
| 77.33 | 8.84E+00 | 1.72E+00 | 2.84E-01 | 0.1121 |
| 80.75 | 1.05E+01 | 2.02E+00 | 3.35E-01 | 0.1089 |
| 84.25 | 1.17E+01 | 2.25E+00 | 3.72E-01 | 0.1048 |

| | | | | |
|---|---|---|---|---|
| 87.83 | 1.33E+01 | 2.54E+00 | 4.20E-01 | 0.1013 |
| 91.47 | 1.54E+01 | 2.92E+00 | 4.81E-01 | 0.0984 |
| 95.19 | 1.78E+01 | 3.33E+00 | 5.48E-01 | 0.0957 |
| 98.97 | 2.00E+01 | 3.72E+00 | 6.11E-01 | 0.0930 |
| 102.82 | 2.42E+01 | 4.41E+00 | 7.23E-01 | 0.0915 |
| 106.74 | 2.84E+01 | 5.09E+00 | 8.32E-01 | 0.0899 |
| 110.71 | 3.25E+01 | 5.73E+00 | 9.33E-01 | 0.0882 |
| 114.74 | 3.95E+01 | 6.75E+00 | 1.09E+00 | 0.0870 |
| 118.83 | 4.50E+01 | 7.51E+00 | 1.21E+00 | 0.0861 |
| 122.97 | 5.20E+01 | 8.43E+00 | 1.36E+00 | 0.0851 |
| 127.16 | 6.40E+01 | 9.84E+00 | 1.57E+00 | 0.0848 |
| 131.40 | 7.77E+01 | 1.13E+01 | 1.79E+00 | 0.0844 |
| 135.68 | 9.25E+01 | 1.26E+01 | 1.98E+00 | 0.0840 |
| 139.99 | 1.18E+02 | 1.44E+01 | 2.25E+00 | 0.0840 |
| 144.35 | 1.52E+02 | 1.62E+01 | 2.51E+00 | 0.0840 |
| 148.73 | 2.01E+02 | 1.77E+01 | 2.73E+00 | 0.0838 |
| 153.15 | 3.78E+02 | 1.96E+01 | 2.99E+00 | 0.0839 |
| 157.59 | | 2.11E+01 | 3.20E+00 | 0.0838 |
| 162.04 | | 2.27E+01 | 3.40E+00 | 0.0838 |
| 166.52 | | 2.40E+01 | 3.58E+00 | 0.0838 |
| 171.01 | | 2.52E+01 | 3.74E+00 | 0.0839 |
| 175.50 | | 2.60E+01 | 3.84E+00 | 0.0839 |
| 180.00 | | 2.62E+01 | 3.87E+00 | 0.0838 |